

Improvement of NiCrBSi sprayed coatings performance by electromagnetic induction remelting

Teză destinată obținerii titlului științific de
doctor inginer la "Universitatea
Politehnica Timișoara" în domeniul
ȘTIINȚA MATERIALELOR
de către

Ing. Petru Cristian Vălean

Conducător științific: Viorel-Aurel Șerban

Timișoara, 2022

Foreword

The present thesis was elaborated during my activity at the Politehnica University of Timisoara, in cooperation with the Department of Materials Science and Testing from Westphalian University of Applied Sciences, Gelsenkirchen, Germany and the company Karl Schumacher GmbH, Bochum, Germany.

The thesis addresses material and industrial engineers and all interested in knowing and understanding the remelting process of self-fluxing alloys. Deposited with the Oxyacetylene flame and remelted by induction.

I believe this thesis represent a solid scientific support for future research and industrial application of the NiCrBSi coatings.

Acknowledgments

I would like to express my sincerely appreciations to my scientific supervisor Prof.Dr.Eng Viorel-Aurel Serban from Polytechnic University of Timișoara who provided valuable guidance during my studies. I would also like to say thankyou to Dr.rer.nat.Gabriela Marginean from Westphalian University of Applied Sciences, Gelsenkirchen for continuous and permanent support before and during this thesis.

Special thanks to Eng. Thomas Conrad from Karl Schumacher GmbH for his help and trust, for giving me the opportunity to test everything on machines and for all the materials provided.

I was also very lucky to have the support of my colleagues Dr.Eng. Dragos Pascal, Dr. Eng. Norbert Kazamer and Dr. Eng. Roxana Muntean at the beginning of my research and during all the laboratory tests.

Furthermore, I would like to thank, Prof.Dr. Eng Mircea Vodă, Assoc. Prof. Dr. Eng. Bogdan Radu, Prof. Dr. Eng. Ion Dragoș Uțu, and Assoc. Prof. Dr. Eng. Cosmin Codrean from Polytechnic University of Timisoara for being part of my guidance committee and for their countless suggestions and advices regarding my scientific research

Last but definitely not least, I am extremely grateful to my family for their unconditional support, for trusting me and encouraging me to make important steps in my life.

June 2022

Petru Valean

Contents

| | |
|---|----|
| List of figures | 7 |
| List of tables | 9 |
| 1. Introduction | 11 |
| 1.1. Background and motivation | 11 |
| 1.2. Aim of the study | 12 |
| 2. State of the art | 14 |
| 2.1. Theoretical aspects regarding thermal sprayed coatings | 14 |
| 2.1.1. Preparation prior to thermal spraying | 14 |
| 2.1.2. Designing of the components for thermal spraying | 19 |
| 2.2. Thermal spraying processes classification | 20 |
| 2.2.1. Wire flame spraying | 21 |
| 2.2.2. Arc spraying | 22 |
| 2.2.3. High velocity oxy-fuel spraying | 24 |
| 2.3. Post-processing of sprayed coatings | 25 |
| 2.3.1. Surface remelting methods | 25 |
| 2.3.2. Induction heating | 28 |
| The law of electromagnetic induction | 29 |
| The skin effect | 30 |
| Proximity effect | 36 |
| Variation of steel properties in the heating process | 36 |
| The loop effect | 37 |
| Distribution of current density in the inductor and in the heater using electromagnetic flux concentrators | 37 |
| 2.4. Wear of materials | 39 |
| 2.4.1. Abrasive wear | 39 |
| 2.4.2. Erosion Wear | 40 |
| 2.4.3. Adhesion Wear | 41 |
| 2.4.4. Fatigue Wear | 41 |
| 2.5. Corrosion | 41 |
| 3. Equipment and methodology for experiment and testing | 43 |
| 3.1. Equipment and materials | 43 |

6 Table of contents -

| | | |
|--------|---|----|
| 3.2. | Powder deposition | 44 |
| 3.3. | Mechanical testing..... | 45 |
| 3.3.1. | Microhardness tester..... | 45 |
| 3.3.2. | Wear testing and wear measurements..... | 45 |
| 3.4. | Microstructural Characterization | 46 |
| 3.4.1. | Metallographic preparation..... | 46 |
| 3.4.2. | Thermogravimetric analysis (TGA)..... | 46 |
| 3.4.3. | Scanning electron microscopy (SEM)..... | 47 |
| 3.4.4. | Energy Dispersive X-ray Spectroscopy (EDX) | 48 |
| 3.5. | Corrosion investigation | 49 |
| 4. | Results and discussion | 51 |
| I. | Oxy-acetylene flame spraying | 51 |
| 4.1. | Characteristics of the feedstock powders..... | 51 |
| 4.1.1. | Morphology..... | 51 |
| 4.1.2. | Phase composition | 55 |
| 4.2. | Substrate material..... | 57 |
| 4.3. | Parameters of the oxy-acetylene flame/fuel spraying process | 58 |
| 4.4. | Characteristics and properties of as-sprayed coatings | 61 |
| II. | Electromagnetic induction remelting..... | 64 |
| 4.5. | Selection of the inductor geometry | 64 |
| 4.6. | Remelting process optimization..... | 68 |
| 4.6.1. | Full Factorial Design | 69 |
| 4.6.2. | Taguchi method | 69 |
| 4.6.3. | Working distance | 75 |
| 4.6.4. | Extra Hardening..... | 82 |
| 4.7. | Characteristics and properties of remelted coatings | 83 |
| 4.7.1. | Deposition coating thickness | 83 |
| 4.7.2. | Phase composition | 84 |
| 4.7.3. | Porosity | 87 |
| 4.7.4. | Hardness..... | 89 |
| 4.7.5. | Adhesion | 89 |

| | | |
|--------|--|-----|
| 4.7.6. | Tribological behaviour..... | 91 |
| 4.7.7. | Corrosion behaviour..... | 93 |
| 5. | General conclusion, unique contributions and upcoming work | 102 |
| 5.1. | General Conclusion | 102 |
| 5.2. | Personal contributions..... | 103 |
| 5.3. | Future work..... | 104 |
| | Bibliography | 107 |

List of figures

| | | |
|-------------|---|----|
| Figure 1.1: | Schematic of the experimental part | 13 |
| Figure 2.1 | Thermal spraying schematics [11] | 14 |
| Figure 2.2 | Surface processes applied prior to thermal spraying [12]..... | 15 |
| Figure 2.3 | Designing components for spraying [9] | 19 |
| Figure 2.4 | Thermal spraying process classification according to the sources of energy [20] | 20 |
| Figure 2.5 | Schematic diagram of wire spraying..... | 21 |
| Figure 2.6 | Cross section through hand spray head and the nozzle [9]..... | 21 |
| Figure 2.7 | Solid (a) and powder filled wires (b) | 22 |
| Figure 2.8 | Principle of arc spraying | 22 |
| Figure 2.9 | Arc formation [26] | 23 |
| Figure 2.10 | Arc spraying coating building [29]..... | 24 |
| Figure 2.11 | Principle diagram of HVOF process | 25 |
| Figure 2.12 | Laser cladding schematics [38]..... | 26 |
| Figure 2.13 | Electron Beam melting [42] | 27 |
| Figure 2.14 | Induction rapid heating..... | 27 |
| Figure 2.15 | Schematic illustration of an induction coil [44]..... | 28 |
| Figure 2.16 | Schematic of induction heating [46] | 28 |
| Figure 2.17 | Explanatory figure for solving electromagnetic field equations and deducing formulas for resistors and reactants..... | 30 |
| Figure 2.18 | Dependence on current density and magnetic field strength as a function of depth | 32 |
| Figure 2.19 | Current distribution to the proximity effect [61]..... | 36 |
| Figure 2.20 | Electro-magnetic field distribution [68] | 37 |
| Figure 2.21 | Electromagnetic flux concentrators [68]..... | 38 |
| Figure 2.22 | Two-tree body abrasive wear [85] | 40 |
| Figure 2.23 | Erosion wear [88] | 40 |
| Figure 2.24 | Adhesive wear [88] | 41 |
| Figure 2.25 | Fatigue wear [88] | 41 |
| Figure 3.1 | Flame spraying principle | 44 |
| Figure 3.2 | SEM operation system [99] | 48 |
| Figure 3.3 | EDX principle [101]..... | 49 |
| Figure 3.4 | Electrochemical Cell configuration | 50 |

8 List of figures -

| | |
|--|----|
| Figure 4.1 EDX spectrum of NiCrBSi powders | 52 |
| Figure 4.2 SEM micrograph of the NiCrBSi powder: a) KS-IC-45, b) KS-IC-55S | 52 |
| Figure 4.3 SEM cross section micrograph of the NiCrBSi powder: a) KS-IC-45, | 53 |
| Figure 4.4 DTA curve of IC-KS-45 powder..... | 54 |
| Figure 4.5 XRD diffraction pattern KS-IC-45..... | 55 |
| Figure 4.6 XRD diffraction pattern KS-IC-55S..... | 56 |
| Figure 4.7 XRD diffraction pattern KS-IC-55..... | 56 |
| Figure 4.8 As-sprayed (left) and remelted (right) bars..... | 58 |
| Figure 4.9 Sand blasted samples | 59 |
| Figure 4.10 Cross-section SEM micrographs of as-sprayed KS-IC-45: a) near to surface, b) at the interface, c) whole coating..... | 62 |
| Figure 4.11 Friction coefficient and wear track of as-sprayed KS-IC-45..... | 63 |
| Figure 4.12 Friction coefficient and wear track of as-sprayed KS-IC-55S..... | 63 |
| Figure 4.13 Friction coefficient and wear track of as-sprayed KS-IC-55..... | 63 |
| Figure 4.14 Magnetic lines and temperature distribution cilinder heated by 4-turn inductor [113, 114]..... | 64 |
| Figure 4.15 a) Remelting element 3 spirals, b) Optimised remelted sample..... | 65 |
| Figure 4.16 Non remelted edge with 3 spiral elements..... | 66 |
| Figure 4.17 Coil design [116] | 66 |
| Figure 4.18 Sample remelted with circle cross element section | 67 |
| Figure 4.19 Sample remelted with rectangular cross element section | 68 |
| Figure 4.20 Charts showing parameter level v/s Signal to noise ratio | 73 |
| Figure 4.21: Exfoliate coating a) on the surface, b)cross-section..... | 74 |
| Figure 4.22 Crack's example: a) On the surface b)cross-section | 74 |
| Figure 4.23 Temperature influences a) to low, b) to high | 75 |
| Figure 4.24 Element and coating destruction | 75 |
| Figure 4.25 Substrate structure a) 7mm b) 12mm c) 20mm working distance | 76 |
| Figure 4.26 Substrate before heating | 77 |
| Figure 4.27 Structure of 42CrMo 2 mm from surface | 77 |
| Figure 4.28 Sorbite lamellar structure on the interface with perlite-ferite inclusions | 78 |
| Figure 4.29 Micro indentation on substrate remelted with 7 mm working distance | 78 |
| Figure 4.30 Sorbite lamellar structure on the interface | 79 |
| Figure 4.31 Micro indentation on substrate remelted with 12 mm working distance | 80 |
| Figure 4.32 Micro indentation on substrate remelted with 20 mm working distance | 80 |
| Figure 4.33 Martensitic lamellar structure on the interface | 81 |
| Figure 4.34 42CrMo4V cooling diagram [124]..... | 82 |
| Figure 4.44 Ceramic ball hardening..... | 83 |
| Figure 4.35 Coating cross section a)KS-IC-45, b)KS-IC-55S, c)KS-IC-55 | 84 |
| Figure 4.36 Overlapped XRD diffractograms | 85 |
| Figure 4.37 XRD Diffractogram of KS-IC-45 inductive remelted (left) and cross-section LM-micrograph (right) | 85 |
| Figure 4.38 XRD Diffractogram of KS-IC-55S inductive remelted (left) and cross-section LM-micrograph (right) | 86 |
| Figure 4.39 XRD Diffractogram of KS-IC-55 inductive remelted (left) and cross-section LM-micrograph (right) | 86 |

| | |
|--|-----|
| Figure 4.40 Example for marking the porosity of the as-sprayed coating (a) with help of the measurement software (b)..... | 87 |
| Figure 4.41 KS-IC-45 porosity: a) before, b)after measurement | 88 |
| Figure 4.42 KS-IC-55S porosity: a) before, b)after measurement | 88 |
| Figure 4.43 KS-IC-55 porosity: a) before, b)after measurement | 88 |
| Figure 4.45 Micrographs of Brinell indentation 187.5 kgf | 90 |
| Figure 4.46 Micrographs of Vickers indentation, applied forces: 1200N | 90 |
| Figure 4.47 Friction coefficient and wear track of KS-IC-45 | 91 |
| Figure 4.48 Friction coefficient and wear track of KS-IC-55S | 92 |
| Figure 4.49 Friction coefficient of KS-IC-55 | 92 |
| Figure 4.50 Corroded cylinder sample..... | 94 |
| Figure 4.51 Polarization curves of NiCrBSi coatings | 95 |
| Figure 4.52 Polarization curves of NiCrBSi coatings in 3.5% NaCl + 5% H ₂ SO ₄ , passivating part..... | 95 |
| Figure 4.53 Sample before salt spray test | 96 |
| Figure 4.54 KS-IC-45 before Salt spray test | 97 |
| Figure 4.55 KS-IC-45 after 480 hours Salt spray test | 97 |
| Figure 4.56 Attacked area of KS-IC-45 | 98 |
| Figure 4.57 Corrosion depth on KS-IC-45..... | 98 |
| Figure 4.58 KS-IC-45 before(left) and after (right) salt spray test..... | 99 |
| Figure 4.59 Cross section of KS-IC-45 coating after salt spray test..... | 100 |
| Figure 4.60 KS-IC-55S before(left) and after (right) salt spray test..... | 100 |
| Figure 4.61 KS-IC-55 before(left) and after (right) salt spray test..... | 101 |
| Figure 4.62 Cross section of KS-IC-55S(left) and KS-IC-55 (right) coating after salt spray test | 101 |

List of tables

| | |
|--|----|
| Table 2.1 Advantages and disadvantages of cleaning agents | 16 |
| Table 2.2 Advantages and disadvantages of covering materials | 17 |
| Table 2.3 Types of blasting materials | 18 |
| Table 2.4 The depth of penetration of the current | 35 |
| Table 4.1 Powder used in thermal spraying process..... | 51 |
| Table 4.2 Physical tests of NiCrBSi powder | 53 |
| Table 4.3 Chemical composition of substrate material..... | 58 |
| Table 4.4 Deposition layers of KS-IC-45 | 60 |
| Table 4.5 Spraying parameters..... | 60 |
| Table 4.6 Ball on disk parameters | 62 |
| Table 4.7: Factors that affect remelting process..... | 70 |
| Table 4.8 Selected factors and their levels | 70 |
| Table 4.9 Power constant - 980°C..... | 71 |
| Table 4.10 Power constant - 1010°C | 71 |
| Table 4.11 Power constant - 1050°C | 71 |
| Table 4.12 Power constant - 1080°C | 71 |
| Table 4.13 Orthogonal Array with Control Factors | 71 |

| | |
|---|----|
| Table 4.14 Porosity measurements | 72 |
| Table 4.15-Average S/N ratio for each Factor | 72 |
| Table 4.16 Optimum Parameters..... | 73 |
| Table 4.17 Optimised parameters | 75 |
| Table 4.18 Indentation values of remelted samples | 89 |
| Table 4.19 Wear measurements | 93 |
| Table 4.20 Corrosion values of NiCrBSi coatings | 96 |

1. Introduction

Society is in a continuous progress, in order to survive for long term, communities of people need energy. This energy is taken from different sources, however, any type of source requires processing toward to extract the maximum amount of usable power. To achieve this maximum, in addition to optimizing work processes, the life of raw material processing equipment must be extended

1.1. Background and motivation

According to statistics, the world rises constant consumption of energy, if around 7.5 billion metric tons oil equivalent were consumed in the early 1990s, over the next 20 years an annual increase in energy consumption of up to about 13.5 billion metric tons oil equivalent is expected [1]. To obtain this amount of energy, both from non-renewable sources (fossil) and from renewable sources (hydro-, tidal-, wave-, wind power) is urgently needed an improvement in the quality of the acquisition process of the raw material in case of non-renewable sources, and capture energy when we talk about the renewable energy.

An important direction of approach, in relation to the increase of the demand on the energy market, refers to the identification of new technological solutions of manufacture, of reduction of the costs related to the maintenance, repair, rehabilitation, of increase of service life of the equipment. A suggestive example is the development of new more durable assemblies, with improved wear behavior and a very high corrosion resistance in extremely aggressive environments (coal mines, offshore atmosphere, hydropower plants).

For example, machines which are working in these environments, in order to have the necessary force, are equipped with hydraulic cylinders. Because they are in a continuous movement, these parts are susceptible to premature wear and to intense corrosion, as well. According to a study made by the US Federal Highway Administration, in 2002, direct corrosion costs amounted to around \$ 272 billion [2]; it is currently estimated to raise these costs globally to around \$ 2.5 trillion annually, which is corresponding with 3.4% of world GDP. Besides these costs, if it is taken a single set of components, the costs can be divided into three major categories. The first and the most expensive category is in the year zero of the assembly: where the costs being the initial construction investment of the structure. In the second category are the costs associated with maintenance, repair, rehabilitation, and also the costs related to non-functioning time for the whole assembly. The last category includes the costs related to removal of the installation and after that a new cycle can begin.

The afore mentioned structures are designed to be in use for a certain amount of time. Maintenance costs may be reduced if some active parts of the plant can be rebuilt relatively easily, and the entire component does not have to be restored. Therefore, a protective coating is used for active parts of the cylinder and the costs are much diminished [3]

Leaving the economic side, the technical part comes into play, namely surface engineering. The aim of this is to solve the requirements of the interface (e.g. wear and corrosion resistance, close dimensional tolerance, hardness) for components which are in direct contact with an aggressive environment or directly with another assembly part, without destroying the mechanical resistance requirements, also it is

desirable not to destroy the properties of the underlying material (e.g. ductility tensile strength, high toughness, low density) [4].

Since the 1970s the surface properties of these components were improved by depositing a hard chromium coating. In this process the working pieces are coated with a chromium metal with coating thickness in range of 2,5 μm up to maximum 500 μm [5]. Due to the harmful chromium compounds: Chromite (Cr (III)) and Chromate (Cr (VI)) [6], it had been tried to decline the electroplating chromium method, optimizing new coating types and processes for machine parts industries.

Thermal spraying is a popular solution in replacing the hard chromium plating process and is currently used to enhance product lifetime and also to restore components that have emerged from nominal sizes by wear or corrosion. The foundations of this process were laid by the Dr. Max Ulrich Schoop at the beginning of XX's century, he is also called "the Father" of thermal spraying. On 28th April 1909 in Berlin was applied the first patent for a metal spraying process, after that it took four years for the imperial patent office to grant it [7]. However, a technological expansion did not occur until after World War II period, during this time the powder used as feedstock and plasma spraying were developed and introduced in industry at a large scale.

The greatest advantage of this process is that a variety of materials can be used to obtain coatings, theoretically any material which is not decomposing at the melting point can be used in the process [8].

Due to the high deposition rate and having a wide range of coating thickness from a few micrometres up to millimetres, thermal spraying is known to be one of the most effective deposition methods, besides other methods of material depositing

1.2. Aim of the study

From all the flame-deposition methods the cheapest and more productive one is oxy-acetylene powder flame deposition. Following the literature, it is known that the coatings obtained by this process consists of several layers with a lamellar structure, very high porosity and imminent threat of delamination [9]. In this case of powder deposition, the major disadvantage is that at the interface the particle shows a mechanical anchorage to the substrate and has the risk of exfoliating upon exposure of an external agent/force

The purpose of the work was to obtain high-quality coatings (in terms of corrosion resistance and wear) in two steps, succeeding the simple and inexpensive procedure of deposition (step I) by applying a subsequent process of heating them by high-frequency currents (step II).

Objectives- the study aim is to develop NiCrBSi coatings with good wear and corrosion resistance in aqueous environment and with improved adhesion to the substrate. These novel coatings will find application in the coating industry, especially in the field of hydraulic cylinders.

The activities that are necessary to achieve the assumed objective are: deposition of coatings, construction (design) and optimization of the elements (components) used in the inductive remelting process, optimization for the remelting parameters, microstructure characterization, determination of the phase composition, examination of the adhesion to the substrate, evaluation of the corrosion and wear

behaviour of the remelted coatings, influence of the heating process on substrate material .

Consequently, the present work is structured in following chapters: in Chapter one (introduction) is presented the motivation and aim of this work. The second chapter presents the theoretical aspects regarding thermal spraying, engineering methods of protection against friction, wear, corrosion and also methods of improving mechanical properties; The third chapter is about equipment and methodology used in current work; chapter four contains the experimental program shown in Figure 1.1. Chapter five and six present the conclusion, pointing out some further research and original contributions presented in this work.

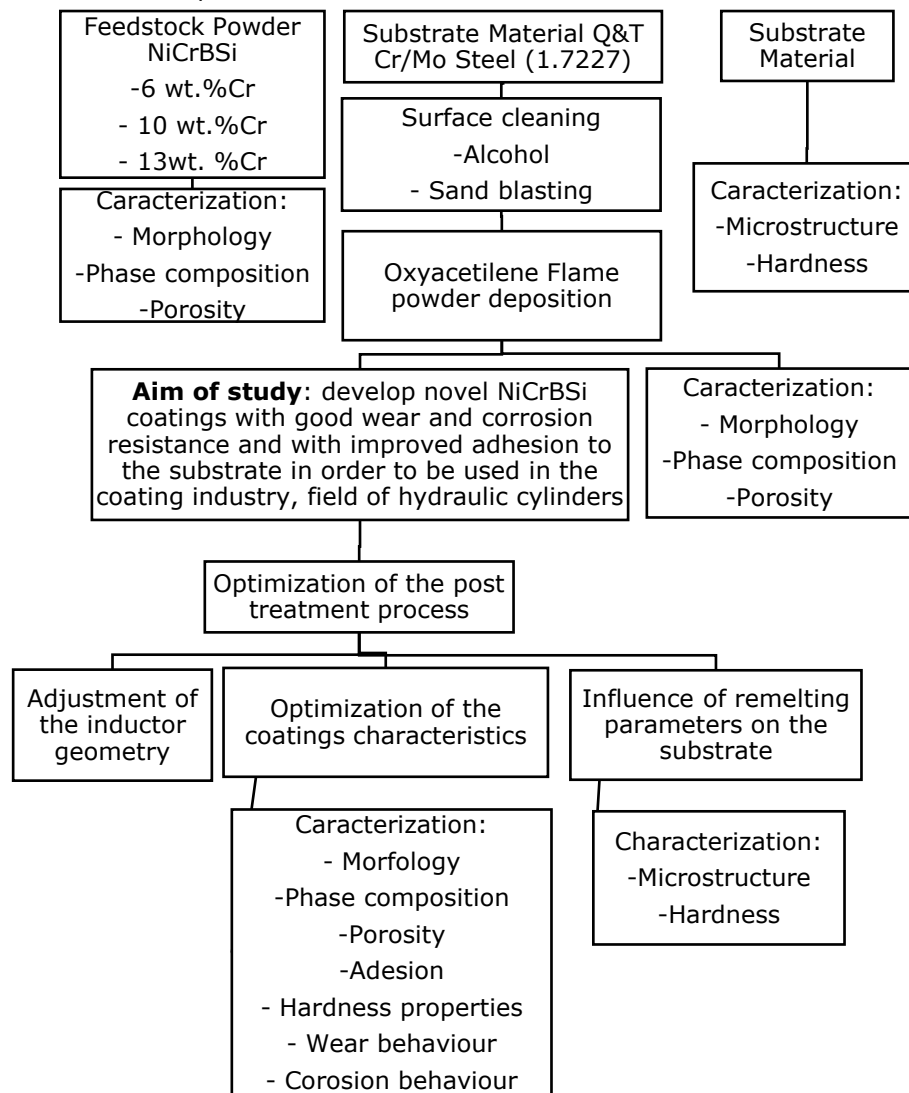


Figure 1.1: Schematic of the experimental part

2. State of the art

2.1. Theoretical aspects regarding thermal sprayed coatings

Nowadays more and more parts/components need a coating that gives them an increased durability while working in aggressive environments and not only.

These components can be subjected to different mechanical, chemical, or thermal stresses. The individual stresses can be the following and can lead to:

- Chemical stresses: Corrosion
- Thermal stresses: ageing and creep
- Mechanical stresses: fatigue and wear

In reality most of the time it cannot appear just a single stress, these tensions being combined with each other some of them are defined by the following types:

- Mechanical-chemical: friction corrosion and cavitation
- Mechanical-thermal: high-temperature fatigue
- Chemical-thermal: high-temperature corrosion.

A large majority of processes have been developed and come up with the same goal: that the process needs to have a high quality, efficiency, and reproducibility.

Thermal spraying is a process by which a metallic, ceramic, cermet or polymeric material is deposited on a substrate, providing a protective coating (see Figure 2.1). The spraying consumables material is fed to an equipment that will transform it into a semi-melted state and will accelerate it using a gas jet to the substrate. Several layers are deposited on the surface of the base material in the form of thin lamellar, which overlap and anchor mechanically to each other [10].

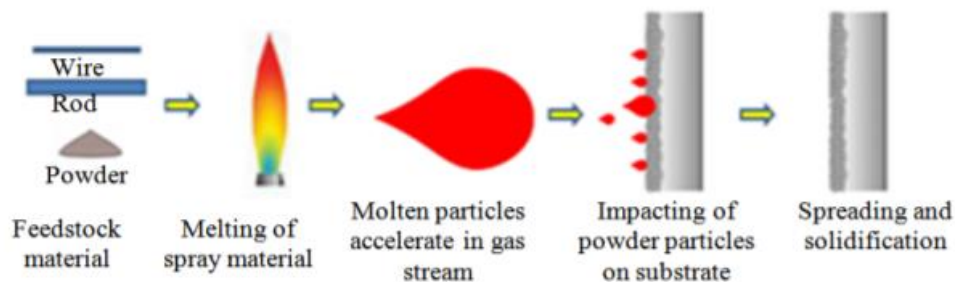


Figure 2.1 Thermal spraying schematics [11]

2.1.1. Preparation prior to thermal spraying

The correct preparation of the substrate is a decisive component in the success of the final coating. Most of the coats deposited by thermal spraying are fixed to the substrate by the mechanical bonding. This bond depends not only on the type of particle sprayed and its speed but also depends on the cleaning level of the substrate and its roughness. For these reasons in practice, pre-treatments are required. The common pre-treatment processes are listed in the Figure 2.2. The coatings that need

2.2 Theoretical aspects regarding thermal sprayed coatings 15

a subsequent treatment by means of remelting could be subject of different processes, like in the case of this work where high frequency currents were applied. Further alternative methods can be remelting by an oxyacetylene flame or even in a vacuum oven. All these methods lead to a good bond of the coating material to the substrate.

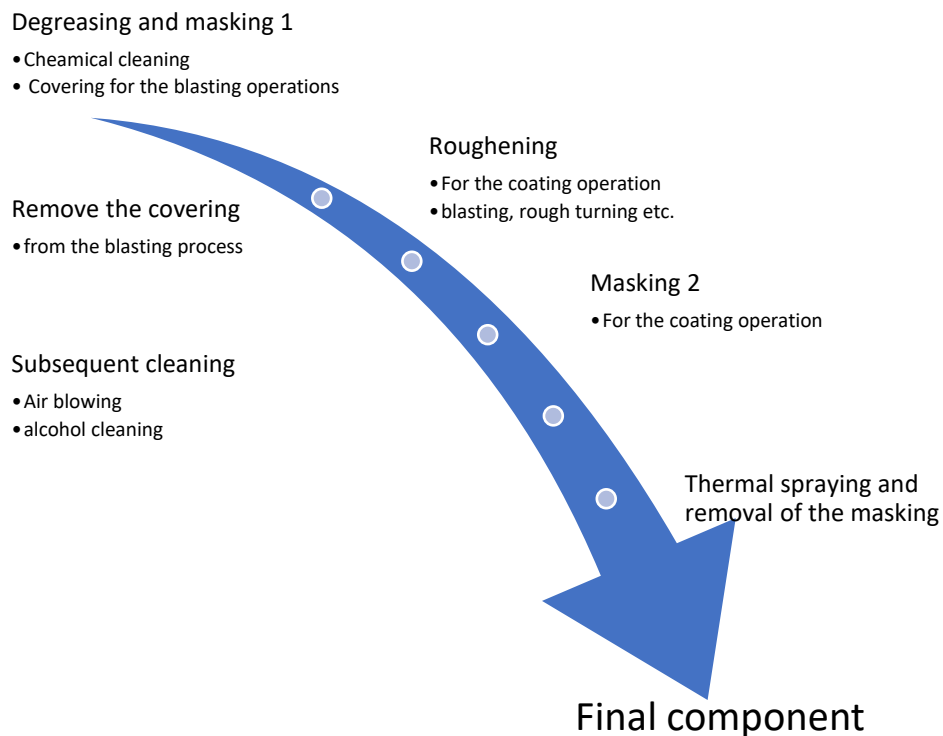


Figure 2.2 Surface processes applied prior to thermal spraying [12]

a) Chemical cleaning

The initial condition before putting into use a material, part or device is that it is clean, without traces of oil, grease or substances that adhere to the base substrate in order to be used in the thermal spraying process.

One of chemical degreasing processes used is combustion using high furnace temperatures, or with the flames of a welding torch.

Degreasing in ovens or furnaces is another technique utilised when there are old machine parts, especially cast components that are covered with oils, greases or other paints on the inside where it is very difficult to reach with the help of liquid solvents.

Greases can be dissolved using chemical cleaning agents such as Acetone, Alcohol, spirit, Nitrocellulose varnish solvent [13].

Acetone is characterized by: colorless, low viscosity, highly flammable and can form explosive mixtures.; also this can be diluted with water or mixed with most of the organic solutions in almost any concentrate ratio

Alcohol is also colorless, for technical use only (not good for human consumption).

Nitrocellulose varnish solvent is a mixture of various hydrocarbons, most often used to clean nitrocellulose varnishes; is harmful to health.

In the case of all chemical cleaning agents one must to take into account the technical safety data [14].

Alkaline aqueous solutions(similar to soap-based solutions) and hot water vapor can be used to remove greases, as well.

Toxic pericocular products such as methanol, perchlorethylene, triperchlorethylene should not be used as they can seriously affect human health.

In conclusion in the case of chemical cleaning, it cannot be said that one is better than the other. We can make an analysis according to which, depending on the costs and advantages and disadvantages, it is the right material to choose for the degreasing of the surface that will be covered with a layer of protective metal. The advantages and disadvantages are presented in Table 2.1

Table 2.1 Advantages and disadvantages of cleaning agents

| Method | Disadvantages | Advantages |
|--------------------------------|---|---|
| Combustion | due to high temperatures, it can produce distortions in the material, produce oxides on the surface, emit smoke when burned | cleanses all grease on the surface, even hard to reach spots, has no effect on human health |
| Acetone | Easily volatile and inflammable, relative expensive, skin degreasing effect. | very good degreaser |
| Alcohol, spirit | Can causes states of intoxications, easily inflammable | good solvent , favourable cost |
| Nitrocellulose varnish solvent | Harmful for health, easily inflammable | better grease solvent than alcohol, favourable cost if it is produced in large quantities |
| Alkaline aqueous solutions | Component drying required | not inflammable |

b) Covering for the blasting operations

Covering materials are required to be used for all regions where there is no additive material in the form of a protective coating needed these parts should not be sandblasted. The materials used for surface protection are different.

There are materials that can be used only once, such as self-adhesive tapes or materials that can stand out for many uses, such as metal strips or rubber-coated masks, which stand out for many uses [15]. A classification of the advantages and disadvantages are summarized Table 2.2

Table 2.2 Advantages and disadvantages of covering materials

| Covering material | Advantages | Disadvantages |
|--------------------|---|--|
| Self-adhesive tape | easy to use | precise position depending on the worker, no temperature resistance, cannot be used for HVOF sandblasting, can be used only once |
| Separating Agent | Favourable cost, immediately utilisation, water soluble | not suitable for blasting (just for spraying) imprecise delimitations because of paintbrush |
| Solid metal mask | exact covering, can be reused for identical parts, favourable costs | depends on design, high prices. requires processing beforehand |
| Sheet metal mask | often in combination with adhesive tapes. suitable for all sprayed coatings | depends on design, high prices. Possibility of distortion at high operating temperatures |
| Silicon mask | favourable costs for series parts, accurate coverage, ideal for critical contours | high price, cannot be immediately used |

c) Roughening for the coating operations

The roughening of the surface which needs to be thermally coated has as its main purpose the improvement of the mechanical adhesion for the coating on the substrate. At the same time, is pursued to remove all impurities from the surface, such as oxides or contaminants of any kind, in order to obtain an active surface. In practice there were 3 methods which have international acceptance, namely: rough turning, rough grinding and blasting.

Rough turning it produces a surface similar to a thread or sawtooth. It is mainly used for forging parts because by this process the forging defects can be eliminated, and later a prominent coating of up to a few mm thickness can be deposited. For this procedure, the tooth or thread surface deep must be at least 0.5 mm or more. A disadvantage of this structure is that this structure must first be filled, after which the formation of the coating thickness can be considered.

Rough grinding it is a rarely applied method and like the rough turning it was often used in the past. It similar to blasting but grinding operations is carried out in an cross grinding pattern with an coarse grindstone) [9]

Blasting it is most common method

In the case of the most commonly used installations for blasting metal parts, the agent used is thrown to the surface with the help of compressed air. Its acceleration results in a kinetic energy that can be increased using special blasting nozzles (Laval Nozzels) [16]. The atomic forces of attraction (Van der Waals bonds, adhesion or cohesion) are activated and increased by the sandblasted surface, which

improves the adhesion of the layer [17]. Adhesion of the coating to the substrate for sandblasted surfaces is time-dependent. According to the adhesive pull strength test, the adhesion capacity is halved at an interval of 4 hours after sandblasting. Consequently, this means that in practice the material must be covered within a maximum 2 hours after blasting.

Five types of materials have proven to be suitable for use in the mechanical sandblasting process. Depending on their advantages and disadvantages, they are presented in the Table 2.3

Table 2.3 Types of blasting materials

| Blasting Material | Cost | Advantages | Disadvantages | Standard DIN EN |
|-------------------|------------------|-----------------------------------|---|----------------------------|
| Slag | Particularly low | Economical viable | Suitable for precleaning, can be used once | ISO 11126-3 ISO 11126-4 |
| Steel grit | Low | Long service life, High toughness | Used just for components made from weakly alloyed steels | ISO 11124-2 |
| Corundum, pure | Medium | Very pure, Utilised frequently | Low toughness, relative short service life | ISO 11126-7 |
| Corundum, alloyed | Medium | Pure, utilised frequently | Better toughness, does not break so fast as pure corundum | ISO 11126-7 |
| Silicon Carbide | High | Very hard | Reacts to cobalt, short service life related to the costs | |

Steel grit is one of the most commonly used blasting materials, it is made of cast steel, angular, martensitic with carbide inclusions, its hardness is higher than 60 HRC. A second type is made of chromium steel, angular, with a hardness of 60 HRC or third one made of nickel chromium steel, round, with a hardness of 45HRC. These 3 materials are the most used due to the low price and high life service. Also, the residues that remain after the blasting process and the subsequent cleaning with compressed air jet, should not influence the function of the component to be thermally covered. They are suitable for the coatings to be subjected to a subsequent heat treatment, because they have a high melting temperature, they will not be melted together with the coating and will not change its properties [18].

In selecting and using the materials necessary for blasting for a certain circumstances, the following parameters must be taken into account, which decisively influence the blasting process:

- Blasting angle
- Blasting distance
- Blasting pressure

2.2 - Theoretical aspects regarding thermal sprayed coatings 19

- Size and shapes of blasting materials
- Blasting materials
- Blasting principle
- Hardness of the component- influence the cleaning speed
- Recycling of blasting materials – the media must be collected cleaned and reused in function of the efficiency of the cleaning process
- Care of blasting materials

2.1.2. Designing of the components for thermal spraying

Because the spray jet is always in a straight line, only the parts in front of it can be sprayed. For the inside diameters it is always necessary that the size of these to be taken into account by design, the sprayed hole must be larger than the torch head plus the minimum spray distance, if the inside diameter is larger than the respective process can be used, otherwise we should search for another metal coating process which doesn't need this spray distance. Depending on the spraying process, there are different angles of flame. The optimal angle of impact of the sprayed particles and approaching to the base material is $80-90^\circ$. deviations of up to 45° are possible in exceptional cases but with poorer coating quality and a lot of over spraying particles. Examples on this subject are included in the DVS 2308 Technical bulletin [19].

If surfaces with right angles or grooves are sprayed, the coating will always be much more pronounced at the sharp tip and corner of the groove, which will not give stability to this coat and also the adhesion will not be standard. In order to eliminate this problem, the gun should always move when it reaches this groove or the 90° angle. Figure 2.3 shows the preferred sketches for thermal spraying in which we will not have problems during the process. It can be observed that it is desirable that the edges, they must be rounded so as not to be stress concentrators and in time the coating will crack. On the other hand at 90° angles it would be indicated that the deposited coating always ends in a groove at a distance of at least 5 mm from the shoulder. At the same time the coverings in the groove should be at least twice the thickness of the coating as width. Also is not indicated that they have straight edges, the most indicated is that their exits should be in a arc circle, preferably as large as possible.

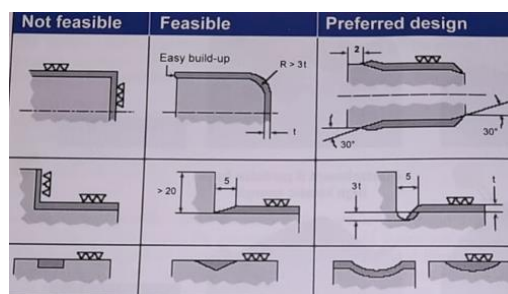


Figure 2.3 Designing components for spraying [9]

2.2. Thermal spraying processes classification

Depending on the energy source used, the thermal spray processes can be sort into several main groups, among which we list: energy from molten liquid, energy from gas combustion, kinetic energy, electric discharge or electron beams [20].

Each of the groups listed has its distinctive characteristics such as enthalpy, speed of coating deposition, thickness of the coating that can be deposited, the temperature at which the process takes place. These characteristics have a direct influence on the coating quality. These including porosity, adhesion of the coating to the substrate, internal connection between particles, oxides present in the each layer that forms the final coating [21].

In order to select the optimal deposition process, the following characteristics must be taken into account:

- the type of application in which the final component will work;
- the base material on which the coating will be deposited;
- the type of material to be deposited;
- the shape and dimensions of the part to be deposited.

The type of thermal spraying is often chosen according to the dimensions of the part or the place where they are incorporated. For example , small dimensions of the pieces can be deposited in the thermal spray chambers, instead plates that are already incorporated in the assemblies (for examples on the oil platforms) must be sprayed on that place.

In many situations an easier process will be chosen to handle under the given conditions, even if the quality is a little lower but acceptable.

Figure 2.4 shows a classification of these processes according to the energy [20]

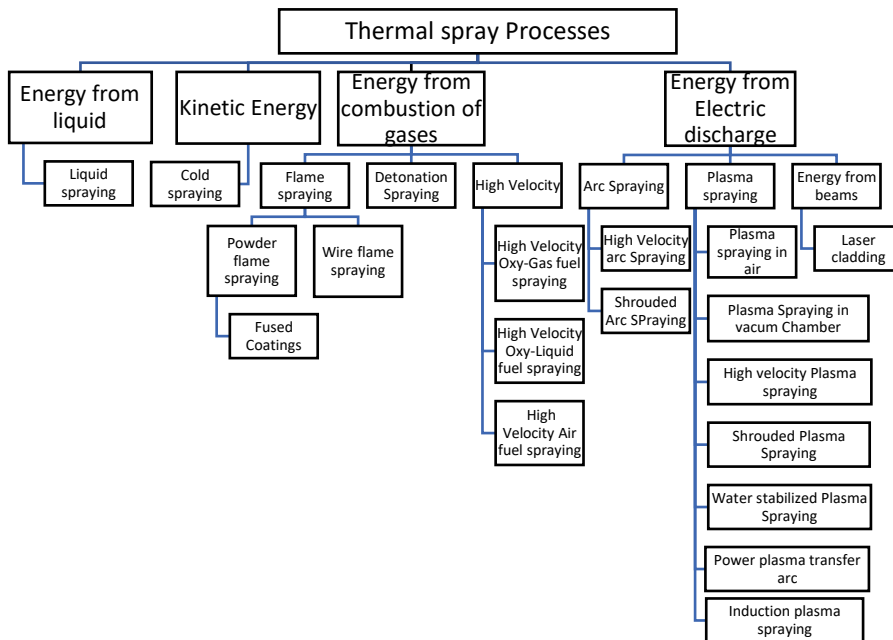


Figure 2.4 Thermal spraying process classification according to the sources of energy [20]

2.2.1. Wire flame spraying

In addition to thermal spraying with oxygas and electric arc, thermal spraying with wire is one of the oldest coating processes. This is one of the most feasible procedures for reworking in construction site because it does not require high transportation costs, also the materials to be deposited do not need to be prepared in advance, the feed system is a mechanical one, with too little electronic involvement in the transport of the wire which has to be melted. In this process material to be deposited it is found in the form of wire, this is melted with the help of oxygen/gas type fuel. Propane, hydrogen or most commonly Acetylene can be used as the fuel gas. Particle velocity can reach approx. 100m/s [22]. This process is portrayed schematic on the Figure 2.5

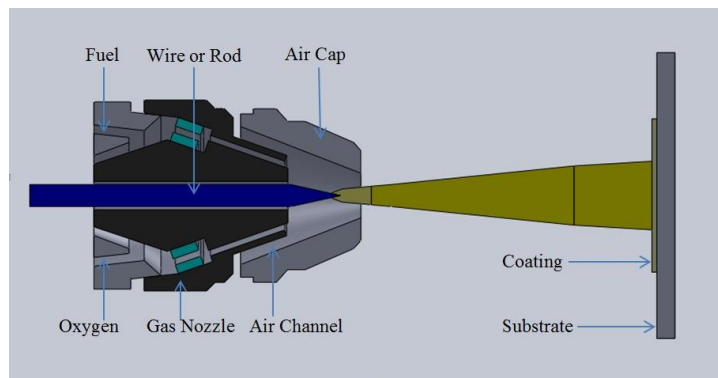


Figure 2.5 Schematic diagram of wire spraying

The design of the spray head differs from application to application, there are spray heads specially designed for industrial robots that are mounted in specific locations and have rigid dimensions. For inside diameters spraying the flame can be extended up to one meter and the spray jet is deflected with up to an angle of more than 45 degrees. For manual operator spraying, the spray head must be as light as possible and should be handled very easy so that it can be used for simple operations or minor repairs [23].

In the Figure 2.6 show the project manual using head

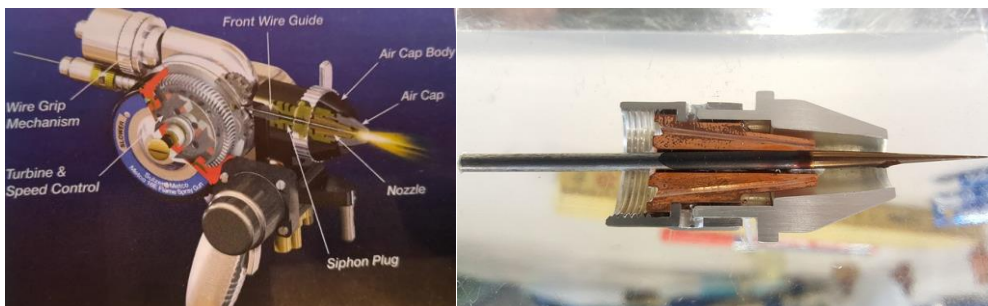


Figure 2.6 Cross section through hand spray head and the nozzle [9]

The types of wires used for spraying can be of several types. solid wires, powder-filled wires (Figure 2.7)(the wires that contain the powder are covered by a core/shell that holds the powder together until it reaches the flame, the core is also melted in the fame), foldable wires, electrodes for ceramic materials - the powder is cold pressed together with a special glue, after which it can be sintered or left in a pressed state

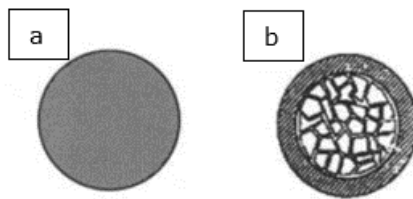


Figure 2.7 Solid (a) and powder filled wires (b)

2.2.2.Arc spraying

Electric arc spraying was described by M.U Schoop in 1914 [24].He patented a twin ark spray gun. He is considered the "father" of thermal spraying. His research in this field has been going on for almost four decades [25].

In the 1930's, the first patent for various applications was introduced. Because of the little knowledge of the process and the development of current source supply , led to its application only in 1950.

In the case of arc spraying, two conductive wires of the same chemical composition or of different compositions (in this case the result is a pseudoalloy) are pushed into the spray head at a constant controlled speed. The current is transferred with the help of the wire guide contacts (in most cases they are made of copper) See Figure 2.8

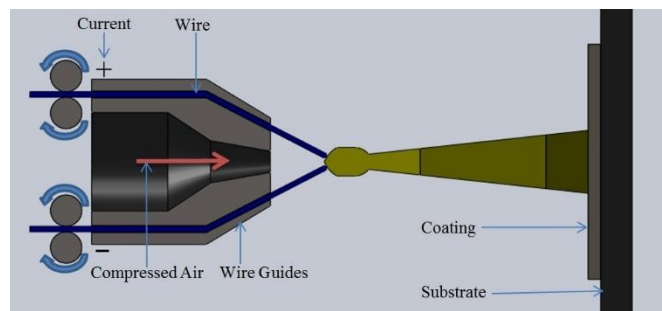


Figure 2.8 Principle of arc spraying

2.2 - Thermal spraying processes classification 23

After the feed system has been started, the wires connected to the anode and cathode advance through their guides until they touch. The short circuit that is formed results in an overheating of those two wires which results in the vaporization of the material and the formation of the electric arc. Figure 2.9 shows the arc formations on the right and the normal working gun on the left. The temperature formed in the arc reaches up to 5000 degrees Celsius. The melted material is transferred with the help of an air jet coming from the centre of the gun. This gas atomizes the molten material, accelerating the particles by up to 150 m/s and throws them on the surface which need to be coated.

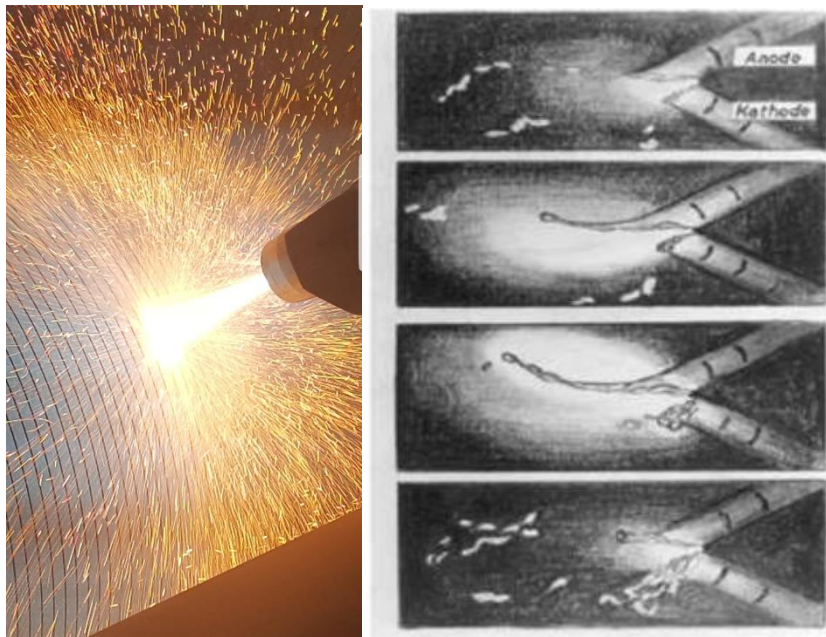


Figure 2.9 Arc formation [26]

The process allows depositions of any electrically conducting feedstock wires. Diameter of wires can be between 1.6 and 4.8 mm

Due to the fact that compressed air is used in the transfer of the material, the resulting layer may contain oxides, unsuitable particles or porosity. Also due to the fact that compressed air is used, depending on the pressure set for the compressed air, the resulting layer is more compact when the pressure is higher. Deposition rate is between 8-20 Kg/h and reach up to 30 kg/h for St alloys and 50 Kg/h for the Zn alloys [27].

The use of this type of process is suitable for bearings where the requirements are that the wear coating should be porous with a high porosity, so that this porosity is always filled with lubricating material. At the same time, this process has a mechanical adhesion to the substrate, and due to the low particle velocity, the adhesion on the substrate is much lower than other thermal spraying processes [28]. It is a cheap and feasible process for many industry applications. In Figure 2.10 it can be seen the building of an arc spraying coating

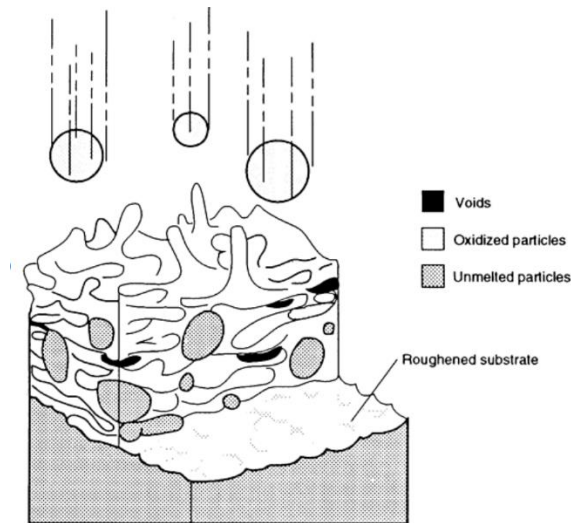


Figure 2.10 Arc spraying coating building [29]

2.2.3. High velocity oxy-fuel spraying

The high velocity oxy-fuel spraying process is characterized by a speed of entrained particles of up to 800 m/s theoretically, in normal practice it reaches an average of 600-700 m/s [30]. During the process the particles are heated to a temperature between 1600 and 2200 degrees Celsius [31]. During the process, oxygen and fuel material are mixed in the combustion chamber at high flow rates and pressures, reaching up to 12 bar [32]. The fuels used for this process can be: Kerosene, natural gas, acetylene, propylene, hydrogen or propane [33].

The process is a relatively new one in which the hypersonic speed of the flame greatly shortens the interaction time between the flame and the particles. The kinetic energy stored in the particles gives to the coating a good cohesion with the substrate and between the particles, also a coating with low porosity and a high hardness and density is obtained [34].

The design principle of the spray gun is shown in Figure 2.11. The torch is of older generation and is cooled exclusively with compressed air, or in case of long use the cooling is done with nitrogen. powder injection is done through the center of the gun, they lead to good efficiency because the spray jet is formed symmetrically

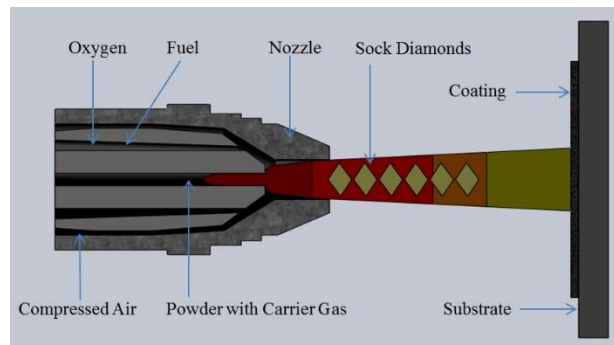


Figure 2.11 Principle diagram of HVOF process

High velocity oxy-fuel spraying process can be considered today one of the most used layer deposition techniques

Until now the next group of materials have been tried with successfully results in utilisation of HVOF spraying procedures:

- Cermets (carbide coatings, WC-Co, WC CoCr, WC-Ni, Cr₃C₂-NiCr and TiC-Ni)
- Nickel and cobalt alloys (MCrAlY, manufactures designations such as Tribaloy, stellite, Hastelloy or Inconel)
- Self-fluxing Ni Cr B Si alloys
- High alloyed steels (CrNi18-8 steel, Type 316 L and Cr steels)
- Cooper alloys (Cu, bronze, Al bronze and lead bronze)
- Aluminum alloys (Al Si) and composite materials
- Molybdenum (Mo, Mo-MoO₂ and Mo-Mo₂C)
- Oxides (Al₂O₃, Al₂O₃-TiO₂, and Cr₂O₃) [9]

2.3. Post-processing of sprayed coatings

In order to change the microstructure of the coatings, they are subsequently subjected to different surface treatment procedures [35]. These processes aim to improve density, reduce oxides, reduce internal stresses etc. According to J.R. Davis, there are three main categories in which they are divided to improve the quality of the resulting layer [36]:

- Physico-chemical treatments: chromium plating, aluminization, sealing;
- Thermal processes: fusion, heat treatments, diffusion, isostatic pressing, laser glazing;
- Mechanical treatments: milling, turning, sandblasting, polishing, work hardening;

2.3.1. Surface remelting methods

Surface melting are part of the thermal process group and are used to improve the functional properties of the surface of compact materials or coatings made by different technologies. The most common methods are laser melting or electron beam melting and induction melting.

Laser melting

To use technology of laser melting, powders produced by a micronization process are used. The shape of the powder granules should be as spherical as possible to allow a greater distribution during the laying phase. The dimensions may vary depending on the results to be obtained, but there is a tendency to create powders with a constant particle size, 15 - 45 μm or 20 - 63 μm are the most used. The material to be deposited can be transferred to the surface of the substrate by several methods: powder injection, pre-placed powder on the substrate or by wire feed. Of these methods, powder injection has been shown to be most effective (Figure 2.12). In this process, the laser beam melts the powder particles and a small portion of the moving substrate, thereby depositing a thin layer of powder particles on the surface of the substrate. A wide variety of materials can be deposited using laser injection powder coating leading to the formation of layers with thicknesses between 0.05 and 2 mm and widths of up to 0.4 mm [37].

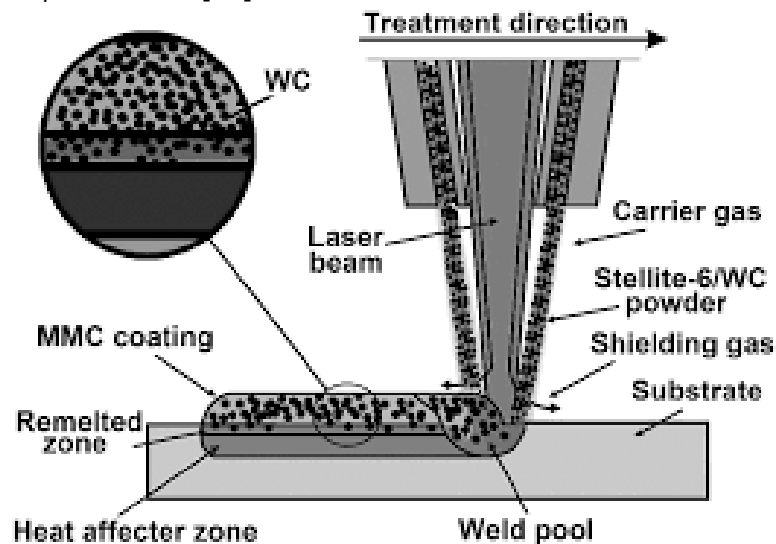


Figure 2.12 Laser cladding schematics [38]

The most commonly used materials are pure powders of various materials, such as aluminum, copper, tungsten (tungsten is very suitable for this technology due to the high melting temperature) or steel alloys, cobalt chrome alloys, Inconel 625 and 718, aluminum and titanium [39].

As usual applications, it is used to obtain on the hydraulic cylinders, molten powder in order to form a wear-resistant protective coating. Also 3d- printing of supports for aeronautical instrumentation, both in civilian and military fields. Examples are jet engine injectors developed by General Electric or rocket engine parts developed by SpaceX [40].

Electron beam remelting

The electron beam strikes the surface to be remelted, bringing the surface to a melting temperature but below the evaporation temperature of the coating material.

2.3 - Post-processing of sprayed coatings 27

This beam heats the material locally. Due to the fact that the beam it moves it will generate a line that is melted and also thermally influenced area. The dimensions of the remelted area and the thermally influenced area depend entirely on the strength of the electron beam and the geometry of the focus point on the surface to be remelted [41]. The process should take place in an vacuum chamber, it is not suitable for large samples. The process is presented in Figure 2.13

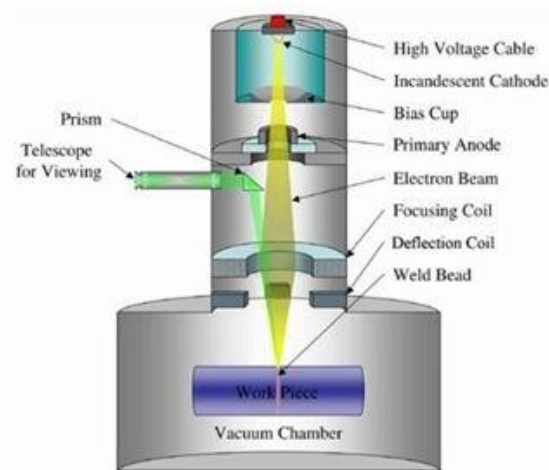


Figure 2.13 Electron Beam melting [42]

Induction remelting

One of the best-known applications of induction heating along with Preheating Prior to Metalworking, Heat Treating, Welding, Brazing, Soldering, Sintering and melting.

Induction heating has a number of advantages over furnace heating (such as rapid heating see Figure 2.14, smaller scale loss, quick start, energy savings) and compared to laser melting or electron beam it provides high production rates and much wider applicability in industry

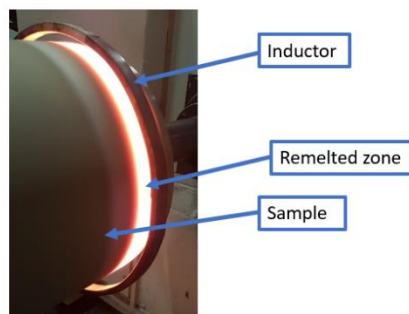


Figure 2.14 Induction rapid heating

Due to the fact that in the technological route a superficial remelting, with the help of electromagnetic induction was used, this process will be presented in detail.

2.3.2. Induction heating

Induction heating is a method of heating metallic materials by electromagnetic induction. The process is based on the property of high frequency currents induced to flow to the surface of the conducting parts at a depth dependent on the frequency of the current.

2.3.2.1 Process fundamentals

A high frequency electricity source is used to conduct a large alternating current through an induction coil. This heating inductor is known as a working coil [43]. See Figure 2.15

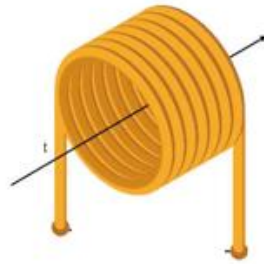


Figure 2.15 Schematic illustration of an induction coil [44]

The passage of current through this heating inductor generates a very intense and fast magnetic field in the space in the working coil. The workpiece to be heated is placed inside this intense alternating magnetic field [45].

The alternating magnetic field induces a current flow in the conductive workpiece. The arrangement of the work coil and the workpiece can be considered as an electrical transformer. The work coil is like the primary one in which the electricity is supplied, and the workpiece is like a secondary coil that is short-circuited. This causes the currents to flow through the piece. These are known as eddy currents.

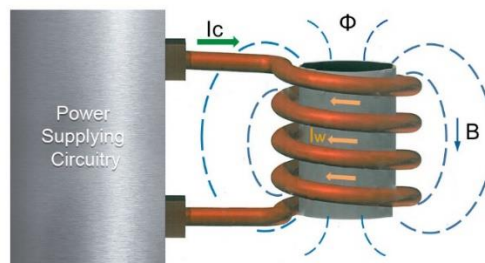


Figure 2.16 Schematic of induction heating [46]

In addition, the high frequency used in induction heating applications give rise to a phenomenon called the skin effect. This skin effect forces the alternating current to flow in a thin layer to the surface of the workpiece. The skin effect increases the effective resistance of the metal to the passage of high current. Therefore, the induction heating effect of the induction heater caused by the induced current in the workpiece greatly increases [47].

The method of inductive heating is based on the following laws and phenomena (effects)

1. The law of electromagnetic induction
2. The skin effect
3. Proximity effect
4. Variation of steel properties in the heating process, important for surface heat treatment [48]

The use of the inductive heating method must also take into account the existence of other phenomena that influence the distribution of currents in the inductor and in the part to be heated [49]. In some cases they can be useful in others harmful. These phenomena are known, however in almost all fields of technology, except for the phenomenon of electromagnetic induction, they are insignificant.

The law of electromagnetic induction

For the inductive heating method, the importance of electromagnetic induction consists first of all in the possibility of transmitting electromagnetic energy in the part to be heated, without using contacts [50]. The use of contacts considerably complicates the process, and in a number of cases it leads to the impossibility of its realization (for example: the superficial hardening of the crankshaft cranks, complicated shaped parts, etc.).

The induced electromotive voltage in a contour can be determined based on the law of electromagnetic induction [51]:

$$e = - \frac{d\psi}{dt} \quad 2.1$$

Where:

- e - instantaneous value of the induced electromotive voltage in V
- $\psi = w\Phi$ - The total flux that embraces the contour formed by w turns, each magnetic flux Φ , expressed in Wb

The expression of the total flux Φ is valid if the magnetic fluxes of all coils are the same, a condition fulfilled in many cases of interest, with sufficient accuracy.

If the variation of the total flux Φ in time is close to the sinusoidal one, the effective value of the induced electromotive voltage can be written:

$$E = 4.44fw\Phi \text{ [V]} \quad 2.2$$

Where:

- f - frequency measured in Hz
- Φ - is the amplitude of the magnetic flux measured in Wb

Power can be determined by expression:

$$P = E I \cos\varphi = 4.44 f \omega I \Phi \cos\varphi \text{ [W]} \quad 2.3$$

Equation 2.3 shows that the power P is proportional to the frequency. Therefore, as the frequency increases, the energy that is transmitted in a given volume increases. This explains the small size and light weight of high frequency transformers as well as the use of higher frequencies when heating small parts.

The skin effect

The skin effect is the basis of the inductive heating method, especially for surface hardening. It consists in the irregular distribution of the current on the section, the current density being the maximum towards one of the surfaces of the conductor [52].

To highlight the film effect, take as an example the incidence of a plane electromagnetic wave with the conducting half-space. Its physical properties, magnetic permeability and electrical resistivity are constant at all points [53]. This being a much simplified case idealized, however, for the analysis of electromagnetic phenomena in real conductors in conditions of pronounced skin effect.

The magnitudes of the electromagnetic field in the conducting environment satisfy Maxwell's equations [54]:

$$\text{rot } H = J + \frac{\partial D}{\partial t} \quad 2.4$$

$$\text{rot } E = - \frac{\partial B}{\partial t} \quad 2.5$$

Where:

- $B = \mu_0 \mu H$ - electromagnetic induction
- $D = \epsilon_0 \epsilon E$ - electrical induction
- $\mu_0 = 4\pi \cdot 10^{-7}$ H/m - electrical vacuum permeability
- μ - the relative magnetic permeability of the environment
- $\epsilon = \frac{1}{4\pi \cdot 9 \cdot 10^{-9}}$ F/m - vacuum permittivity
- ϵ - relative permittivity of the environment
- J - conduction current density

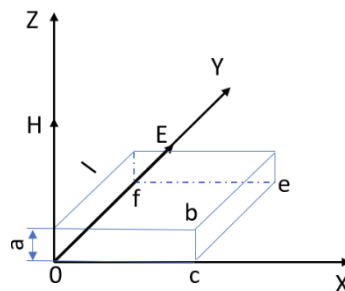


Figure 2.17 Explanatory figure for solving electromagnetic field equations and deducing formulas for resistors and reactants

2.3 - Post-processing of sprayed coatings 31

The differential equations 2.4 and 2.5 express the laws of magnetic circuit and electromagnetic induction. The second term on the right side of the equation 2.4 represents the displacement density, insignificant in conductive environments.

Because in a plane wave, the vectors H and E have only one component (in the case analyzed in Figure 2.17 the vectors H_z and E_y are observed) equations 2.4 and 2.5 become:

$$-\frac{\partial H_z}{\partial x} = J_y = \frac{E_y}{\rho} = \gamma E_y \quad 2.6$$

$$\frac{\partial E_y}{\partial x} = -\frac{\partial B_z}{\partial t} = \mu_0 \mu \frac{\partial H_z}{\partial t} \quad 2.7$$

Where:

- ρ - resistivity of the conductive environment measured in $\Omega \cdot m$
- γ - electrical conductivity measured in S/m

Further the y and z indices will not be written. If E and H are sinusoidal functions of time then:

$$\begin{aligned} \underline{H} &= H_m e^{j(\omega t + \theta_H)} = H_m e^{j\theta_H} e^{j\omega t} = \underline{H}_m e^{j\omega t} \\ \underline{E} &= E_m e^{j(\omega t + \theta_E)} = E_m e^{j\theta_E} e^{j\omega t} = \underline{E}_m e^{j\omega t} \end{aligned} \quad 2.8$$

Where:

- H_m and E_m , \underline{H}_m and \underline{E}_m - are the real and complex amplitudes of the intensity of the magnetic and electric fields, respectively
- θ_H and θ_E - the corresponding initial phases
- ω - pulsation

Replacing expression 2.8 in equations 2.6 and 2.7 are obtained:

$$-\frac{d\underline{H}_m}{dx} = \underline{J}_m = \gamma \underline{E}_m \quad 2.9$$

$$\frac{d\underline{E}_m}{dx} = -j \omega \mu_0 \mu \underline{H}_m \quad 2.10$$

After replacing in Equation 2.10 the expression \underline{E}_m from Equation 2.9 is obtained:

$$\frac{d^2 \underline{H}_m}{dx^2} = j \omega \mu_0 \mu \gamma \underline{H}_m = j 2 k^2 \underline{H}_m \quad 2.11$$

$$k = \frac{1}{\delta} = \sqrt{\frac{\omega \mu_0 \mu \gamma}{2}}$$

Where: δ - penetration depth of the current

$$\delta = \sqrt{\frac{2}{\omega \mu_0 \mu \gamma}} = \sqrt{\frac{2\rho}{\omega \mu_0 \mu}} \approx 503 \sqrt{\frac{\rho}{\mu f}} \quad 2.12$$

The solution of equation 2.11 is designed like

$$\underline{H}_m = A e^{\alpha_1 x} + B e^{\alpha_2 x} \quad 2.13$$

Coefficients α are determined from the characteristic equation $\alpha^2 = j 2 k^2$ and have values:

$$\alpha_{1,2} = \mp k\sqrt{2j} = \mp k(1+j) \quad 2.14$$

Since at infinity the field must have a finite value $B=0$. The condition on the surface of the conducting space $x=0$, on which the amplitude of the intensity of the magnetic field \underline{H}_{me} is given, determines the second integration constant, $A=\underline{H}_{me}$. By choosing the initial phase $\theta_H=0$ it is obtained $\underline{H}_{me}=H_{me}$ is obtained. Then the expression for \underline{H}_m has the form:

$$\underline{H}_m = \underline{H}_{me} e^{-k(1+j)x} = H_{me} e^{-(1+j)x/\delta} \quad 2.15$$

From equation 2.9 it determinates:

$$\underline{E}_m = \rho J_m = -\rho \frac{dH_m}{dx} = \sqrt{2} \frac{\rho}{\delta} H_{me} e^{j\frac{\pi}{4}} \cdot e^{-(1+j)x/\delta} \quad 2.16$$

Modules for this expressions are:

$$H_m = H_{me} e^{-x/\delta} \quad 2.17$$

$$E_m = \rho J_m = E_{me} e^{-x/\delta} \quad 2.18$$

On the surface where $x=0$ it will be obtained:

$$E_m = E_{me} = \sqrt{2} \frac{\rho}{\delta} H_{me} \quad 2.19$$

$$J_m = J_{me} = \frac{E_{me}}{\delta} = \sqrt{2} \frac{H_{me}}{\delta} \quad 2.20$$

The corresponding phases are determined from the equations 2.15 and 2.16 and are :

$$\theta_H = -\frac{x}{\delta} \quad \text{and} \quad \theta_E = -\frac{x}{\delta} + \frac{\pi}{4} \quad 2.21$$

Dependency $\frac{H_m}{H_{me}} = \frac{E_m}{E_{me}}$ as a function of relative depth $\frac{x}{\delta}$ is shown in Figure 2.18

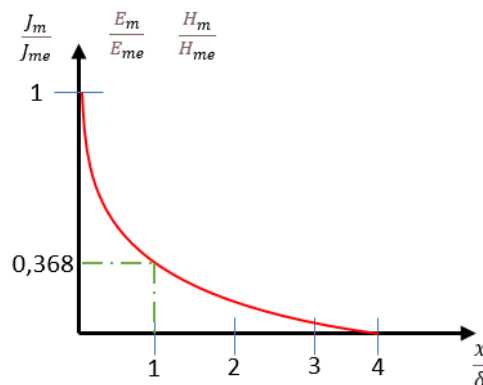


Figure 2.18 Dependence on current density and magnetic field strength as a function of depth

At depth $x=\delta$ the $\frac{J_m}{J_{me}} = \frac{H_m}{H_{me}} = \frac{E_m}{E_{me}} = \frac{1}{e} = 0.368$.

This shows the significance of the concept of depth of current penetration. Using this allows us to simplify many calculations [55]. Especially the calculation of resistance and reactance. Let the parallelepiped with the edges of length l and a in the directions of the OY and OZ axes and infinitely long edge in the direction of the OX axis placed in the conductive space (see Figure 2.17)

The amplitude of the current I_m passing through the width band a it will be determined by applying the law of the magnetic circuit on the OabcO contour. It will be obtained the following equation:

$$\oint_{OabcO} H dl = a H_{me} = I_m \quad 2.22$$

Because the component of the magnetic field strength in the direction of the OX axis is zero and the side bc is far apart (at a sufficient distance) where $H = 0$. From equation 2.22 it is observed that this current is in phase with the intensity of the magnetic field on the surface. Taking into account the relation 2.20 the current I_m is expressed by the current density:

$$I_m = a \frac{J_{me}}{\sqrt{2}} \delta \quad 2.23$$

It is calculate the voltage u that balances the electromotive voltage induced by the magnetic flux that crosses the parallelepiped section perpendicular to the OZ. For this, the law of electromagnetic induction on the OcefO contour is applied (Figure 2.17)

$$\oint_{OcefO} E dl = - \frac{d\Phi}{dt} = -u \quad 2.24$$

Taking into account that $E_x=0$ and that the component of the integral $E_{yce}=0$ (due to the distance of the side ce) the following equation is obtained:

$$\underline{U}_m = j\omega \Phi_M = E_{me} l \quad 2.25$$

Where: Φ_M - the magnetic flux that pierces the contour OcefO

The expression of the corresponding impedance of the band of width a and length l on the surface of the space is using the relations 2.22 and 2.25:

$$\underline{z} = \frac{\underline{U}_m}{I_m} = \frac{l E_{me}}{a H_{me}} = r + jx_M \quad 2.26$$

Where:

- r - electrical resistance of the band
- x_M - internal reactance, corresponding to the magnetic flux passing through the section OabcO

Substituting the E_{me} value from equation 2.16 and modifying $x=0$ is obtained:

$$\underline{z} = \frac{l}{a} \sqrt{2} \frac{\rho}{\delta} e^{j\frac{\pi}{4}} ; \quad z = \frac{l}{a} \sqrt{2} \frac{\rho}{\delta} \quad 2.27$$

$$r = x_M = l\rho/a\delta \quad 2.28$$

The magnetic impedance Z_m of the parallelepiped is:

$$\underline{Z}_m = \frac{\oint_{OabcO} H dl}{\Phi_M} = \frac{aH_{me}}{\Phi_M} = \frac{I_m}{\Phi_M} = j\omega \frac{I_m}{U_m} \quad 2.29$$

It is obtained:

$$\underline{Z}_m = \frac{j\omega}{z} = R_m + jX_m \quad 2.30$$

Where: Z is the total impedance

The magnetic impedance module is:

$$Z_m = \frac{\omega}{z} = \sqrt{R_m^2 + X_m^2} \quad 2.31$$

Apparent power inside the parallelepiped:

$$\underline{P} = \frac{1}{2} \underline{U}_m I_m^* \quad 2.32$$

Where: $\underline{U}_m = j\omega \Phi_M$ and $\underline{I}_m = \Phi_M \underline{Z}_m$ If we replace in the power equation:

$$\underline{P} = \frac{1}{2} j\omega \Phi_M \Phi_M^* \underline{Z}_m^* = \frac{1}{2} \omega \Phi_M^2 (X_m + jR_m) = P_a + jP_r \quad 2.33$$

From the obtained relation it is seen that the real part R_m of the magnetic impedance corresponds to the reactive power and also to the component of the electromotive voltage that is in phase with the magnetic flux Φ_M . The imaginary part X_m is proportional to the active power - the losses in space - and corresponds to the component of the magnetomotive voltage that is in phase with the voltage U_m (usually in electrical machines this component is small while in the induction heating is defining the process [56]). For example, in the analyzed case, of the conductive space with $\rho = \text{constant}$ and $\mu = \text{const}$, $R_m = X_m$. If $l = a = 1\text{m}$ the so-called impedance per unit area is obtained:

$$\underline{Z}_0 = r_o + j\underline{\chi}_0 = \frac{E_{me}}{H_{me}}; \underline{Z}_{m0} = R_{m0} + jX_{m0} = \frac{j\omega}{z_0} \quad 2.34$$

Therefore:

$$\underline{z} = \frac{l}{a} \underline{z}_0; \underline{Z}_m = \frac{a}{l} \underline{Z}_{m0} \quad 2.35$$

It is specified that when was obtained the equations 2.22, 2.25, 2.26 and 2.30 no hypothesis was made on the dependence of the resistivity and the permeability of the x coordinate. It is specified that when obtaining the equations 1.2 1.2 12. 12.3 no assumption was made on the dependence of the resistivity and the permeability of the x coordinate. These dependances are general and are also used in more complicated forms of the skin effect. For example, if H and E are sinusoidal functions of time, they are replaced by equivalent sinusoids - the first harmonic functions of $H(t)$, $E(t)$ and $J(t)$.

Formulas 2.24 and 2.28 explain the meanings of the concept of depth current penetration, allowing properly to consider that the induced current passes only in

2.3 - Post-processing of sprayed coatings 35

layer δ but with uniform density equal to $J_{me}/\sqrt{2}$, and beyond the limits of this layer is zero. By this the resistance of the space is considered as the resistance in direct current of a plate, its thickness being equal to the depth of penetration of the current δ . For calculations, especially thermal ones, it is essential that within the limits of the depth of current penetration, the most important part of the energy is released. Using the expression 2.18, the power is determined in a band of width a and length l (Figure 2.17). The elemental power in the layer with thickness dx , at depth x will be:

$$dP = \frac{1}{2} (aJ_m dx)^2 \frac{\rho l}{a dx} = al \frac{1}{2} \rho J_{me}^2 e^{-2x/\delta} dx \quad 2.36$$

The total power passing through the surface $S = al$ of the conductive space is:

$$P = al \frac{\rho J_{me}^2}{2} \int_0^{\infty} e^{-2x/\delta} dx = al \frac{J_{me}^2 \rho \delta}{4} = alp_0 \quad 2.37$$

Where: p_0 is specific power per unit area measured in W/m^2

Within the limits of a layer of thickness x we have:

$$P_{0-x} = al \frac{\rho J_{me}^2}{2} \int_0^x e^{-2x/\delta} dx = alp_0 (1 - e^{-2x/\delta}) = al(p_0 - p_x) \quad 2.38$$

Where:

- P_{0-x} – Power in the layer with thickness x
- P_x – Specific power on depth x

Within the delta thickness layer, replacing $x=\delta$ is obtained:

$$P_{0... \delta} = alp_0 (1 - e^{-2}) = 0.865 alp_0 \quad 2.39$$

This creates the premise that in the approximate calculations, it can be admitted that in layer δ the whole thermal energy is released.

Table 1 gives the values of the depth of penetration of the current at various frequencies for the steel at ambient temperature, the steel heated over the Curie point and for copper

Table 2.4 The depth of penetration of the current

| Frequency Hz | δ in Cm | | |
|-----------------|---|--|--|
| | Copper | Steel | |
| | At 15°C $\rho=1.8 \cdot 10^{-8} \Omega \cdot m; \mu=1$ | At 15°C $\rho=2 \cdot 10^{-7} \Omega \cdot m; \mu=40$ | At 800°C $\rho=10^{-6} \Omega \cdot m; \mu=1$ |
| 50 | 1.0 | 0.5 | 7.0 |
| 500 | 0.3 | 0.15 | 2.2 |
| 2500 | 0.13 | 0.067 | 1.0 |
| 10000 | 0.07 | 0.034 | 0.5 |
| 10^5 | 0.022 | 0.011 | 0.16 |
| 10^6 | 0.007 | 0.0034 | 0.05 |

In real conditions the conductors have finite dimensions and are not always flat. However, even in these cases the notion of penetration depth does not lose its meaning, because the current density becomes a negligible at a distance $(2...3)\delta$ from the surface, and the power even faster [57]. At x greater than 2δ the power is practically zero, so the bend of the surface or the thickness of the conductor often does not influence the accuracy of the result obtained by formulas 2.6-2.39

Proximity effect

Figure 2.19 shows the approximate structures of the magnetic fields of two conductors of circular section, in the case of currents with the same direction (left, phase difference is zero) and opposite direction (right, phase difference is equal to 180°) [58]. The highest field intensity in the system, having currents in the same direction is observed at its outer surfaces of the conductors, and in the system when the currents directed in the opposite direction, on the inner surfaces [59].

It is obvious that most of the electromagnetic energy absorbed by the conductor comes from the strong field area, and related to this fact, there is also the highest current density, as shown in the Figure 2.19 (the thickness of the reddish layer is proportional to the density of current) [60]. The depth distribution of the current is subject to the laws of the skin effect analyzed above. The proximity effect itself is a variant of the skin effect, and consists in the concentration of current in certain areas of the conductor surfaces, as a result of the interaction of the electromagnetic fields of all the current conductors entering the analyzed system.

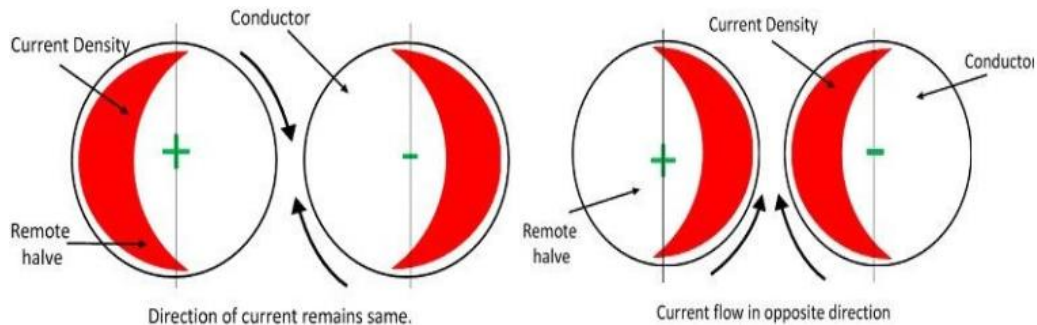


Figure 2.19 Current distribution to the proximity effect [61]

Using the proximity effect, by choosing the appropriate inductor shape, it can concentrate the heating in certain parts of the part [62]. For example, if the inductor is ring-shaped and surrounds the part to be heated, then a current of the opposite direction is introduced, the path of which is also circular in shape. The current is concentrated in a segment whose width differs very little from the width of the inductor [63]. The proximity effect is stronger if it is a shorter distance between the conductors. The stronger the skin effect, the higher the ratio between the thickness of the conductor and the depth of penetration of the current [64].

The distribution of current in the conductor should not be confused with the proximity effect or with the electrodynamic interaction between the conductors. Conductors with currents of the same direction are attracted, and those with currents in opposite directions are rejected.

Variation of steel properties in the heating process

When heated, the steel changes its resistivity and magnetic permeability, namely the resistivity increases to the Curie point, after which its growth decreases.

At temperatures above 800°C the resistivities of steels of different qualities are almost the same. On average it can be considered that the resistivity in the range $800\text{-}900^\circ\text{C}$ is approximately equal to $10^{-6}\Omega\cdot\text{m}$ [65].

The loop effect

It is known that if a ring or a spiral is made of a conductor and an alternating current is passed through it, then the maximum current density will be on the inside of the conductor spiral [66]. This phenomenon called the loop effect will be stronger with the higher ratio between the conductor size and the diameter of the ring, and the stronger the skin effect. The loop effect is a variant of the skin effect and is explained by the asymmetry of the magnetic field of the spiral or solenoid. In the inner gap of the loop (Figure 2.20) it is considerably stronger than outside; as a result, the main part of the electromagnetic energy enters inside the conductor. The loop effect worsens the use of the conductor section, increasing the active electrical resistance. For the calculation of the resistance of the cylindrical and oval inductors, inside which the heating piece is placed, it will be considered that the current intensity is concentrated only on the inside of the conductor [67].

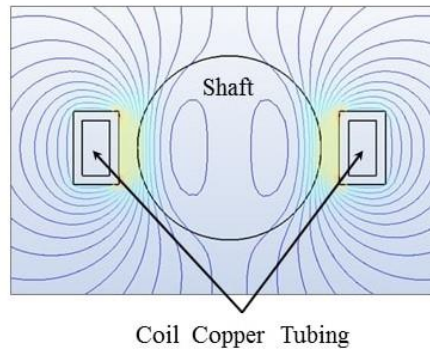


Figure 2.20 Electro-magnetic field distribution [68]

The strengthening of the magnetic field inside the inductor due to the proximity effect increases the heating efficiency for the parts embraced by the inductor. In this case the loop effect is useful, although it increases the active resistance of the inductor.

However, it makes it difficult to heat the interior surfaces, acting inversely to the skin effect, reducing the intensity of the magnetic field on the surface to be heated.

Distribution of current density in the inductor and in the heater using electromagnetic flux concentrators

The Figure 2.21 shows the structure of the magnetic field of the inductor inside which a metal shaft is inserted.

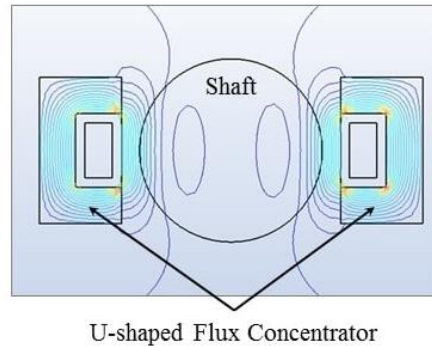


Figure 2.21 Electromagnetic flux concentrators [68]

The inductor current under the influence of the loop effect, the proximity effect and the U-type magnetic flux concentrators is concentrated on its inner surface of the ring [69]. The density is approximately uniform and decreases towards the corners of the inductor. This is explained by the fact that the current lines flowing at the corners of the inductor are covered by a smaller magnetic flux than those found in the middle part [70].

2.3.2.2. Component parts of the installation and heating methods

The installation for inductive heating of metals usually consists of the following basic elements [71]:

- High frequency generator (with lamps, rotary or static converter);
- Inductor, represented by a spiral of the desired shape of the cross section, or a conductor of any shape depending on the type of object to be heated;
- Capacitor battery that compensates for the low power factor of the inductor;

Often in surface hardening installations the inductor is almost always connected to the generator by a descending transformer [72]. Multi-coil heaters and inductors are usually connected to the generator without transformers [73].

In a number of cases, the industrial frequency is used for heating. When supplying a single-phase load, a device is installed instead of the generator, which transforms the three-phase system into a single-phase system, which ensures the symmetrical charging of the network [74].

The heating piece is placed inside the inductor or next to it according to the requirements. The alternating magnetic field causes an induced current to appear in the part, as a result of which it is heated by the Joule-Lenz effect [75].

There are two basic methods of heating:

Simultaneous heating method. The inductor covers the entire surface of the part to be heat treated, it's heating being done at all points simultaneously. The surface temperature and its distribution in depth depending on the heating time T_K , of the energy transmitted in the piece during this time and the frequency of the induced current. Voltage heaters that work in this way are usually called periodically heating heaters [76].

Simultaneously successive heating method. A thin inductor moves along the part to be heated. In order to harden the surface, from the inductor or from a special device mounted next to them, called the hardening shower, the cooling medium is sent to the heated area. In this case, the depth of hardening and the surface temperature are determined by the speed of movement of the inductor, its width, the power that develops in the part to be heated and of course the frequency used [77].

In thermal calculations the notion of heating time is used, for any element of the surface being under the inductor for a certain time.

$$\text{Heating time} \quad T_k = \frac{a}{v} \quad 2.40$$

Where

T_k - heating time of the element in the surface

a - inductor width

v - the moving speed of the inductor or the part if the inductor is static

This method is widely used for heating bulk, bar or pipe type semi-finished products [78].

When heating short products, or other similar parts that are used in the subsequent hot forging process. The parts are inserted in a long inductor with the help of a pusher, they are inserted at a predefined short time interval t_0 , called in industry supply or push rate. This method is a variant of the simultaneous-successive heating method [79]. The installations working in this mode are called continuous action heaters.

2.4. Wear of materials

Wear is usually defined as the removal of material from solid bodies, caused by contact and relative motion, which changes the initial state of the contact surfaces. Consequently the wear is the result of a tribological contact that takes place between two moving surfaces [80]. Wear occurs in all cases where there is friction, whether it is useful or harmful. The result of the wear process is expressed in units of length, volume, mass, operating time until decommissioning. The specialized literature in the field of tribology offers a wide variety of classification of types of wear and possible solutions to wear problems. The version proposed by Barwell in 1957 regarding 4 basic types of wear is generally accepted [81]:

- abrasive wear
- erosion wear
- adhesion wear
- fatigue wear

2.4.1. Abrasive wear

In some cases, especially in research, wear rates are determined using abrasive tools, however, about one-third of total economic losses are due to abrasive wear. This type of wear is caused by hard particles from the wear process or from the outside, which come between the contact surfaces (see Figure 2.22) [82]. The additional feature of the abrasion process is that the abrasive usually has sharp

angular edges, which produce a cut or shear on the surface exposed to damage [83]. The necessary condition for the appearance of abrasive wear is the difference in hardness between surfaces [84]. The form of destruction by abrasive wear can be:

- fragile - with groove formation
- quasi-fragile - with microplastic deformation
- tenacious - formation of large deformations on the direction of movement

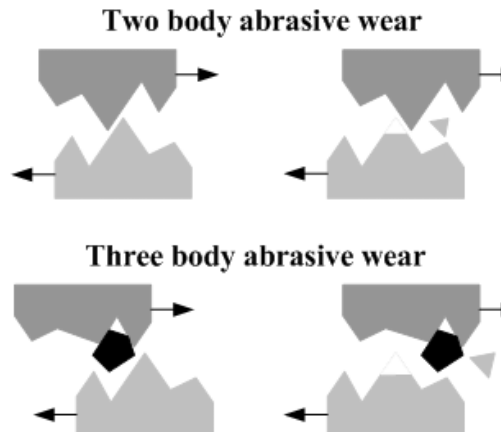


Figure 2.22 Two-body abrasive wear [85]

2.4.2. Erosion Wear

Erosion wear is caused by the repeated impact of a solid or liquid particle with the surface of a solid, resulting in contact, slipping of the particle and gradual modification of the area/surface by deformation [86]. Finally dislocation of material and destruction of the surface [87]. This process of erosion wear is often found in hydro turbine rotors, pump rotors in sludge work systems, aircraft paddles, hydroelectric turbine blades or gas turbine blades. The schematic of wear erosion is presented in Figure 2.23

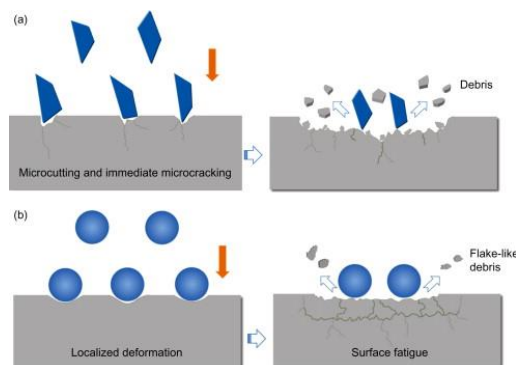


Figure 2.23 Erosion wear [88]

2.4.3. Adhesive Wear

The mechanisms of this type of wear are related to the existence on the contact surfaces of a given roughness, as well as of some patchiness. High local pressures exceeding the flow limit it is obtained (Figure 2.24). In the absence of lubrication, the wear of adhesion occurs in all forms of friction, in the contact microzones appear welding bonds or atomic interactions between roughness in contact. Once welded due to the high engagement forces of the two surfaces, these micro welds dislocate, leaving gaps in the surfaces and the particles leading to abrasive erosion [89].

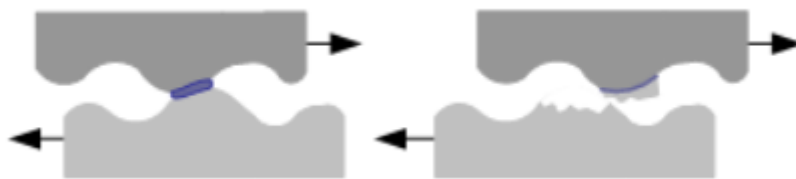


Figure 2.24 Adhesive wear [88]

2.4.4. Fatigue Wear

Fatigue wear is the result of cyclic stresses on the surfaces in contact (Figure 2.25), followed by plastic deformation in the atomic network of the surface layer overlaid on the movement of sliding, rolling or combinations of these movements. Factors that influence fatigue wear are: temperature, type of stress, concentration of stress, frequency of variable stress, part dimensions [90].

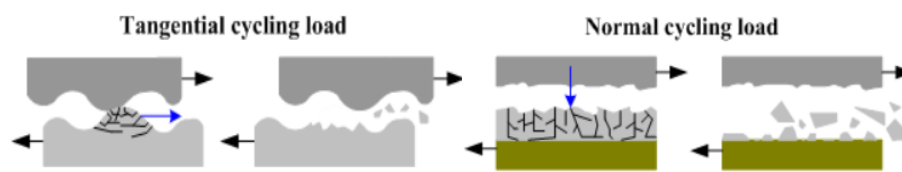


Figure 2.25 Fatigue wear [88]

2.5. Corrosion

Corrosion is a natural phenomenon that includes all electrochemical and chemical processes, which aim to continuously damage metal surfaces. Since most metals are not found as such in nature, but in the form of combinations (oxides), their metallic state is not thermodynamically stable in the presence of other chemical compounds, which in time leads to layer degradation through corrosion [91]

Corrosion is commonly understood as the material transformation of metal surfaces, caused by the influence of the contact environment. As a result, the oxide of the respective metal is composed. In the case of iron this oxide is rust. In economic

terms, it has been observed that only preventing and protecting against corrosion costs 5% of the GDP of an industrialized nation [92].

General corrosion is one of the most common and is characterized by loss of material due to chemical attack or dissolution of metal parts into metal ions. When this occurs at high temperatures, the metal ions combine with other elements besides the formation of oxides.

Atmospheric corrosion is one of the most recognized types of corrosion, also because the atmosphere is the most common environment in which the ensembles carry out their activity. It is formed by the reaction of a metal with the ambient atmosphere and can be classified as dry or wet corrosion [93].

Corrosion resistance depends on the environment, the conditions of exposure and the nature of the material. When it comes to corrosion, each material has a unique behavior that can range from high strength to very low strength. This behavior is often the result of complex interactions between the material and the working conditions (environment) to which it is exposed depending to a large extent on the chemical composition, temperature and many other characteristics [94].

3. Equipment and methodology for experiment and testing

3.1. Equipment and materials

- The equipment necessary for the good development of this work is:
 - Cut-off Machine (Discotom-2, Struers)
 - Hot Mounting Press (ProntoPress-20, Struers)
 - Grinding and Polishing Equipment (RotoPol-V, Struers)
 - Scanning Electron Microscope (ESEM XL 30, Philips)
 - Energy-dispersive X-ray Spectrometer (EDAX)
 - Confocal Laser Scanning Microscope (VK-X, Keyence)
 - X-ray Diffractometer (X'Pert, Philips)
 - Thermogravimetric Analysis Instrument (STA 449 F1 Jupiter, Netzsch)
 - Universal Hardness Tester (KB250, KB Prüftechnik)
 - Micro Vickers Hardness Tester (ZHV μ , Zwick / Roell)
 - Pin-on-Disc Tribometer (TRB, CSM Instruments)
 - Potentiostat / Galvanostat (VoltaLab PGP201, Radiometer Analytical)
 - turning machine (weipert)
 - Thermal spraying pistole (Methaterm MPP 85)
 - Induction system (Ambrell Ekoheat)
 - Corrosion testing system (Liebisch S 1000 M-SC)

- Materials used for this experiment are:
 - Steel: material EN 1.7225 (Heitmann Stahl, Germany)
 - NiCrBSi powder (LSN Diffusion, England)
 - Ethanol, 96% vol., (VWR Chemicals)
 - Sulphuric acid, H₂SO₄ 98% purity (Sigma-Aldrich)
 - Sodium chloride, NaCl, $\geq 99,5\%$ purity (Carl Roth)

- The results were processed using the following software
 - STA 449 F1 Software Netzsch Data Collector
 - Proteus Thermal Analysis, Netzsch Data Processing
 - X'Pert Data Collector, XRD Philips
 - X'Pert HighScore 3.0, PANalytical
 - ImageJ, open access
 - VK-X Analyzer, Keyence
 - VoltaMaster 4, Radiometer Analytical
 - Microsoft Office 365
 - OriginPro 2016
 -

3.2. Powder deposition

Flame thermal spraying uses a siphon block in which the gases are mixed combustible gases (acetylene, propane or hydrogen) in the case of this paper using acetylene mixed with oxygen in controlled proportions, the ratio being 1 to 2. This block siphon is used from two reasons one is to ensure consistent functionality and the second is as safety to prevent back burning

The powder is in a container above the gun and is injected into the burning oxyacetylene flame. due to the gas pressure (maximum 1.5 bar for oxyacetylene and maximum 2.5 bar for oxygen) this powder is propelled to the substrate surface. Due to the relatively large distance between the combustion head and the substrate, the powder has time to be semi-melted, reaching the substrate it sticks to the substrate and solidifies quickly, assimilating the coating. Typical flame temperatures are around 3000 ° C

The functional principle of spraying with oxyacetylene flame is presented in Figure 3.1.

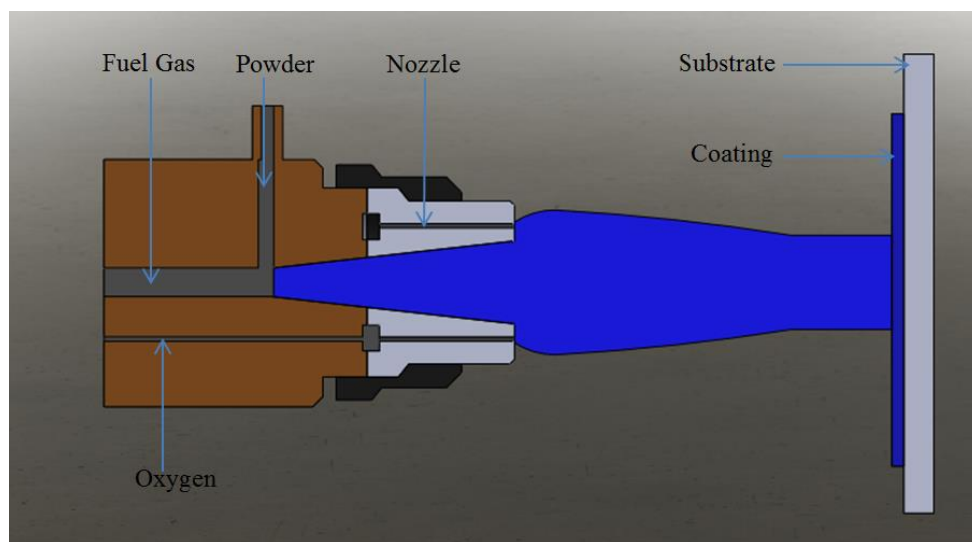


Figure 3.1 Flame spraying principle

The process of thermal spraying with oxyacetylene flame is very similar to that of wire spraying. Except that it has the advantage of using powdered materials as a raw material for coatings. In this field several types of raw materials can be obtained, including ceramics, or another option is to mix two types of powder from different materials that otherwise could not be deposited, see the doctoral thesis of Mr. Kazamer [95]

Advantages:

- Spray costs are quite low;
- Particle speed is from 50 to 100m / s;

3.3. Mechanical testing

3.3.1. Microhardness tester

The hardness of the coatings was determined using a Zwick / Roell YHV μ S microhardness test machine using a Vickers microindenter (ISO 6507).

Microindentation hardness testing is widely called as microhardness testing, it is mainly used to measure the hardness of materials that are in the form of coatings, these being thin films or thin layers, the measurement is not influenced by the substrate. An indentation is made with precision and the indenter is pressed in the sample with a specific load in the test material, set between 0.01Kg and 2 KG

The heat treatment industry has used this technique to evaluate the heat treatment applied to the parts and to detect and evaluate the possible decarburization of the surfaces. In laboratories specialized in metallography and defect analysis, this tool is often used to evaluate the homogeneity of materials, the characterization of welds and the identification of phases. For small parts in automotive industry, it is also possible to test the surface hardness on the finished part without needing to damage it.

In the Vickers test, a pyramidal diamond indenter penetrates the surface of the specimen, the load is applied smoothly, without impact. The indenter is held in the test piece for 10 or 15 seconds. The use of diamond allows the Vickers test to be used to evaluate any material (except diamond) and, in addition, has a very important advantage of putting the hardness of all materials on a single continuous scale [96].

The samples can be further evaluated (sometimes automatically) with software attached to the indenter or using conventional optical microscopy measuring the two diagonals of the indentation correlated with the test load, by mathematical calculation will give the value of hardness. Furthermore, the indentation technique can be used to see the adhesion of a layer deposited on a support material

3.3.2. Wear testing and wear measurements

In the present work the friction and sliding wear tests were performed with an CSM instruments investigation tool equipped with a ball-on-disc type arrangement, following the instructions from the DIN 50324 standard.

With the help of tribology, important information can be determined, such as friction resistance, wear of materials or their lubrication under predefined conditions. In practice there are several standardized methods designed to simulate a certain type of wear in certain applications.

The pin-on-disk test (POD) is considered a relatively simple investigation, which provides a quick response to the wear resistance of materials to abrasion. Typically, in a pin-on-disk wear test arrangement, a pin is loaded on a flat rotating disk specimen so that the instrument describes a circular wear track. This type of equipment can be used to evaluate the wear and friction properties of materials in dry or lubricated slip conditions. In our case the disc serves as a test sample, but there are cases in which the pin or ball is the test sample and the disc is counterbody, different shapes and chemical compositions of the pins can be used for testing. The most convenient approach is to use balls of commercially available materials such as

bearing balls, carbide balls (tungsten, silicon) or alumina as static partners. That is why the name ball on disk is used more frequently and not pin on disk

The testing device consists of a simple mechanism in which a partner is stationary, in this case the ball which it is placed on the test sample, which is fixed in a rotating chuck, the ball is pressed with a constant force. The pin can have other types of geometries, in practice spherical geometry (given by the ball) is used to simplify the contact geometry and automatically future calculations that give us the wear rate.

3.4. Microstructural Characterization

In order to obtain the optimal parameters for this work and after for implementation in large-scale production, a multitude of tests were performed. To correlate the parameters used to obtain the sample with the resulted coatings, a severe characterization of these samples was necessary. Therefore, the thermal coatings resulting from the deposition processes and the subsequent inductive heating process were analysed. An scanning electron microscopy (SEM) combined with energy dispersive X-ray spectrometry (EDX) for morphological and structural characterization was used these being correlated with investigations using X-ray diffraction (XRD) to identify the chemical composition and phases.

At the same time, the adhesion to the substrate and the porosity were investigated, in the preliminary phases the cracks that appeared in the remelted layer were also studied. Thermogravimetric analysis (TGA) was used to verify the thermal behaviour of the powder and to correlate the data with those of the manufacturer.

3.4.1. Metallographic preparation

In order to be able to characterize the samples microstructurally, they require mechanical cutting processing, followed by a well-defined metallographic preparation, in order to be subject to further investigation processes. The samples were sectioned using a Struers cutting machine, after that they were incorporated into the epoxy resin after which they were ground and polished until the surface necessary for the investigations was reached.

3.4.2. Thermogravimetric analysis (TGA)

Thermal analysis (TGA) is frequently used to observe and measure chemical or physical changes in a material as the temperature rises. Common thermal analysis techniques include differential analysis (DTA), thermogravimetric analysis (TGA) thermomechanical analysis and scanning calorimetry

Thermogravimetric analysis accurately measures the weight of the sample as a function of temperature and time. In order to work, this method requires a very good precision in data collection, the test sample is placed in a heat-resistant crucible and which is based on a precision scale. the crucible is constantly heated in a controlled manner and with a predetermined inclusion rate, programmable oven. Inside the heating chambers where the crucible is located the atmosphere can be of two types, interactive with the sample such as gases: oxygen and nitrogen or non-interactive such as helium or argon

DTA measures the temperature difference using a differential thermocouple between the material to be analysed and a reference material

In the present work, a STA 449 F1 Jupiter® device from Netzsch (Germany) was used to determine the thermal behaviour of the samples, as well as the melting temperature of the raw material powder.

The device used has a top charging system, the programmable oven is made of silicon carbide and can heat up to a temperature of 1600 degrees Celsius. The system can measure samples up to 5 grams being equipped with a digital resolution in the nanometric range (0.025 µg). The working atmosphere is controlled with 3 mass flow regulators for the purification and protection gases, offering an optimal control. Heating and cooling can be chosen in the range of 0.001 K min⁻¹ to 50 K min⁻¹.

3.4.3. Scanning electron microscopy (SEM)

Scanning electron microscopy is considered one of the most important methods of investigating microstructure for a very wide range of materials used in industry today. This meter can provide various information such as:

- crystalline structure
- surface topography
- chemical composition
- other properties of the specimen

To obtain an image, the device uses electrons produced by a thermal emission source, in this case it is a tungsten filament that produces electrons by heating. They are accelerated and passed through a set of lenses and diaphragms to produce an electron-focused beam [97]. The beam once focused hits the surface of the sample and interacts with the atoms, the whole process taking place under a high level of vacuum. Once the beam strikes the sample its interaction with atoms produces secondary electrons, backscatter and Auger electrons, as well as characteristic X-rays and light. All these data are collected by different detectors mounted inside the working enclosure [98]

Figure 3.2 shows a principle diagram of the scanning electron microscope. In order to fully characterise the sample a microscope built by Philips codenamed XL 30 ESEM was used in this experimental program. Its main features are:

- acceleration voltage up to 30 kV
- resolution up to 2 nm
- magnification range between 25X - 250 000X

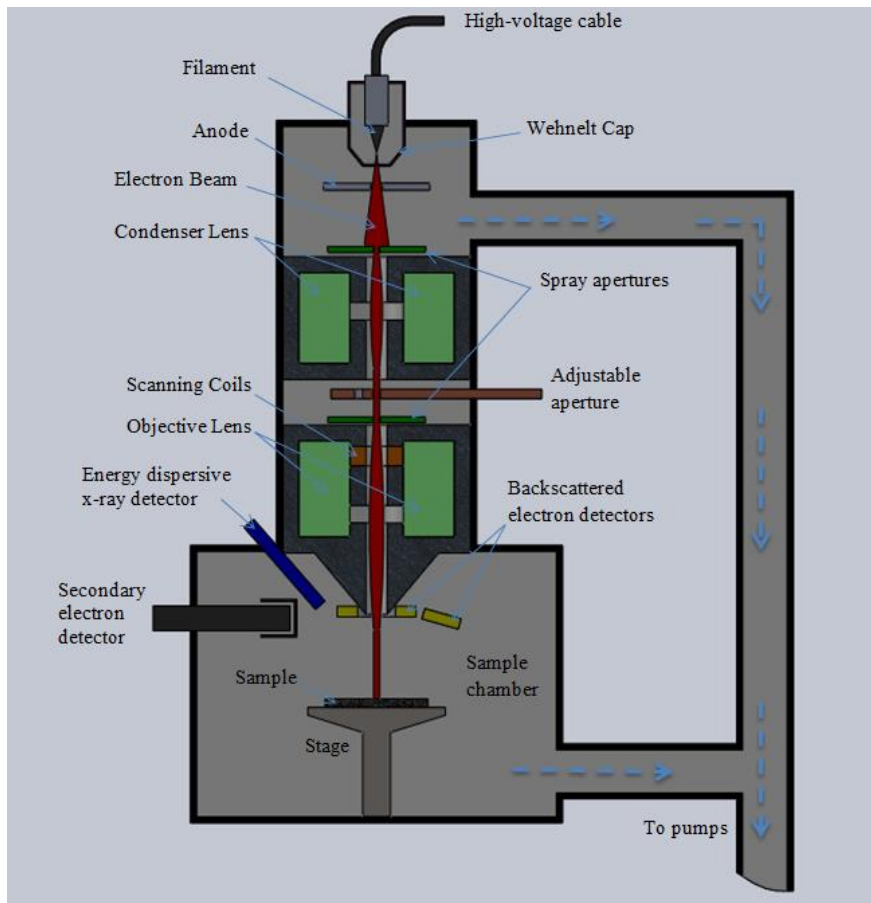


Figure 3.2 SEM operation system [99]

3.4.4. Energy Dispersive X-ray Spectroscopy (EDX)

The SEM described above is additionally equipped with an EDX spectrometer. this technique is used to analyze the constituent elements in the part to be analyzed.

To obtain an X-ray emission necessary to characterize the part, an accelerated electron beam is focused on the desired surface. Atoms on the surface contain unexcited electrons. When the incident beam acts on the surface, it excites the electrons in the inner shell, expelling them and creating free spaces for other electrons. From the outer shell another electron will fill this empty space with a higher energy, the energy difference between them is released in the form of X-rays. Given that X-ray energy is known between 2 atomic shells, the elemental composition of the surface can be measured. EDX can detect the complete spectrum of X-rays for an analyzed sample except for the composition of the first 4 chemical elements in mendelev's table [100]. EDX principle is presented in Figure 3.3

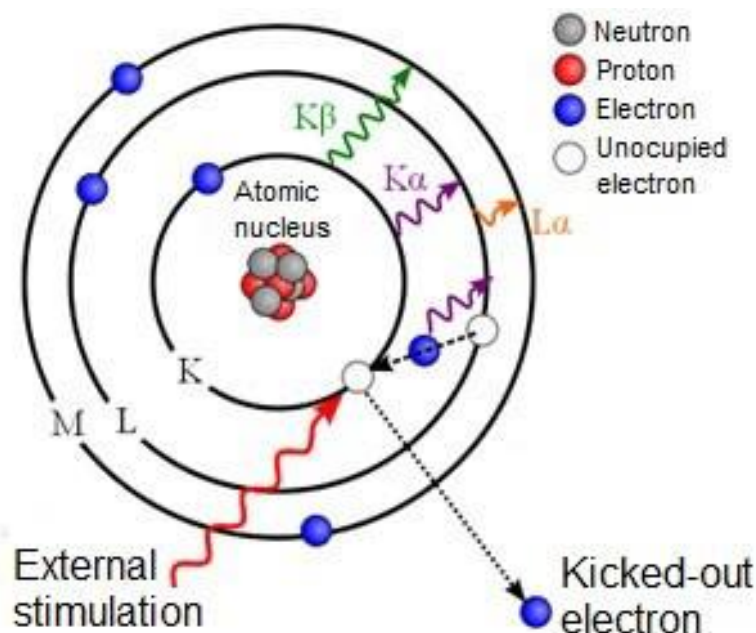


Figure 3.3 EDX principle [101]

3.5. Corrosion investigation

In an electrolyte solution one of the most widely used methods for investigating electrochemical corrosion behavior is linear voltammetry. This is by definition the variation of the working electrode potential over time with a linear scan rate (ν) of 2 different values, initial (E_i) and final (E_f), while measuring the value of the current density (i).

In order to use this technique, the potentiostatic configuration of the electrochemical cell must be composed of three electrodes: working electrode or sample of interest (WE), reference electrode (RE) and counter electrode (CE), placed in the electrolyte solution. These 3 electrodes are connected to an electronic working instrument called a potentiostat

The counter electrode is usually made of inert materials (gold, platinum, graphite) it practically affects the electrical circuit not being involved in electrochemical reactions

The reference electrode is always an electrode in which the potential is well known, with its help the potential of the entire measuring system is measured and controlled. A saturated calomel reference electrode (SCE) was used in this paper. To minimize electrolyte resistance, a Luggin-type capillary was used as the reference electrode. A simple principle of the corrosion cell is presented in Figure 3.4 The

samples were embedded in the resin, leaving a working surface of 1 cm², which was taken as the working electrode.

Working mode: The current will flow between CE and WE, the response of the latter will be detected by RE.

These potention-dynamic Experiments provide information on the behavior of pitting, passivation of specific test systems / solutions, as well as on the corrosion of cracks or imperfections in the study material. At the same time, the results collected from the linear analysis can be processed using software to determine the corrosion rates (Slope Tafel), passivation rates or active / passive characteristics of the tested material.

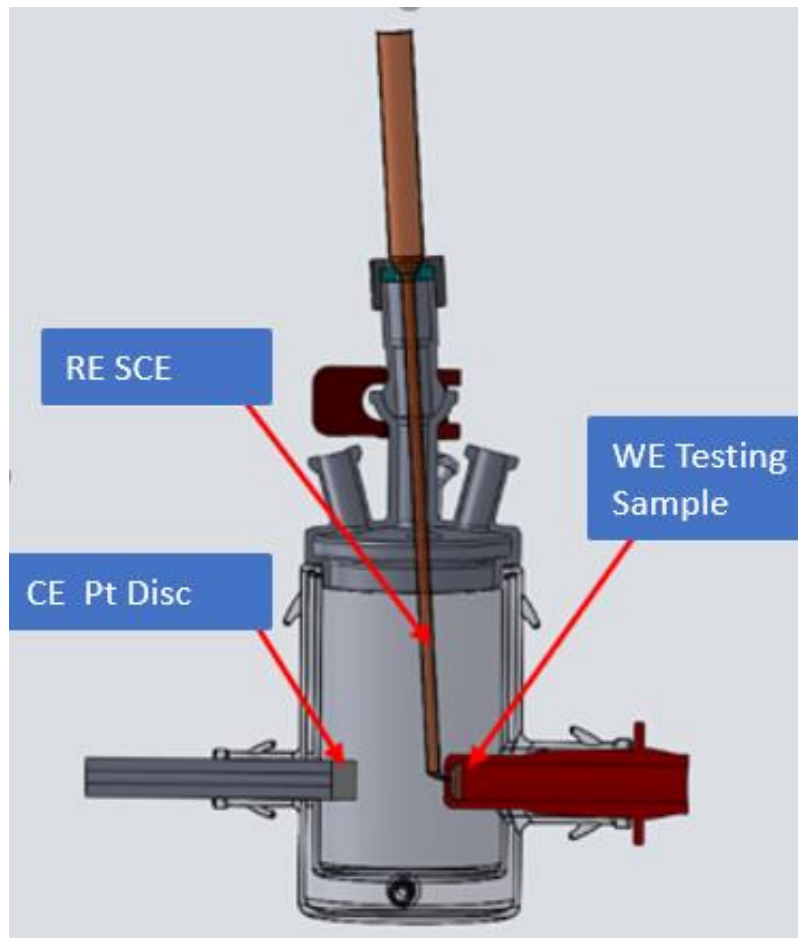


Figure 3.4 Electrochemical Cell configuration

4. Results and discussion

I. Oxy-acetylene flame spraying

Due to the fact that we are following a technological cycle in order obtaining a new product in the first part of this cycle, the coating layer is deposited using NiCrBSi spheroid powder.

4.1. Characteristics of the feedstock powders

The majority and inescapable problems of the mobile and mechanical components in the automotive, mining, aerospace and renewable energy industries are wear and corrosion. Both affect the service life of the components as well as reducing the performance of the whole assembly. Currently, on a large scale, cermet materials are used to improve wear and corrosion resistance in the vast majority of industrial applications [102, 103, 104]. The cermets are made of a metal matrix (Cr, Co, Ni) and a reinforcement material embedded in it (WC and Cr_xC_y), the majority of the thermal sprayed coatings consist of these two powder components [105, 106].

In the present work, nickel-based powders without ceramic reinforcer were used, intending to obtain improved results for wear and corrosion resistance of the final coatings. For comparison, three types of powder with different chromium content were used. The powders were manufactured by LSN Diffusion, Llandybie, United Kingdom, one type of powder being commercial and the other two types being specially developed for the Karl Schumacher Company, Bochum, Germany.

4.1.1. Morphology

Powder composition and particle size are presented in *Table 4.1*. KS-IC-45 powder is commercially available as LSN 330, as about KS-IC-55S and KS-IC-55 are only available through Karl Schumacher. The company has given its consent for the processing of data, the composition in *Table 4.1* may differ with an error margin of up to 2% compared to the powder used in the factory after completion of this study

Table 4.1 Powder used in thermal spraying process

| Trade name | Ni[%] | Cr[%] | B[%] | Si[%] | Fe[%] | C[%] | Grain Size [μm] |
|------------|-------|-------|------|-------|-------|------|------------------------------|
| KS-IC-45 | Bal. | 6.02 | 1.12 | 4.19 | 1.5 | 0.25 | +106-45 |
| KS-IC-55S | Bal. | 10.10 | 2.49 | 3.51 | 4.0 | 0.40 | +106-45 |
| KS-IC-55 | Bal. | 13.02 | 2.80 | 4.19 | 5.12 | 0.42 | +106-45 |

The Cr and B elements, which are present in the chemical composition of the powder, increase the wear resistance due to the fact that they are carbide forming elements. The presence of Si and B promotes wettability and deoxidation (self-fluxing) during the remelting process [107]. In addition, these elements reduce the rate of unremelted particles following the deposition process and after heat treatment [108]. An EDX analysis on all three powders can be seen in Figure 4.1 the most important peak observed in the figure is that of Nickel followed by the detection of chromium and silicon, Fe element was also detected, this elements encourages chromium segregation to the boron-rich regions and conducts to chromium-borides formation [109].

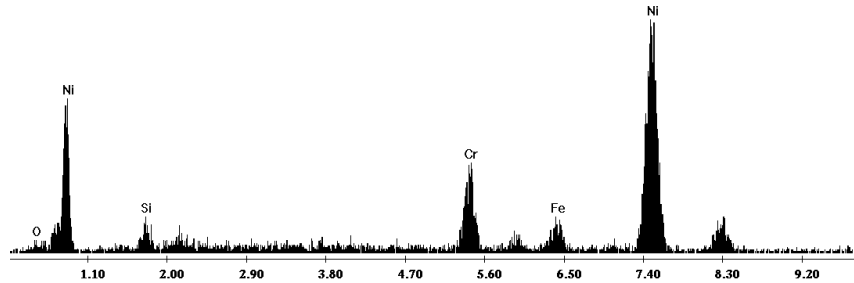


Figure 4.1 EDX spectrum of NiCrBSi powders

The particle morphology and size distribution of NiCrBSi type powders are illustrated in Figure 4.2, as observed for each type of powder, the particle dimensions are in the same range as those given by the manufacturer. As shown in Figure 4.2, NiCrBSi powder with the name KS-IC-55S has a non-uniform particle size distribution, which can lead to a much more porous coating obtained during the spraying process than for equally size dimension powders. At the same time, the powder with smaller dimensions is heated much faster than the powder with larger dimensions resulting in more oxides in the as-sprayed coating and particle inclusions in the coated samples.

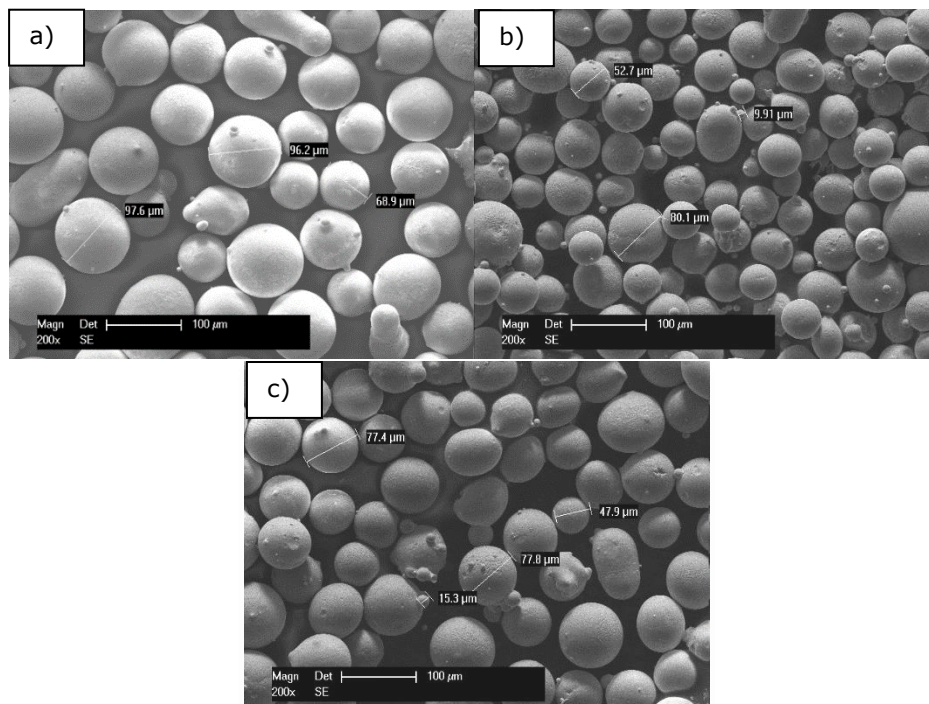


Figure 4.2 SEM micrograph of the NiCrBSi powder: a) KS-IC-45, b) KS-IC-55S c)KS-IC-55

4.1 - Characteristics of the feedstock powders 53

All three types of powders are obtained by the gas atomization process with water collection, consequently the completely spherical shape. This method has a high production efficiency and combines the obtained properties between gas and water atomization

An eliminating condition for the industrial production of thermally coated parts by powder spraying is that the powder mixtures need to have a free flow. A good flowability increases productivity, at the same time increases the consistency of the obtained coatings. To characterize powders on a large scale, the Hall Flow Method is used, it was established as an international standard by MPIF (Metal Powder Industries Federation) in 1945 [110]. There is also an international standard for this method, namely ISO 4490: 2008. Table 4.2 presents the results of the physical tests of the powders, both the flow properties and their apparent density.

Table 4.2 Physical tests of NiCrBSi powder

| Powder Type | Apparent density [$\text{g}\cdot\text{cm}^{-3}$] | Hall Cup Flow [sec/50g] |
|-------------|--|-------------------------|
| KS-IC-45 | 4.7 | 15.3 |
| KS-IC-55S | 4.4 | 14.1 |
| KS-IC-55 | 4.7 | 15.1 |

For a more detailed characterization of the powder, it was embedded in the epoxy resin after which it was polished to observe its cross section.

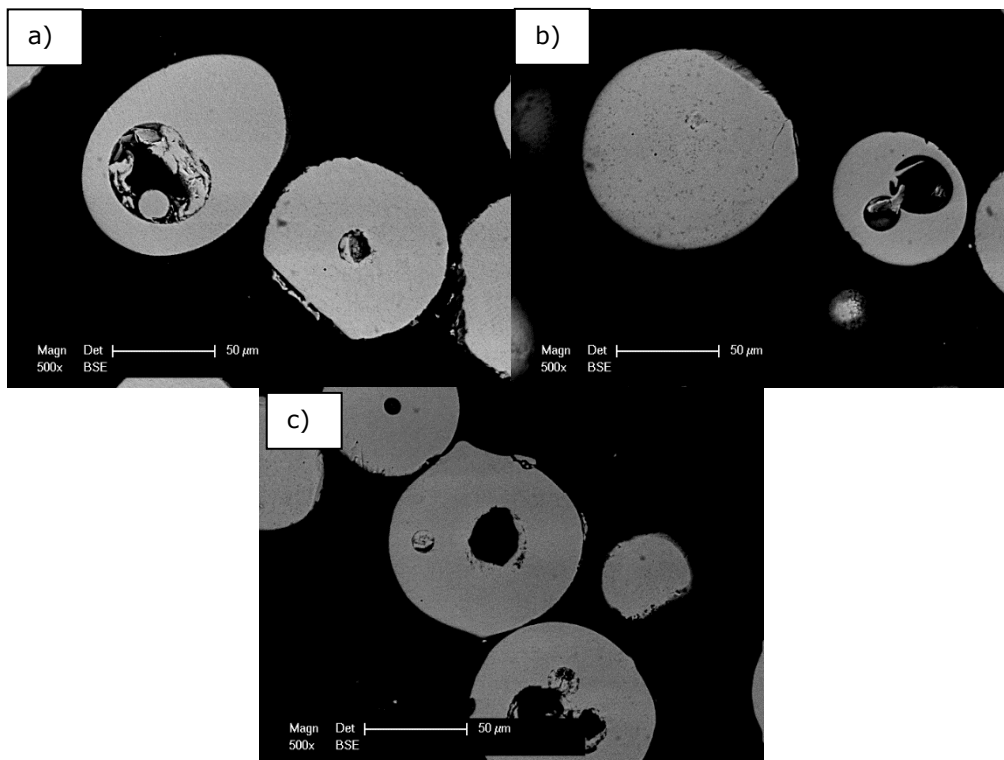


Figure 4.3 SEM cross section micrograph of the NiCrBSi powder: a) KS-IC-45, b) KS-IC-55S c)KS-IC-55

Figure 4.3 shows all the 3 powders used, it is observed that they all have particles in cross section with quite large gaps inside them. These gaps lead during the spraying process to an overheating of the particle, due to the fact that the material to be heated is much less, which indicates to a more pronounced oxidation of them. Resulting a coating with two types of porosity, interconnected porosity resulted from the process of coating formation, layer by layer, and a closed porosity that is inside an percentage of the particles.

Due to this fact, a subsequent heat treatment is suitable that brings the coating in a molten state, closing not only the pores obtained during the process and also the pores inside the particles.

In order to have a starting point in optimizing the remelting process, knowing the melting point of the investigated material has a major importance. A thermogravimetric measuring device was used to determine this point. 100 grams of powder was placed in the Al_2O_3 melting crucible, the heating was completed made from room temperature up to 1200 degrees Celsius with a constant heating of 15 K min^{-1} . All testing was done in an N_2 controlled atmosphere.

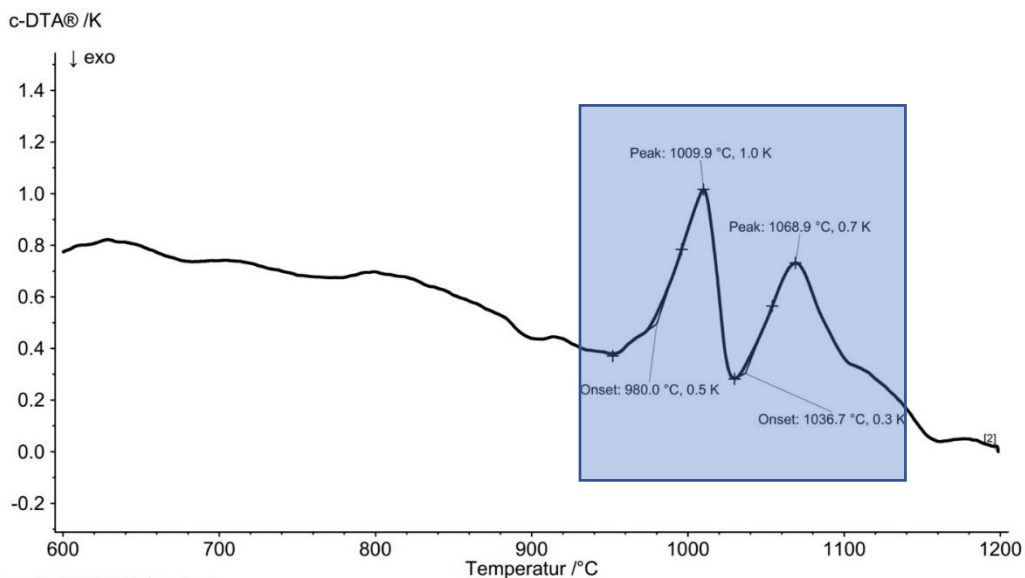


Figure 4.4 DTA curve of IC-KS-45 powder

Following the thermogravimetric analysis, a major importance is the interval between 920°C and 1120°C . It is observed on the thermogram in Figure 4.4 that the starting point of melting is at 1010°C and the investigated material is completely melted at 1069°C . In order to observe which is the optimal point to produce the remelting in chapter 4.6, were taken 4 different temperatures as working variants on the relevant range. Similarly, if the chemical composition is changed, the starting melt point is translated, the point as well where the material is completely melted. Knowledge of these points leads to a slight optimization of the parameters obtained for one type of powder, to their implementation for the other types.

4.1.2. Phase composition

In order to characterize and compare the three types of powder, an XRD analysis was performed, following this analysis the component phases of each type of powder were accurately determined. The powders were scanned at the 2θ angle between 20° and 100° after the manufacturer's details regarding the chemical composition of the powder, it can be seen in all three figures (Figure 4.5, Figure 4.6 and Figure 4.7) as the most intense peak is nickel, it is identified at the theta angle of approx. 44° .

Figure 4.5 shows the NiCrBSi powder with the code name KS-IC-45 in which it is observed that most of the interpretation diagram is represented by Nickel with a percentage of 70% and a cubic crystallization system. The second constituent phase is composed of silicon nickel with a percentage of 14% and an orthorhombic structure. The third phase is also an orthorhombic structure consisting of nickel and boron. The fourth one consists of iron silicon phase with an amount of 3% of the total, and a hexagonal crystallization structure. At the end with a percentage of only 2% of the entire constituents of this powder is represented by the hard phase formed from chromium and boron and is crystallized in the tetragonal system.

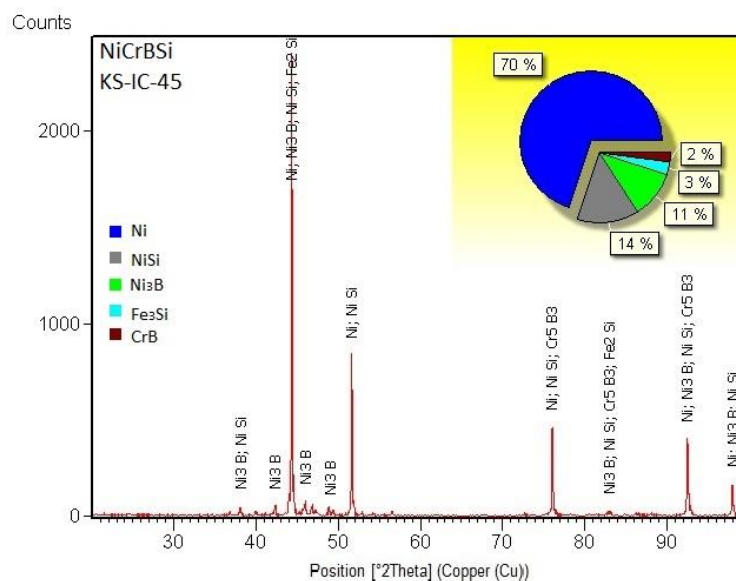


Figure 4.5 XRD diffraction pattern KS-IC-45

The powder with the code name KS-IC-55S presents in the structure only 48% Nickel, besides this there are the chromium-nickel-silicon phases with a percentage of 36% and the chromium-nickel phase with 5%, all three of them are crystallized in the cubic crystallization system. The fourth phase is a hard phase consisting of chromium and boron with a percentage of 11%, and an orthorhombic crystallisation system. The pattern of this powder is represented in Figure 4.6.

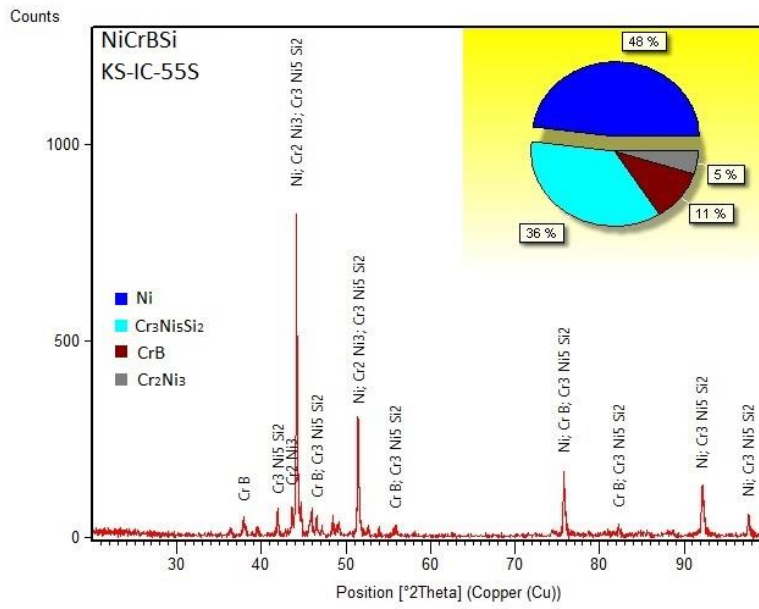


Figure 4.6 XRD diffraction pattern KS-IC-55S

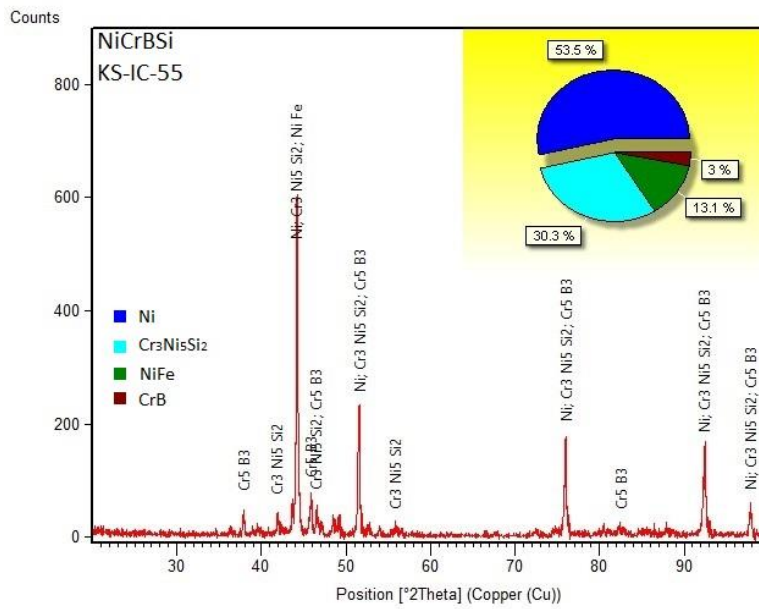


Figure 4.7 XRD diffraction pattern KS-IC-55

The last investigated powder called KS-IC-55 and represented in Figure 4.7, shows like the other two more than half of the phase composition represented by nickel 53.5% with a cubic crystallization system. The next phase is formed from chromium-nickel-silicon with about one third of the total phase composition and also with a cubic crystallization structure, the third constituent iron-nickel phase with a presence of 13%, this phase is crystallized in the monoclinic system. Finally, with the smallest percentage the hard chromium-boron phase is present with 3% and crystallized in the tetragonal system.

4.2. Substrate material

Choosing of the substrate material is very important for the working pieces, it must take over all the loads and stresses which appear during the exploitation of the workpiece. 42CrMo4 quality steel (material EN 1.7225) is a low alloy temperature steel and belongs to the group of hardening steels. The steel used as substrate in the present work is a temperate steel derived from 1.7225, i.e. 42CrMoS4 + QT (material EN 1.7227 DIN – before was named 42CrMo4V) contains at least more sulphur (approximately 0.05%), which, however, significantly improves processability. The mechanical properties of the two types are the same. The delivery condition of 42CrMo4 is mostly + tempered (+ QT quenched and tempered) or + A annealed. In QT state, this alloy has a relatively high strength and high toughness, also present a good wear resistance.

The heat treatment of 42CrMo4 is of central importance for processing. It is suitable for high strain components in the machine industry. Due to the hardness in the tempered state, round steel rods are usually cold drawn until a diameter of about 20 mm. Larger sizes are mostly turned on lathe. This steel has significantly higher susceptibility to appearance of surface cracks in cold and hot rolled conditions, than in the case of other common steel types. Like all hardening steels with a relatively high carbon content, this type of steel is difficult to weld [111]. The carbon content greatly reduces the critical cooling rate (increasing mechanical strength). 42CrMo4 is calmed with silicon (Si) and manganese (Mn), among others. Silicon (Si) improves yield strength, tensile strength, wear resistance and increases hardening by lowering the cooling rate. On the other hand, silicon, especially in larger quantities, deteriorates the solubility of ferrite (iron) for carbon, which reduces the stability of cementite (Fe_3C -iron carbide). Manganese content below 10% can be dissolved in ferrite (mixed crystal) [112]. Similar to silicon, manganese lowers the critical cooling rate and is one of the cheapest and most effective alloying elements in terms of hardening. Manganese binds sulphur to manganese sulphides (MnS), which prevents the formation of low-sulphur iron (FeS).

Steel grade 42CrMoS4 + QT has a higher sulphur content, which facilitates processing. With 42CrMo4 the phosphorus content is kept as low as possible since causes cold fragility. In order to increase the hardness significantly, the steel grade 42CrMo4 is allied with approximately 0.9% - 1.2% chromium (Cr), this element increases the hardness of the alloy due to its carbide formation effect.

Molybdenum (Mo) content of 0.15% - 0.3% in 42CrMo4 improves temperature resistance, reduces the risk of brittleness, and increases heat resistance. The wear resistance of this type of steel is also increased by the carbide forming effect (Mo_2C) of molybdenum.

Table 4.3 shows the chemical composition of the substrate steel given by the steel supplier. Hardness measurements was performed on the base material, using a Zwick Micro Hardness tester, the applied load used for determining the Vickers microhardness was 3N for 15 seconds, distance between measurements was 10mm. The results showed that this steel has a standard deviation Vickers hardness of 315 HV0.3.

Table 4.3 Chemical composition of substrate material

| Steel | C | Si | Mn | P | S | Cr | Mo | Al | |
|--------|------|------|------|-------|-------|------|------|-------|-----|
| 1.7227 | 0.42 | 0.26 | 0.73 | 0.012 | 0.023 | 1.13 | 0.21 | 0.027 | [%] |

4.3. Parameters of the oxy-acetylene flame/fuel spraying process

Prior to the tests for the present work, laboratory tests were performed to see how the material behaves when applying the remelting treatment by electromagnetic induction. Several tests were performed until the optimal parameters for remelting were found. It was observed that at large differences on the preheating side, the final coating was similar. There were no differences in structure or cracks in the coating. The laboratory tests were performed on bars of the same EN 1.7227 turned on a final diameter of 35mm (Figure 4.8). To be able to develop the process and see what the influence of the applying parameters on the coating and the substrate is. The decision was made to pass the tests on diameters of 70mm and 160 mm. these are presented below



Figure 4.8 As-sprayed (left) and remelted (right) bars

Prior to the thermal spray process, the deposited surfaces were subjected to a two-step cleaning process. In the first stage the parts were degreased with alcohol being removed all the organic residues left after the turning process, in the second step they were sandblasted with hard particles of cast iron. This second process was used for 2 well-founded reasons: firstly, to clean the surface of the oxide residues that appeared between the turning, transport, spraying process and the second reason is to obtain an irregular surface, in which it will be possible to mechanically anchor the sprayed particles. In this process the particles were accelerated with the help of compressed air on to the work surface at an angle of 60 degrees, this angle is set to avoid impregnation of the cast iron particles in the substrate. Following the blasting process, all impurities were removed and a roughness of 75 micrometers was obtained. The sand blasted samples can be seen in Figure 4.9.



Figure 4.9 Sand blasted samples

In order to deposit the coatings using the oxy-acetylene deposition technique in the following, the relative deposition velocity was calculated:

a). Calculation of the rotation speed of the cylindrical part on which the deposit is made:

$$n = \frac{V \cdot 1000}{D \cdot \pi} \quad 4.1$$

Where:

- n- rotation speed of the cylindrical shaft [rpm]
- V-Spraying velocity [m/min]
- D- diameter of the shaft [mm]
- π - 3.1415

In order to deposit on our cylinder with a nominal diameter of 160 mm, a stipulated deposition speed of $V=50 \text{ m/min}=833 \text{ mm/s}$ was chosen. From equation 4.1 is resulting a rotation speed of 99.47 rpm. Because the lathe is an older model, the value closest to this value was chosen, that was 95 rpm.

b). Advance speed calculation:

$$V_s = \frac{P \cdot V}{S_c} \quad 4.2$$

Where:

- V_s - Linear advance speed [mm/s]
- P- pitch [mm]
- S_c -shaft circumference [mm]
- V-spraying velocity [mm/s]

To calculate the feed rate of the linear system, a pitch value of 4 mm was chosen because the spray spot has a diameter of approximately 8 mm. Half of the spot was decided for the reason that at each rotation half of the spot will pass over the spray made before. If the step is more than half the layer may be obtained in waves, in the other direction, if the step is smaller the overlap is much larger and the layer is considerably thicker, which can lead to cooling internal stresses even at its cracking.

Spraying velocity = 833mm/s

Nominal diameter of the shaft = 160mm

Pitch=4mm

Replacing all this data in the equation 4.2 it is resulting a $V_s=6.62\text{mm/s}$

Thermal spraying was performed with a mixture of acetylene and oxygen gases using a Methatherm 5P gun, with a total gas flow of 38.7 l / min. The substrate samples were in the dimensions of: turned diameter 158.84 mm and a length of 200 mm, thermal spraying was performed in 6 overlaps up to a final diameter of 161.44, with a coating thickness of 1.3 mm measured (the laps and diameters resulting from each pass can be seen in the Table 4.4), following the process deposit. Subsequent the remelting process the resulting coating was 1.12mm thick, (see Figure 4.36) resulting in a compaction of 15%

Table 4.4 Deposition layers of KS-IC-45

| Lap | Diameter [mm] | Coating per lap [μm] |
|-----|---------------|-----------------------------------|
| 0 | 158.84 | 0 |
| 1 | 159.40 | 280 |
| 2 | 159.75 | 180 |
| 3 | 160.15 | 200 |
| 4 | 160.66 | 255 |
| 6 | 161.00 | 170 |
| 6 | 161.44 | 220 |

All the other parameters used in the process deposition with the help of acetylene oxy flame are presented in the Table 4.5



Table 4.5 Spraying parameters

| Lathe machine | | | |
|----------------------|------------|------------------------|----------------------|
| Name: | Weipert | | |
| Burner | | | |
| Manufacturer | Methatherm | Powder injection type | Internal Powder feed |
| Name | 5P | Powder injection angle | 90° |
| Nozzle | 85-7B-G | | |

4.5 - Characteristics and properties of as-sprayed coatings 61

| Gases | | | |
|------------------------------|---------------|-----------------------|------------|
| Acetylen pressure [Bar] | 1.5 | Oxygen pressure [Bar] | 2.5 |
| Burner control system | | | |
| Total flow | 38.7 | | |
| Acetylen flow [l/min] | 12.8 | | |
| Oxygen flow [l/min] | 25.9 | | |
| Powder doser | | | |
| Transport | Gravitation | | |
| Discharge [g/min] | 100 | | |
| Processing | | | |
| Spraying distance [mm] | 200 | | |
| Spraying angle [Grad] | 90 | | |
| Linear moving soft | Positito 2014 | | |
| Linear speed [mm/s] | 6.5 | | |
| Number of overlaps | 6 | | |
| Coating thickness [mm] | 1.3 | | |
| Aplication | | | |
| Sample drawing | Cylinder | Dimension | Ø160x200mm |
| Base material | 42CrMo4V | | |
| Powder | | | |
| Manufacturer | LSN Diffusion | | |
| Material | KS-IC-45 | KS-IC-55S | KS-IC-55 |
| Particle Size [µm] | +106-45 | +106-45 | +106-45 |

4.4. Characteristics and properties of as-sprayed coatings

Following the deposition process with oxyacetylene flame the samples were investigated to observe the structure.

In the case of NiCrBSi As-sprayed coatings, a network of interconnected pores and unbound particles can be noticed, this can be explained due to the impact, recoil and contraction of the particles once the substrate is reached. All three types of powder have the same coatings structure as a result of the thermal spray process with oxyacetylene flame, also having a poor substrate adhesion, as shown in Figure 4.10. Adhesion that is due only to mechanical anchoring on the substrate, which causes this coating to exfoliate at the action of an external force. Following the deposition, it is suitable to use a subsequent heat treatment to improve the adhesion to the substrate and at the same time to increase the compactness of the coating.

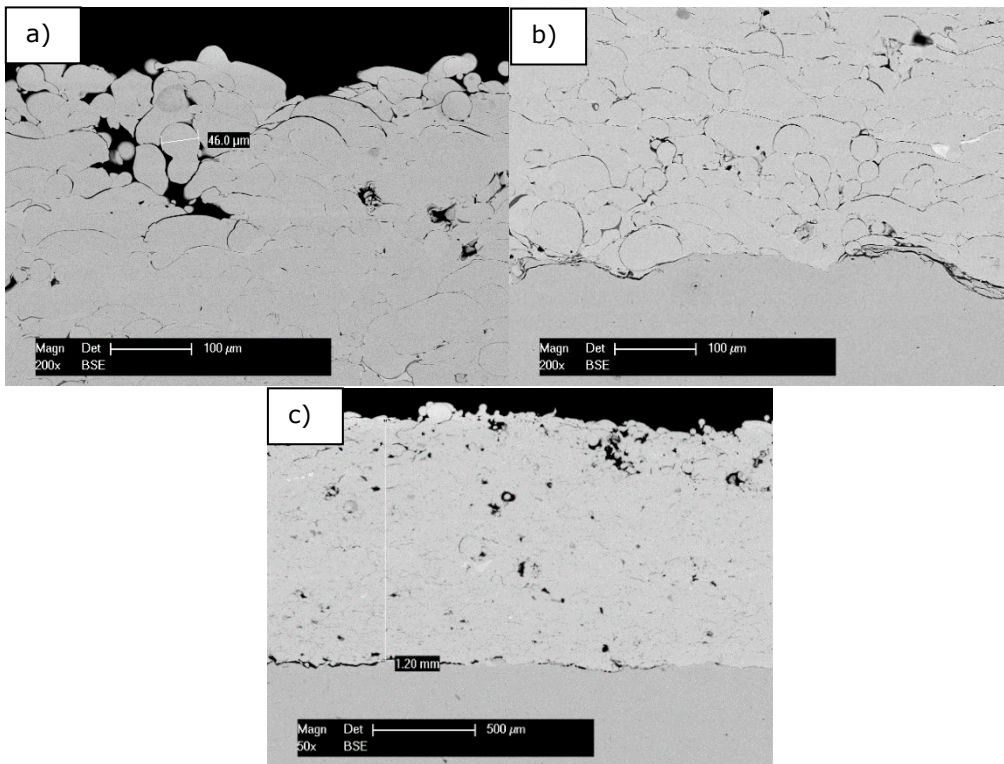


Figure 4.10 Cross-section SEM micrographs of as-sprayed KS-IC-45: a) near to surface, b) at the interface, c) whole coating

Sliding wear was chosen to investigate the as-sprayed layers using a ball on disk arrangement. This method was decided because the test machine is also equipped with a converter that can determine the coefficient of friction.

Before the test, the sample pieces were grinded in order to achieve a flat surface, as they were extracted from cylinders with a diameter of 160 mm, after this process they were cleaned with acetone and dried in hot air. For each type of powder deposition three test were performed. The working parameters used for all of the 3 samples are presented in Table 4.6

Table 4.6 Ball on disk parameters

| Counterbody | Normal Load [N] | Linear Speed [cm/s] | Radius [mm] | Stop Condition [lap] | Sliding distance [m] |
|-------------|-----------------|---------------------|-------------|----------------------|----------------------|
| WC-Co ball | 10 | 15 | 6 | 15.000 | 566 |

As can be seen in Figure 4.10, the particles on the surface of the deposited part don't have a very good bond due to the fact that they have only mechanical adhesion, by clamping to the previously deposited layer. This fact leads to a very unpredictable friction behaviour, it is observed that in all cases the coefficient of friction has not stabilized and presents a deviation quite large compared to the average. In the case of powder type KS-IC-45 it can be said that due to the fact that it has a lower content in Cr which automatically leads to a lower hardness than the

4.5 - Characteristics and properties of as-sprayed coatings 63

other two powders, following the process, after the first 226 meters of testing, it stabilized because the asperities, being a softer material, were flattened, as shown in Figure 4.11.

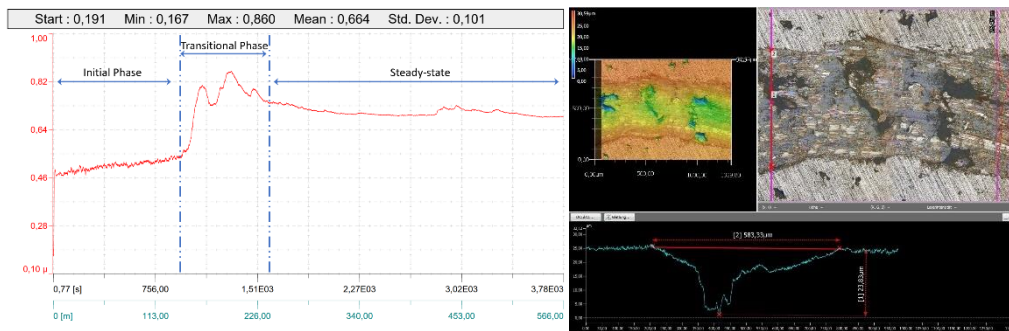


Figure 4.11 Friction coefficient and wear track of as-sprayed KS-IC-45

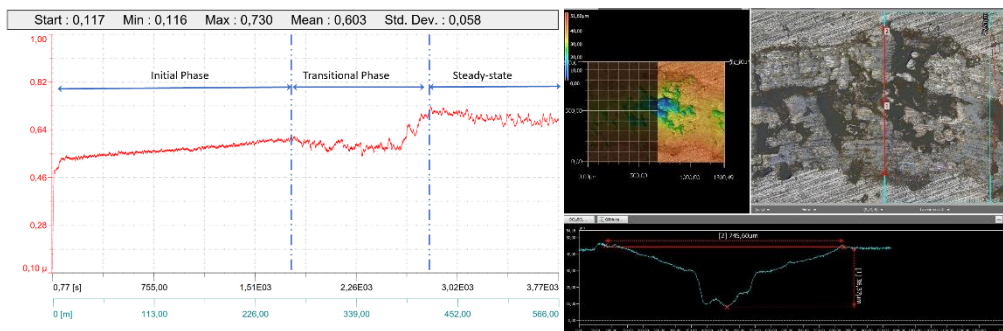


Figure 4.12 Friction coefficient and wear track of as-sprayed KS-IC-55S



Figure 4.13 Friction coefficient and wear track of as-sprayed KS-IC-55

In the case of the other two types of powder, a more unstable friction coefficient is observed, in the case of the KS-IC-55S type powder, it is noticed that the wear trace is much finer (Figure 4.12), it is concluded that this is due to the fact that the powder has finer granulation (Figure 4.2 b.) than the powder type KS-IC-55

shown in Figure 4.2 c). At wear track, it is observed that the hard particles were extracted from the coating and pits appeared, at the same time a very unstable friction coefficient was observed Figure 4.13.

It is also observed that depending on the chemical composition, the initial phase is extended, this remaining at low values (See Figure 4.11 to Figure 4.13). In all types of coating a transitional zone was observed that presents an anomaly, in the case of IC-45 powder, the coefficient of friction jumps to an approximately double value after which at the exit of the transitional zone it stabilizes at an intermediate value entering the zone of stand-states. In the case of the KS-IC-55 coating type, the steady state zone did not appear in the measured range, the tests stopping in the transition zone.

The ball used as a counter part of the WC-Co material that was exposed during the process was worn out on a diameter equal to the width of measured trace, due to the fact that the depth is much diminished, so it is mentioned that the trace left in the material it was much wider because the ball was worn. The width being induced similarly for all three coatings types, the obtaining depths are observed due to the exfoliation of the particles.

II. Electromagnetic induction remelting

As it is observed in the subchapter destined to the characterization of the powders (Chapter 4.1), that they present a non-uniformity of the particles, at the same time some of them present porosity and some are empty spheres. It is imperative to remelt this obtained coating. Before reaching the actual process of optimizing the remelting parameters presented in chapter 4.6, it was considered necessary to optimize the working element, that is the inductor coil.

4.5. Selection of the inductor geometry

Since it is a process of heating by high frequency currents, the study started from the hardening process of steels. First of all, it was considered to obtain a spiral working element formed by a working pipe with a cylindrical section, in order to obtain a high magnetic field strength. As can be seen in Figure 4.14 in order to harder a steel bar, a resulting magnetic field will form which will reach the surface of the part and heat it to the desired temperature.

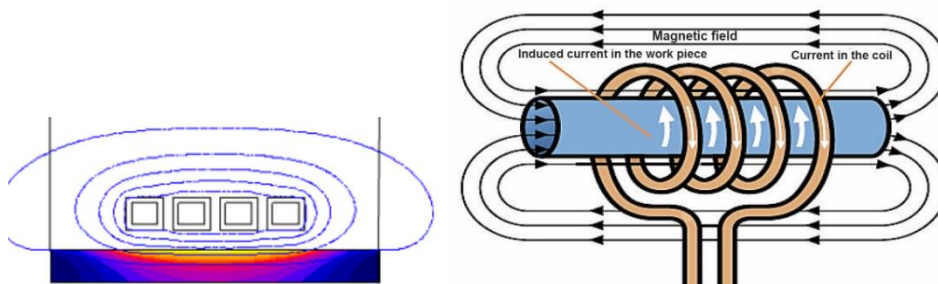


Figure 4.14 Magnetic lines and temperature distribution cylinder heated by 4-turn inductor [113, 114]

4.5 - Selection of the inductor geometry 65

Starting from this premise, an inductor with three spirals was made. After testing it on the NiCrBSi layers, it was observed that the magnetic field given by each spiral intersects with that given by the neighbouring spiral, but has a great influence on the remelted coating, leaving uncoated surfaces in it, surfaces that can be seen optically.

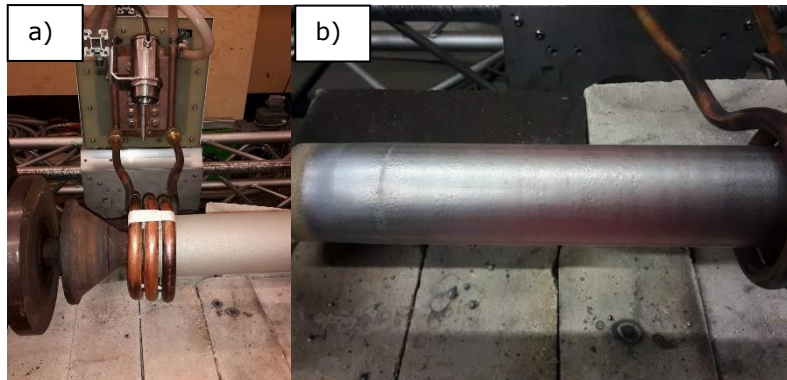


Figure 4.15 a) Remelting element 3 spirals, b) Optimised remelted sample

In Figure 4.15a) an element with 3 spirals is presented. From a technical point of view, this type of element is good for inductive hardening where the steel must be brought into the austenitic field, this phase being a solid one. In the case of NiCrBSi-type coatings, in order to receive improvements, they must be brought to the liquid point. As can be seen in Figure 4.14 inside the working element, the maximum temperature is obtained in the middle of length element. The pyrometer was also positioned directly in the middle of element as a temperature measurement point. After dozens of optimization tests, the part represented in Figure 4.15b) was obtained. It can be observed that due to the irregularly distributed temperature, combined with the translation of the element from left to right, rings of unmelted material were obtained. This is happening for bar type parts with no diameter differences, or tension concentrators. In the case of parts with tension concentrators such as sharp edges or shoulders, the problem is different. In the case of sharp edges, or the end of the cylinders, the edge will overheat which will lead to the flow of the sprayed material. In the case of the shoulders, it was observed that the part did not melt until the intersection of the cylinder with the difference in diameter see Figure 4.16. This is due to the fact that the magnetic field is concentrated towards the inside of the working element. Also, if the melting was to the edge, inside the working spiral the layer is disintegrated and you will flow

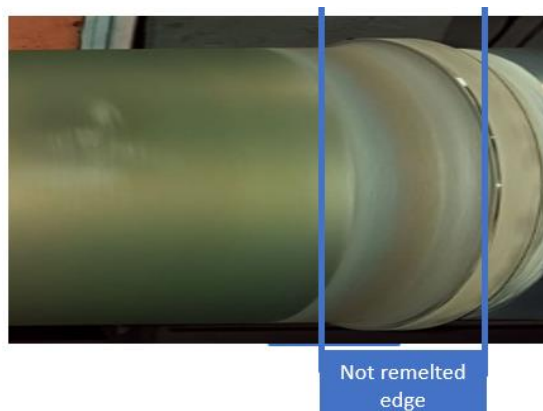


Figure 4.16 Non remelted edge with 3 spiral elements

Due to the fact that no conclusive results were reached for a number greater than 2 spirals that can be further optimized, it was decided to switch from multiple spirals to a single spiral. According to equation 4.3 of the magnetic field intensity, it is observed that the energy required to be introduced in the system in order to be able to bring the material to the same temperature is proportional to the number of turns.

$$H = \frac{nI}{2r} \quad 4.3$$

Where H-Magnetic field strength
 n-number of turns
 I-current intensity
 r- coil radius [115]

In the tests on a single spiral of the inductor, the aim was to maintain the coating intact during the process. It was considered 2 types of sections of the working element, one being a circular section and the other a square or rectangular section.

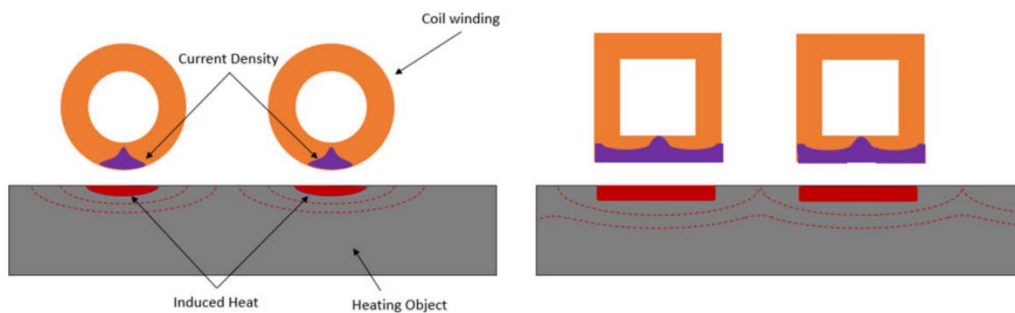


Figure 4.17 Coil design [116]

4.5 - Selection of the inductor geometry 67

Starting from Figure 4.17 where the design for 2 types of elements is presented, the element with cylindrical section was taken into account, for economic reasons and due to the fact that it is easier to process in obtaining a perfect ring. From theory it is known that the magnetic induction (B) is directly proportional to the increase of the magnetic field intensity (H) (equation 4.4) and this is tangent to the field lines, the direction being given by the drill rule.

Magnetic Field:
$$H = \frac{B}{\mu} [25] \quad 4.4$$

Besides the fact that in Figure 4.17 the cylindrical section has a much smaller surface through which the current density is transferred, the magnetic induction is very high and at the same time concentrated, which makes to 'push' the melted coating out from under the inductor, resulting in a coating in waves



Figure 4.18 Sample remelted with circle cross element section

In the last case, the element variant with square and rectangular section was taken into account. The both of them was tested. Due to the fact that inside the working spiral the magnetic field lines are in the form of an ellipse which in the case of magnetic induction B leads it in the center of the working element at an angle close to 0 degrees with the workpiece, succeeding in this way as the element passes over the surface not to push the layer out of the element. According to Figure 4.17 a rectangular element with dimensions of 20 mm x 10 mm was chosen, in order to have a larger working surface.



Figure 4.19 Sample remelted with rectangular cross element section

As can be seen in Figure 4.19, the coating does not show irregularity (which can usually be seen at the beginning or end of the process) due to the shape of the inductor and the applied electric field. In conclusion, the rectangular section inductor was chosen as an element to be used to further optimize the parameters on the three types of powder. The optimization is presented in chapter 4.6

4.6. Remelting process optimization

In order to obtain high quality coatings, it was started from NiCrBSi thermally sprayed coatings which cannot be used in industry in this form and it is urgently necessary to apply a subsequent process to compact them [117]. In order to obtain these high-quality coatings, a process of electromagnetic induction heating was used. Due to the fact that in order to reach a satisfying result a large number of factors and variables come into question, it is not as simple as induction quenching, where, depending on the applied frequency, a certain penetration depth is obtained [118]. In the case of the coatings, a multitude of factors that influence the process appear, among which we list: the preheating temperature, the rotation speed of the shaft, the distance between the element and working the part, the power applied by the transformer and others.

Due to the fact that there are so many variables to be controlled and if all the tests were to be done it would take a long time and is totally inappropriate for the case of the present research. After a brainstorming session was concluded that a solution method should be found in order to use as few tests and in this to include all possible variants. At the same time porosity it was chosen as a factor for determining the quality of the remelted coating.

Taguchi method was chosen, which is presented in detail below:

In 1987 Taguchi and Konishi have developed a statistical method called Taguchi method [119]. At the beginning this method was designed to help the quality development of the manufactured products, with the passing of years this method

has been introduced in other fields of activity: for example Engineering or Biotechnology [120].

The most complete method in the development cycle of a product is considered Design of Experiments (DOE), this statistical approach tries to offer a predictive information of a complex or a multi-variable process in just a few trials. The major methods of DOE are listed below:

4.6.1. Full Factorial Design

In statistics a full factorial experiment is an experiment consisting of two or more factors, each factor having several possible values or levels [121]. The experiment considers all possible combinations resulting in a number of N^k where n is the number of factors that influence the process and k is the number of levels on which the respective factors are divided. For example, a full factorial design for an experiment with 3 major factors, each one divided in 4 levels, has 81 runs.

4.6.2. Taguchi method

The full factorial design method necessitates a large number of experiments to be completed, so the work becomes unreasonable and also difficult if the number of factors is greater than two and has more than three levels. In order to facilitate optimization work, Taguchi suggested a special method of orthogonal design array to study the entire set of parameters, but having the benefits of a much smaller number of experiments being made, also recommended the use of a function that measures the performance of the characteristics that deviates from the anticipated value, after that this function is transformed into a Signal-to-noise (S/N) ratio [122]

Naturally, to characterize this ration, there are three types of performance categories: Nominal the best, higher the best or smaller the best

4.6.2.1 Steps involved in solving coating optimization

In order to use the Taguchi method, we need to take the following steps [123]

- a) Primary function identification and side effects
- b) Identification of noise factors, test conditions and quality characteristics
- c) Identifying the objective function to be optimized
- d) Identifying controllable factors and their levels
- e) Selecting a suitable orthogonal array and building the matrix
- f) Performing experiments
- g) Data Examination; stipulating the optimal factor and its performance
- h) Perform a verification experiment

To optimize the melting process, a NiCrBSi powder deposited on a common chromium-molybdenum steel (42CrMo4V) substrate having a diameter of 160 mm and a length of 250 was used. In accordance with the steps outlined above, a whole series of experiments were carried out at Karl Schumacher GmbH, Bochum, Germany. The entire procedure is presented below

a) Primary function identification and side effects

Main function: Heating at remelting point

Side effects: decreasing the porosity

First of all, before proceeding to the next steps it is essential to find the factors that directly influence the obtained surface and identify the noise factors

Table 4.7: Factors that affect remelting process

| Control Factors | Noise factors |
|------------------------------------|---------------------|
| Applied Power | Substrate material |
| Preheating temperatures | Length of substrate |
| Process remelting temperatures | Operator skills |
| Piece rotation | Room temperatures |
| Linear feed of the melting element | Noise |

After listing the factors that has effect on the heating process, a decision must be taken and only those factors that are believed to have a greater consequence on the final result should be considered in order to obtain the experimental matrix.

b) Identification of noise factors, test conditions and quality characteristics

Quality characteristics: low porosity

Operating machine: Ambrell Ekoheat 35/25 + lathe machine

Testing equipment: DM RM-E Leica light microscope

Remelting element: copper spiral element/ section 20x10 mm

Work piece material: 42CrMo4 steel coated with NiCrBSi

c) Identifying the objective function to be optimized

The main objective of this high frequency current heating is to bring the superficial coating (NiCrBSi powder deposited through the oxyacetylene flame process) into a molten phase in order to close the pores resulted from the first process and at the same time to improve adhesion to the substrate.

Due to these specifications the objective function was chosen: Porosity
Smaller-the-better

$$S/N \text{ ratio for this function: } 10 \log \left(\frac{\mu^2}{\sigma^2} \right)$$

where μ =mean or average, σ = standard deviation or natural variation

d). Identifying controllable factors and their levels

The optimal factors and their levels were chosen considering the TG analyses of the powders and the specifics given by the powder manufacturer, it was also considered the results of "Brain Storming Session" inside Karl Schumacher GmbH, with the working team on the power applied by the high frequency generator. Factors and levels are shown in the Table 4.8.

Table 4.8 Selected factors and their levels

| Factors [Units] | Levels | | | |
|--------------------|--------|------|------|------|
| | 1 | 2 | 3 | 4 |
| Temperature [°C] | 980 | 1010 | 1050 | 1080 |
| Power [KW] | 40 | 60 | 80 | 100 |
| Preheating [°C] | 25 | 100 | 250 | 350 |

e). Selecting a suitable orthogonal array and building the matrix

Table 4.9 Power constant - 980°C

| | | | |
|-----------------|-----------------|-----------------|-----------------|
| E ₁₁ | | E ₁₂ | |
| PO ₁ | Pr ₁ | PO ₂ | Pr ₂ |
| E ₁₃ | | E ₁₄ | |
| PO ₃ | Pr ₃ | PO ₄ | Pr ₄ |

Table 4.10 Power constant - 1010°C

| | | | |
|-----------------|-----------------|-----------------|-----------------|
| E ₂₁ | | E ₂₂ | |
| PO ₁ | Pr ₂ | PO ₂ | Pr ₁ |
| E ₂₃ | | E ₂₄ | |
| PO ₃ | Pr ₄ | PO ₄ | Pr ₃ |

Table 4.11 Power constant - 1050°C

| | | | |
|-----------------|-----------------|-----------------|-----------------|
| E ₃₁ | | E ₃₂ | |
| PO ₁ | Pr ₃ | PO ₂ | Pr ₄ |
| E ₃₃ | | E ₃₄ | |
| PO ₃ | Pr ₁ | PO ₄ | Pr ₂ |

Table 4.12 Power constant - 1080°C

| | | | |
|-----------------|-----------------|-----------------|-----------------|
| E ₄₁ | | E ₄₂ | |
| PO ₁ | Pr ₄ | PO ₂ | Pr ₃ |
| E ₄₃ | | E ₄₄ | |
| PO ₃ | Pr ₂ | PO ₄ | Pr ₁ |

Where E_{xy}- Experiment number

PO_z – Power and z- Level from Table 4.8

Pr_z - Preheating

An analysis of all factors would take into account all the possible combinations between the factors that influence the process and their levels, for this research being 3 factors available on 4 levels, 81 tests should be done. To reduce the number of trials required to obtain results, the number of tests was reduced to an orthogonal array of the L16 type outlined in the tables Table 4.9 to Table 4.12.

f). Performing experiments

In accordance with the orthogonal matrix presented at point e). experiments were made using the factors with their levels presented in Table 4.8. The experimental matrix is shown in Table 4.13 total of 16 tests were carried out.

Table 4.13 Orthogonal Array with Control Factors

| Experiment Number | Control Factors | | |
|-------------------|------------------|------------|-----------------|
| | Temperature [°C] | Power [KW] | Preheating [°C] |
| E ₁ | 980 | 40 | 25 |
| E ₂ | | 60 | 100 |
| E ₃ | | 80 | 250 |
| E ₄ | | 100 | 350 |
| E ₅ | 1010 | 40 | 100 |
| E ₆ | | 60 | 25 |
| E ₇ | | 80 | 350 |
| E ₈ | | 100 | 250 |
| E ₉ | 1050 | 40 | 250 |
| E ₁₀ | | 60 | 350 |
| E ₁₁ | | 80 | 25 |
| E ₁₂ | | 100 | 100 |
| E ₁₃ | 1080 | 40 | 350 |
| E ₁₄ | | 60 | 250 |
| E ₁₅ | | 80 | 100 |
| E ₁₆ | | 100 | 25 |

g) Data Examination; stipulating the optimal factor and its performance

After carrying out the test, porosity of the obtained coatings was investigated in 3 different points, the results are exposed in Table 4.14. The pictures were made at an optical microscopy and the porosity for each specimen was calculated with help of ImageJ Software (Image Processing and Analysis in Java).

Since the purpose of this optimization is to reduce as much as possible porosity in the coating, the S/N ratio was calculated and tabulated in Table 4.14

Table 4.14 Porosity measurements

| Experiment Number | Porosity | | | Mean Value | Standard deviation | S/N ratio |
|-------------------|----------|---------|---------|------------|--------------------|-----------|
| | Value 1 | Value 2 | Value 3 | | | |
| E ₁ | 14.547 | 14.056 | 15.069 | 14.557 | 0.507 | -29.169 |
| E ₂ | 1.901 | 2.172 | 2.299 | 2.124 | 0.203 | -20.381 |
| E ₃ | 4.383 | 4.756 | 4.935 | 4.691 | 0.282 | -24.433 |
| E ₄ | 5.157 | 8.380 | 6.967 | 6.835 | 1.616 | -12.528 |
| E ₅ | 0.541 | 0.615 | 0.794 | 0.650 | 0.130 | -13.974 |
| E ₆ | 7.719 | 7.117 | 7.258 | 7.365 | 0.315 | -27.381 |
| E ₇ | 0.250 | 0.316 | 0.180 | 0.249 | 0.068 | -11.261 |
| E ₈ | 0.328 | 0.412 | 0.374 | 0.371 | 0.042 | -18.917 |
| E ₉ | 0.250 | 0.320 | 0.260 | 0.277 | 0.038 | -17.276 |
| E ₁₀ | 0.150 | 0.180 | 0.200 | 0.177 | 0.025 | -16.927 |
| E ₁₁ | 14.010 | 10.850 | 14.050 | 12.970 | 1.836 | -16.981 |
| E ₁₂ | 0.300 | 0.450 | 0.350 | 0.367 | 0.076 | -13.626 |
| E ₁₃ | 3.500 | 7.320 | 6.350 | 5.723 | 1.986 | -9.195 |
| E ₁₄ | 8.250 | 9.150 | 10.260 | 9.220 | 1.007 | -19.236 |
| E ₁₅ | 15.010 | 10.960 | 13.160 | 13.043 | 2.028 | -16.168 |
| E ₁₆ | 18.000 | 18.250 | 16.260 | 17.503 | 1.084 | -24.162 |

In order to find the best set of parameters and taking into account Table 4.13 and Table 4.14, the mean value of S/N for each factor on their levels was calculated and assembled in the table. Delta was calculated to be able to find the influence of each factor on the process

Table 4.15-Average S/N ratio for each Factor

| | Temperature | Power | Preheating |
|---------------|-------------|---------|------------|
| 1 | -21.627 | -17.403 | -24.423 |
| 2 | -17.663 | -20.981 | -16.037 |
| 3 | -16.202 | -17.211 | -19.965 |
| 4 | -17.190 | -17.308 | -12.478 |
| Δ | 5.425 | 3.770 | 8.386 |
| Influence [%] | 30.86 | 21.44 | 47.70 |

4.6 - Remelting process optimization 73

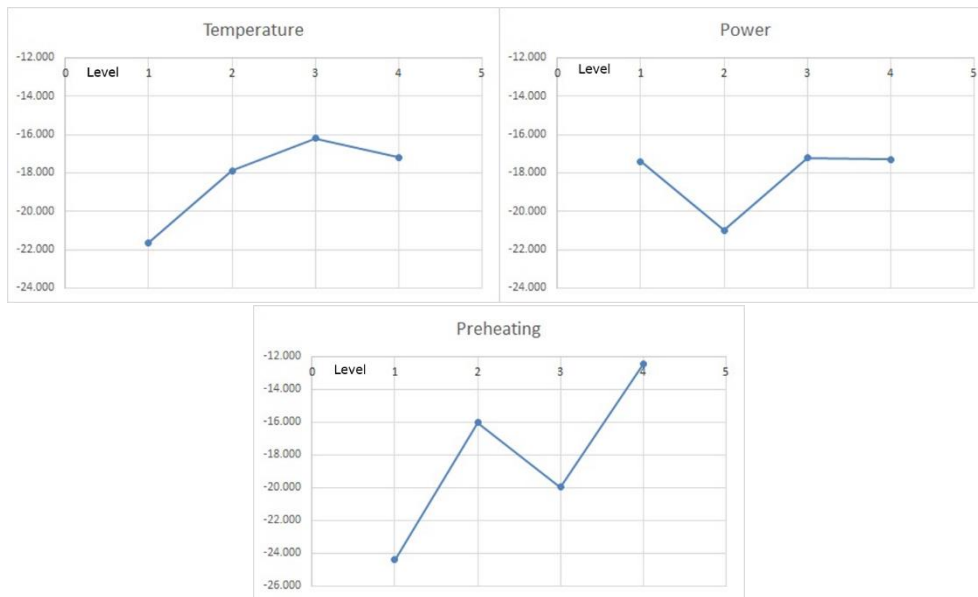


Figure 4.20 Charts showing parameter level v/s Signal to noise ratio

Due to the fact that a lower porosity is required for the process, by analysing Table 4.15 and its schematic diagram presented in Figure 4.20 it was observed that the optimal parameters for remelting process are the one presented in Table 4.16.

Table 4.16 Optimum Parameters

| Parameter | Level | Optimum Value |
|-------------|-------|---------------|
| Temperature | 3 | 1050 °C |
| Power | 3 | 80 KW |
| Preheating | 4 | 350 °C |

Porosity was chosen as the determining factor for parameter optimization, since it is the only factor that can be measured according to the rest of the applied parameters. It was chosen because of the fact that in some sets of parameters the coating was exfoliated, in others the coating overheated and ran on the workpiece and in another test when the applied power was too high this coating resulted in waves because the electromagnetic field it was too strong under the inductor and due to its forces it was pushed out from under the copper spiral. Table 4.14 shows all the porosity results obtained from the optimization process for the KS-IC-45 powder. It can also be observed that some values are very high, these are for the subject where the coating has been exfoliated, which happened when is a poor preheating was applied. In case where the porosity was extremely low the coat was overheated and ran. In the following lines is presented the influence of the parameters applied on:

Following the tests performed and the method used, it can be seen from Table 4.15 that the preheating temperature has a very high influence on the developed coating quality. This is explained in the following rows.

At a low preheating temperature and a high power used for remelting step, it was observed that the coating was exfoliated, the parameters used in this case are

presented in Table 4.13 experiments 11 and 16. Due to the very strong electromagnetic field, the electrons begin to move very quickly, generating internal stress to the interface. Because the substrate is pre-cleaned and roughly 75 microns thick, the peaks of these asperities overheat rapidly and lead to the peeling of the coating as seen in Figure 4.21a. The Figure 4.21b shows the coating in sample section at the end of the crack, it can be seen that the crack propagates across the interface

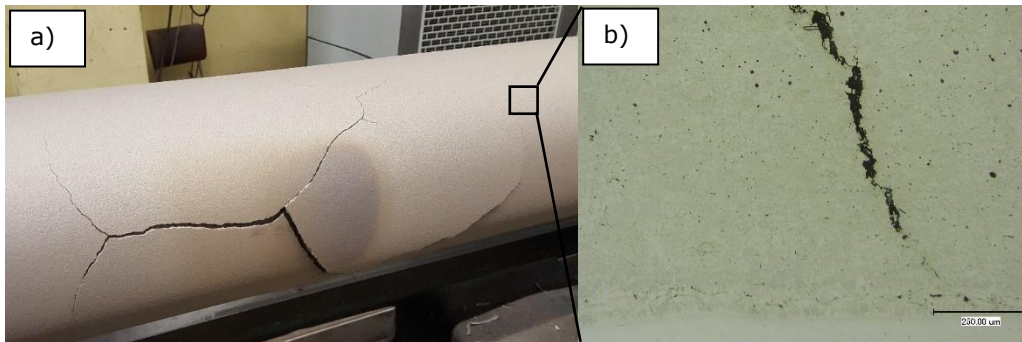


Figure 4.21: Exfoliate coating a) on the surface, b) cross-section

If the preheating temperature is increased then the exfoliation problem is reduced to zero but cracks still occur in the remelted coating, they are observed to be present on the entire surface of the coated remelted area Figure 4.22a. Figure 4.22b shows that the cracks reach the substrate

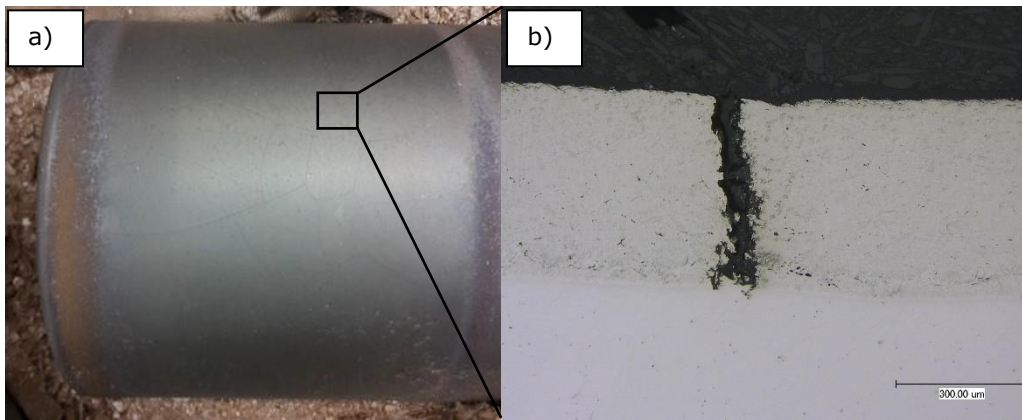


Figure 4.22 Crack's example: a) On the surface b) cross-section

The third parameter, namely the temperature at which the surface of the coating is brought, has a considerable influence, if the temperature is too low combined with a poor preheating, it results in cracks and incompletely remelted coating as shown in Figure 4.23a. If this parameter is above the limit, then the coating is fluidized and begins to flow from the workpiece Figure 4.23b. This can lead, depending on the distance between the working spiral and the workpiece at a short circuit of the installation and erosion on the cooper spiral

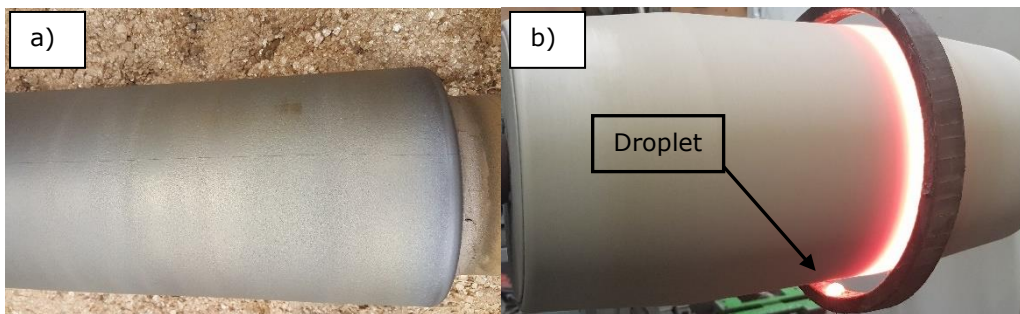


Figure 4.23 Temperature influences a) to low, b) to high

Because for the other two types of powder the optimization process was done according to the same method, it was not considered necessary to rewrite the method again twice, therefore in Table 4.17 only the optimal parameters resulting from the optimization process are presented.

Table 4.17 Optimised parameters

| Parameter | KS-IC-55S | KS-IC-55 |
|-------------|-----------|----------|
| Temperature | 1030 °C | 1000 °C |
| Power | 70 KW | 60 KW |
| Preheating | 400 °C | 550 °C |

4.6.3. Working distance

According to Biot Savart's law (equation 4.5) the magnetic field generated in a point is directly proportional to the proximity of the inductor point [115]. Therefore, it is desirable to have as small as possible distance between the work element and the part to be fused

Biot Savart law:
$$B = \frac{\mu_0 I}{4\pi} \int_{Wire}^0 \frac{dl \times \hat{r}}{r^2}$$
 4.5



Figure 4.24 Element and coating destruction



Figure 4.25 Substrate structure
 a) 7mm b) 12mm c) 20mm
 working distance

For laboratory work the minimum working distance was found to be 5 mm. For shorter distances the magnetic field is much too strong, removing the completely molten coating from under the inductor, no matter how small its intensity. The extrapolation to the industrial dimensions was considered, in this extrapolation the parts to be remelted and the work environment from which they come were taken into account. Was also took interested in the possibility that these parts have internal stresses remaining from previous processing, or in the case of parts in which the coat has to be replaced after a warranty time expires, the stresses accumulated during their operation. Extrapolation was made on a bar of 70 mm and a length of 1000 mm, was observed a deviation from the center axis leading to the destruction of the element and the coating (Figure 4.24)

For this study, the deviation from the central axis up to 5 mm was considered. This can be found in the case of slender bars due to their own weight, or in the case of bars in which a process of de-stressing the metal structure has not been done before. 3 workpieces with a diameter of 70 mm and a length of 200 mm were deposited with KS-IC-45 powder and prepared for inductive remelting. 3 remelting elements with a rectangular section measuring 20x10mm were made. The first element had an inner diameter of 84 mm which means a working distance of 7 mm. The second with the same configuration and the working distance of 12 mm and in the case of the 3rd the inner diameter was 110 mm and the working distance was 20mm.

The applied power and the melting temperature were kept constant for all three types of samples, following the process, the samples were cut and metallographic samples were prepared for all 3 types of inductor, at the same time one of the non-thermally influenced basic material was prepared. . After testing, no major differences were found on the remelted coating, instead, significant differences were observed in transforming the structure of the base material

In Figure 4.26 is presented the structure of the thermally uninfluenced substrate, also in Figure 4.25 Substrate structure a) 7mm b) 12mm c) 20mm working distance the three types of structures resulting from the thermal process can be observed



Figure 4.26 Substrate before heating

4.6.3.1 Influence of working distance 7mm

In the case of the working distance of 7 mm (Figure 4.25 a), a change of structures was observed on a depth of approximately 3-4 mm.

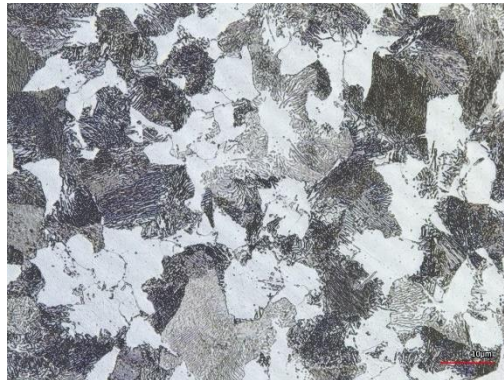


Figure 4.27 Structure of 42CrMo 2 mm from surface

Figure 4.27 shows a structure made of ferrite which has a light colour and in the darker part there is a perlite made of cementite and ferrite. At the interface between layer and substrate on an interval of 20 micrometers the formation of sorbite was observed, which can lead to a weakening of the interface, but due to the fact that the depth is not so extended and the anchoring of the coating to the substrate is a metallurgical connection it does not exfoliate (see Figure 4.46). Also the microhardness HV 0.3 was measured, having a constant value of 300.



Figure 4.28 Sorbite lamellar structure on the interface with perlite-ferite inclusions

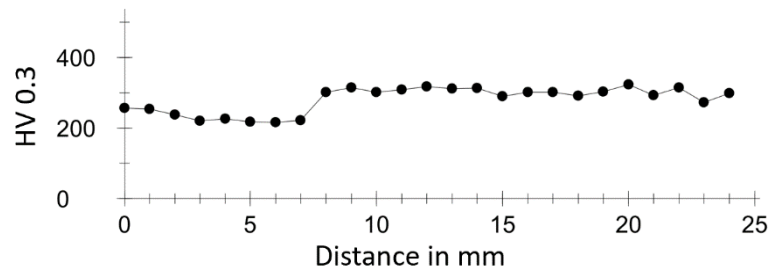


Figure 4.29 Micro indentation on substrate remelted with 7 mm working distance

Due to the small distance between the element and the workpiece, not much energy was introduced into the substrate, which leads to an influence of only a maximum of 7 mm in the substrate, which can be seen from the hardness tests. Figure 4.29 shows the hardness tests made in section starting from the coating-substrate interface, using a step of 1 mm between microindentations.

Correlating Figure 4.29 with Figure 4.34 it is observed that in the range 0-7 mm the hardness results show a hardness on cooling in the Ferite-Perlitic domain

which can be observed also on Figure 4.28 where it is observed that immediately after the first 20 microns ferrite and perlite appear in the structure

4.6.3.2 Influence of working distance 12 mm

In the case of the working element with a distance of 12 mm, according to the Biot Savart 4.5, for the same input parameters the heating time was longer, in order to reach the melting temperature in the surface coating. A much higher influence on the substrate can be seen in Figure 4.25. Also, in the structure at the interface a sorbitic structure can be observed without inclusions of perlite and ferrite, which leads to a more fragile structure at the coating substrate interface, but because it is still present relative over a small distance it does not influence the adhesion of the layer to the substrate. At the same time the ferito-perlitic structure is observed in the depth of the substrate.



Figure 4.30 Sorbite lamellar structure on the interface

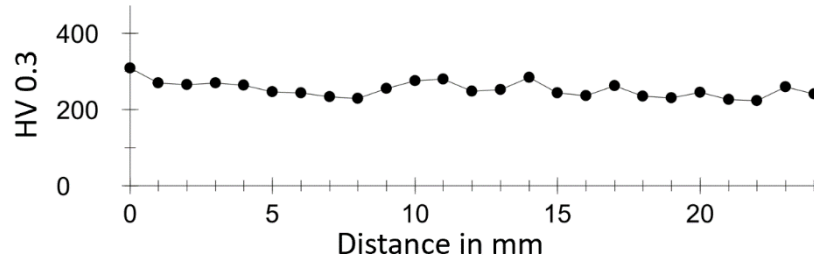


Figure 4.31 Micro indentation on substrate remelted with 12 mm working distance

Figure 4.31 shows a deviation of the hardness measurements from the initial hardness which was 300 HV 0.3. It is observed that up to a depth of 25 mm the coating is thermally influenced, correlating Figure 4.25 b (where it is observed that the microhardness resulting from the treatment is below 290 HV) with Figure 4.34 structure is a rough ferritic-pearlitic structure,

4.6.3.3 Influence of working distance 20 mm

The working distance of 20mm showed that the substrate is completely thermally influenced (Figure 4.25c), and at the interface there is a hard and fragile martensitic structure that is not desirable in the workpiece(Figure 4.33). At the same time, besides the fact that the working time is very high, the energy consumption is also very high. In the same order of ideas, the structure is a rough one that leads to a weakening of the piece, and the probability of being destroyed when the necessary forces are applying in operation.

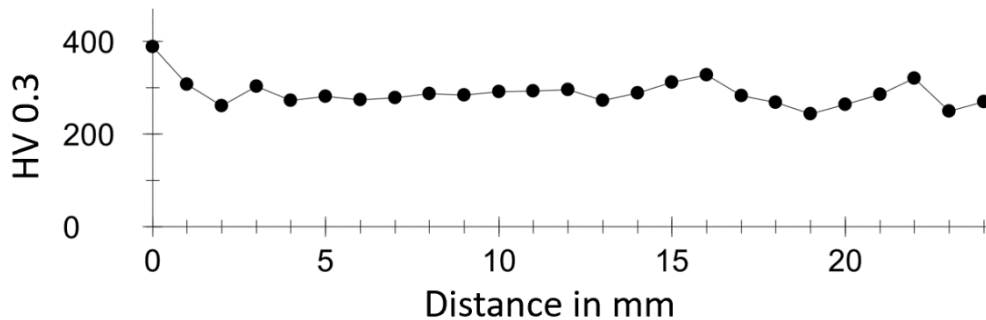


Figure 4.32 Micro indentation on substrate remelted with 20 mm working distance

Figure 4.32 shows that the hardness in the first mm is so high that it takes us in the bainitic field (see Figure 4.34), a few microns from the surface where the indentation was made, in Figure 4.33 it is seen that at the interface is present after the shape of the grains is present Martensite

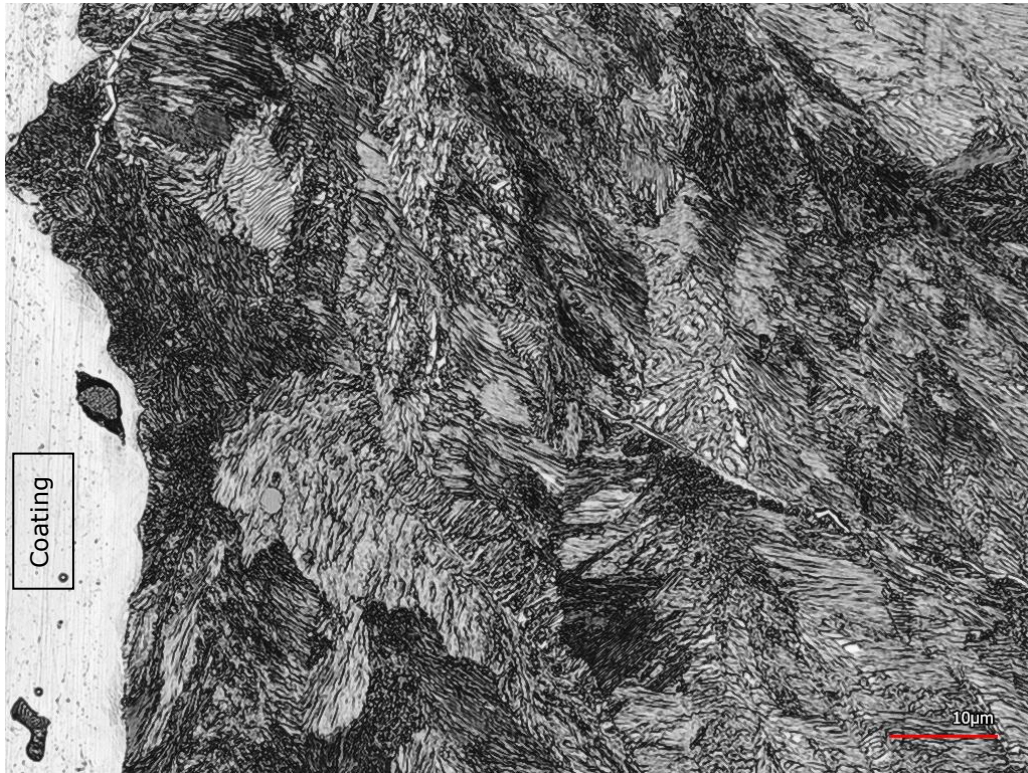


Figure 4.33 Martensitic lamellar structure on the interface

Taking into account the cooling diagram of the 42CrMo4V type steel presented in Figure 4.34 and the substrate structures present in Figure 4.25, the following can be deduced: In the case of the working element with a distance of 7 mm it is observed that a high amount of energy was not introduced in the substrate, the cooling on the interface taking us in the bainitic domain on a distance of only a few micrometers, intersected with the ferrite-perlitic fine structure domain that goes up to 3-4 mm in the substrate, after this distance the substrate is not thermally influenced. In the case of the element with a working distance of 12 mm, at the interface, only the bainitic structure is observed, which leads us to the conclusion that a high amount of energy was introduced in the system, the observed structure show us the conclusion that the substrate was completely brought into the austenitic domain and on the first 0.2 mm the cooling was done quickly, taking us to the bainitic domain. In depth the structure is completely formed of ferrite and perlite, up to 20mm. In the case of the third working element, with a working distance of 20mm, the time of heating was relatively high, which led to the complete heating of the substrate at working temperature, during cooling a martensitic structure was observed at the interface and in the depth of the substrate a rough structure, which is specific to a slow cooling, structure which was also observed in the center of the piece.

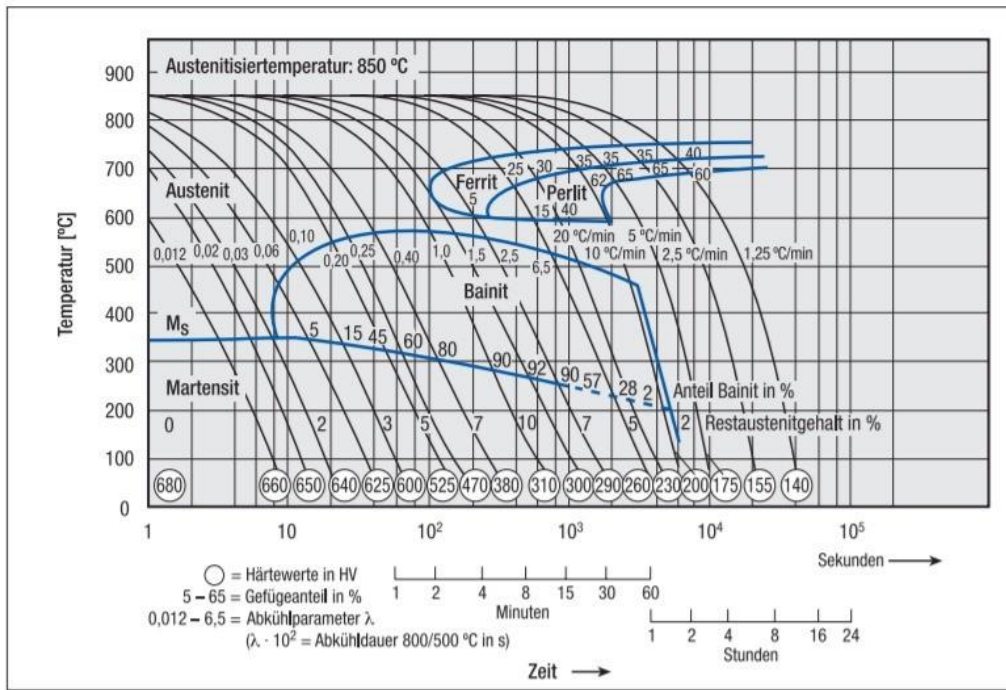


Figure 4.34 42CrMo4V cooling diagram [124]

In conclusion, in this chapter of optimizing the working distance:

- The element with a working distance of 7 mm is optimal because it brings a compact layer, without waves and without an influence on the substrate.
- In the case of repair parts that have already been in the industry and whose internal stress are not known, an element of maximum 15 mm working distance is recommended. In his case the influence on the substrate is relatively small.
- The tests documented in this doctoral thesis were made on cylinders with a diameter of 70mm, extra tests were made on larger diameters, which led to a much lower influence of the depth of penetration of the thermal influence in the substrate, inversely proportional to diameter.

4.6.4. Extra Hardening

The samples were extra hardening with a ceramic ball and a pressure of 200 bar. Figure 4.35 shows the process: a tool with a moving ball is pressed on the rotating bar. Due to the friction force the ball need to be cooled with a cooling liquid. The parts were polished and brought to the final mass after that the hardening process was done, an increase of the hardness was observed with up to 10 HRC units.



Figure 4.35 Ceramic ball hardening

In conclusion, the KS-IC-45 type powder is suitable for use in industry with a hardening process applied before the polishing process because the surface in the first 10 micrometers will be hard and meets the quality requirements, and inside the coating is ductile.

4.7. Characteristics and properties of remelted coatings

The samples were obtained by depositing a coating of NiCrBSi on a steel bar with a diameter of 160 mm and a length of 250 mm. These were sectioned and prepared metallographically in order to characterize them (physically, mechanical and structural).

All cross sections of the coats were investigated using a scanning electron microscope equipped with an energy dispersion spectroscope, also the x-ray diffraction was used to determine the phase composition. Additionally, all three types of coating have been characterized in terms of adhesion on the substrate and hardness.

4.7.1. Deposition coating thickness

The deposited coating has a thickness of over one mm. it was submitted so much due to the fact that the following step is intended to implement these coatings in the hydraulic cylinder construction industry and taking into account the subsequent processing: Turning, rectifying and bringing in nominal measures. Coat thickness is

shown in Figure 4.36. At the same time as it is presented in chapter 4.7.7 Corrosion behaviour, a higher coating thickness is desirable because corrosion on these types of coatings is selective and the thicker the coating, the logic says that reaching the electrolyte at the substrate will be greatly slowed

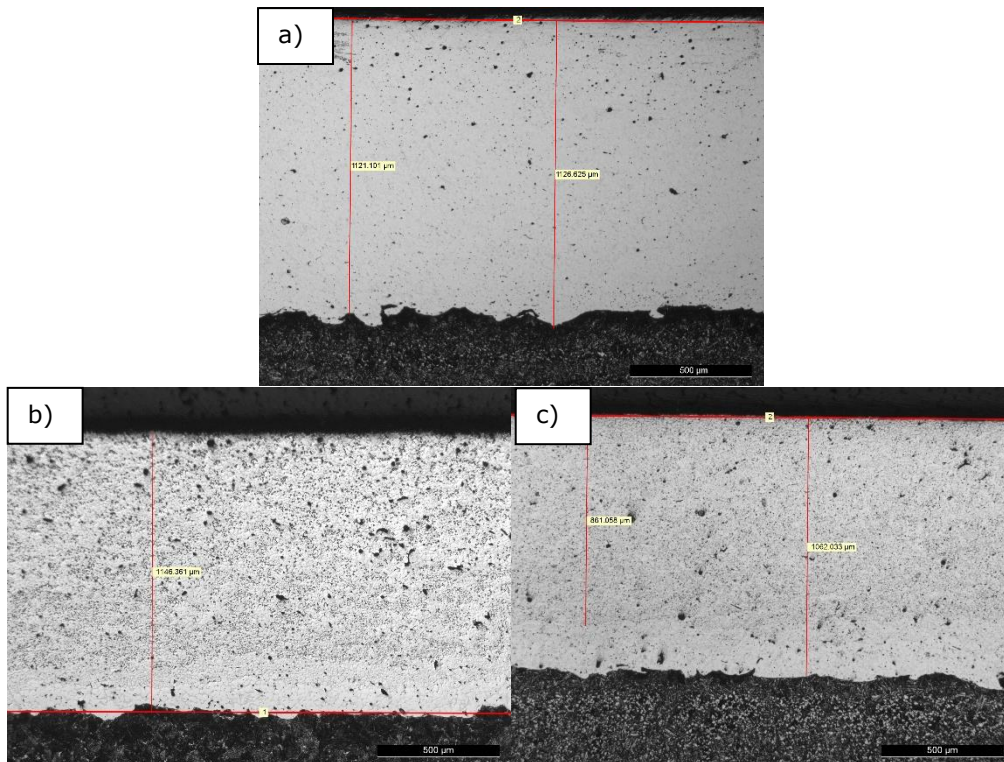


Figure 4.36 Coating cross section a)KS-IC-45, b)KS-IC-55S, c)KS-IC-55

4.7.2. Phase composition

In order to analyse the component phases in the coatings obtained by the two-step process: thermal spray with oxyacetylene flame followed by a heating process at melting temperature with the help of high frequency currents, XRD (X-Ray Diffraction) aid was made, with which the powders can be described and characterized coatings used in this experiment.

Figure 4.37 shows the comparison of coatings from XRD pattern results point of view, it is observed that the peaks corresponding to the component phases are present at the same theta angles but for each type of powder each peak has a different intensity. This results in a different percentage composition of phases for each type of powder. For each type of powder, it is explained in detail in the following rows

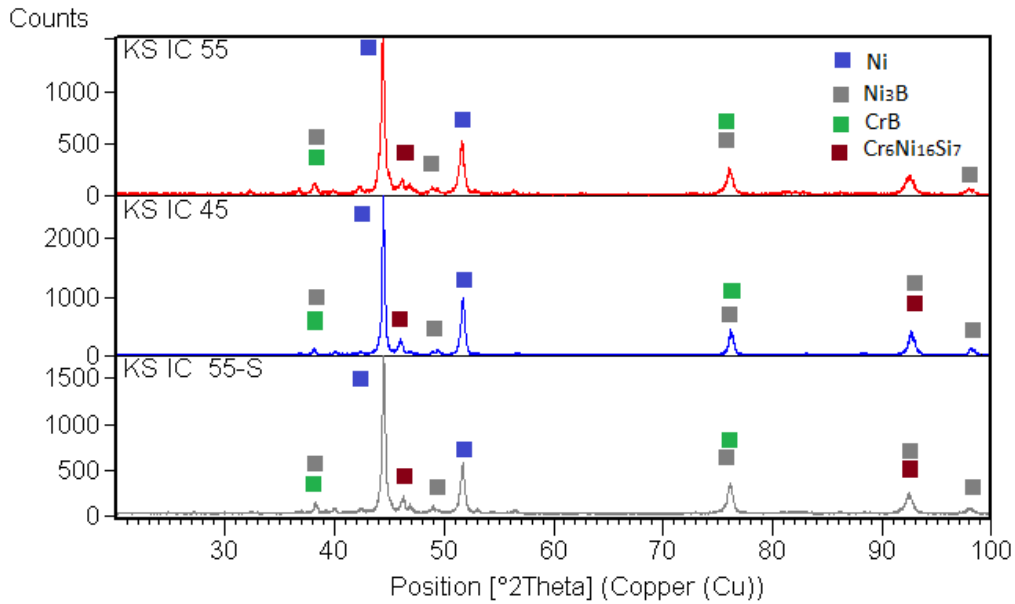


Figure 4.37 Overlapped XRD diffractograms

The three types of coatings were analysed quantitatively and qualitatively from component phases point of view, using a Phillips X'Pert type diffractometer at a working voltage of 45kV and a current of 40mA (Cu K α radiation). In order to obtain the phase diagram, the 2θ angle started from 20 degrees and was taken up to 100 degrees. With the step of $2\theta = 0.015$ degrees and the step time was 1.5 seconds. The data obtained from the process of scanning the crystalline structure of the investigated coating were analysed using the X'Pert High Score software also after that they was contrasted with note patterns from the ICDD and PAN-ICSD databases.

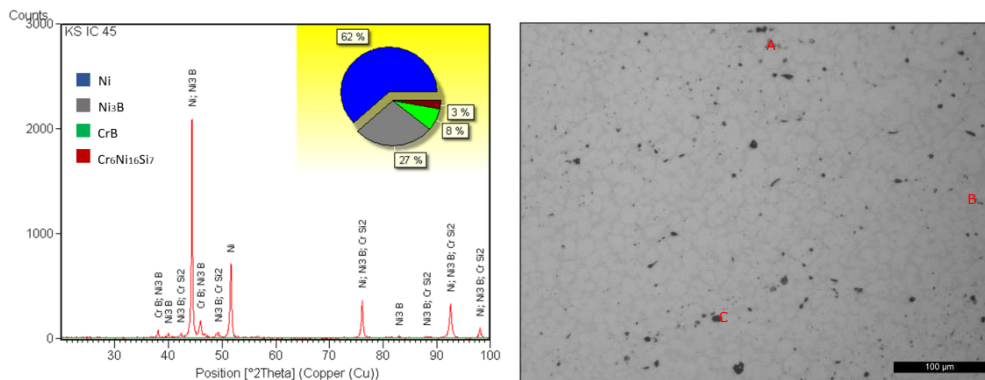


Figure 4.38 XRD Diffractogram of KS-IC-45 inductive remelted (left) and cross-section LM-micrograph (right)

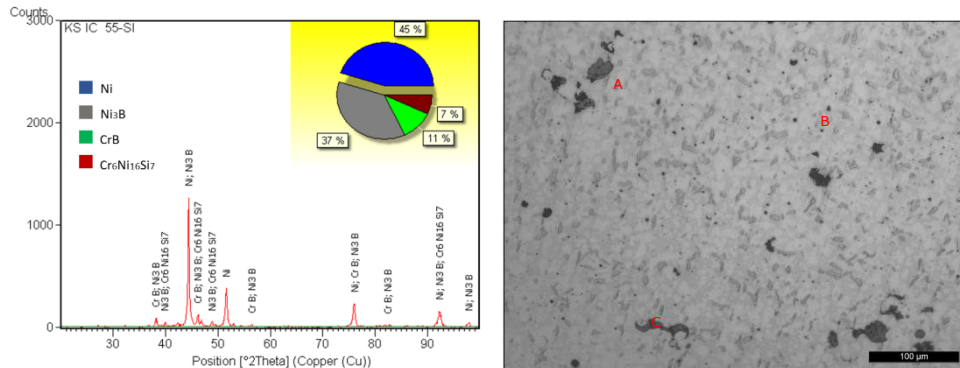


Figure 4.39 XRD Diffractogram of KS-IC-55S inductive remelted (left) and cross-section LM-micrograph (right)

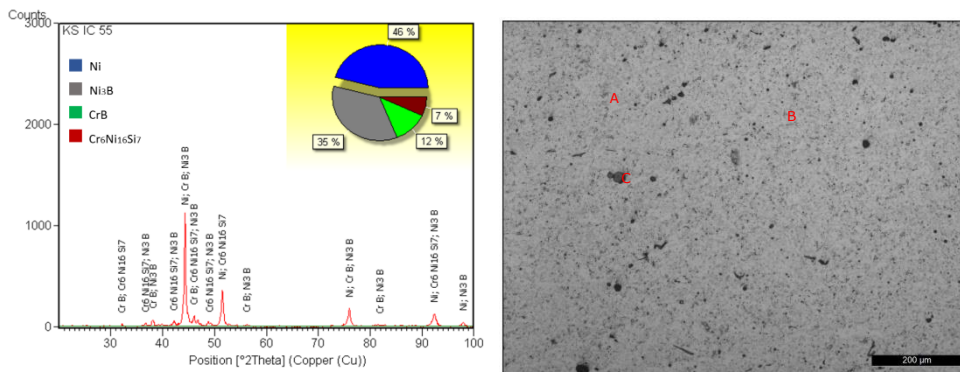


Figure 4.40 XRD Diffractogram of KS-IC-55 inductive remelted (left) and cross-section LM-micrograph (right)

Following the comparison of the peaks obtained from the test with the database, 4 important phases were observed in the composition of the remelted coatings. The nickel matrix, which is predominant in all 3 types of powder, as was also observed in the XRD analysis of the powder. Following the heat treatment, the nickel free phase was reduced from 70% to 62% in the case of type powder KS-IC-45, from 48% to 45% in the case of KS-IC-55S type powder, and in the case of KS-IC-55 type powder from 53.5% to 46%. This soft phase also explains the much lower corrosion behaviour of KS-IC-45 powder, the matrix being prone to corrosion. The dark area marked with B corresponds to the CrB (chromium boride) phase, the phase of nickel boride (Ni_3B) is the bright area marked with A. These two phases are very hard phases which, at the same time, can be observed also in the hardness tests. At the powder type KS-IC 55 it can be observed (Figure 4.40) that these two phases are very finely distributed which leads to an increase in the hardness. The presence of silicides ($\text{Cr}_6\text{Ni}_{16}\text{Si}_7$) in the coating structure increases the stability of the coating at high temperatures, at the same time this phase increases the corrosion resistance.

The silicide are noted with C and are the darkness phase presented in Figure 4.38, Figure 4.39 and Figure 4.40

4.7.3. Porosity

Porosity is generally connected with a high number of unmelted or improperly remelted particles, which are included in the coating. This trapped, unmelted or partially melted, as well as re-solidified particles create a cavity. Corrosion in the sprayed coatings can be promoted by the high proportion of porosity, since the base material can be attacked more easily by oxidizing elements at the interface due to open porosity if this pores are interconnected [8].

The pictures were taken at an optical microscopy after which they were processed with the help of ImageJ image processing software in order to determine the porosity

Following the remelting process the porosity was consistently reduced from about 15% in the case of as-sprayed coatings Figure 4.41, it was reduced to a percentage of 0.5% in the case of KS-IC-45 (Figure 4.42), increasing to 0.9% in the case of KS- IC-55 (Figure 4.44) and in the case of using the KS-IC-55S powder, it had a value of 1.1% (Figure 4.43).

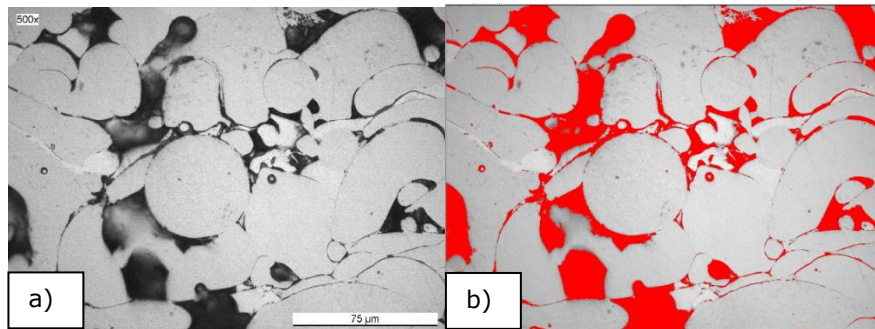


Figure 4.41 Example for marking the porosity of the as-sprayed coating (a) with help of the measurement software (b)

As can be seen in chapter 4.4, the deposited layers are not very compact and require a subsequent treatment of closing pores and improve their adhesion to the substrate. Without this process these coats can be exfoliated by the action of an external force. At the same time, these pores create micro gaps in the piston cylinder assembly, creating a difficult tightness, where the working fluid at each stroke can be extracted from the working environment. Figure 4.41 was taken at a magnification of 500x to be able to observe the non-melted particles embedded in the as-sprayed layer as well as the interconnected porosity. This structure is relevant for all three types of investigated coatings.

In order to investigate the three types of coatings in terms of porosity, after the remelting process, with the help of the optical microscope, pictures were taken at a magnification of 200x in order to have a relatively larger surface to be able to investigate, for each type of sample. 3 pictures were taken in different parts of the coating, porosity was calculated and then averaged.

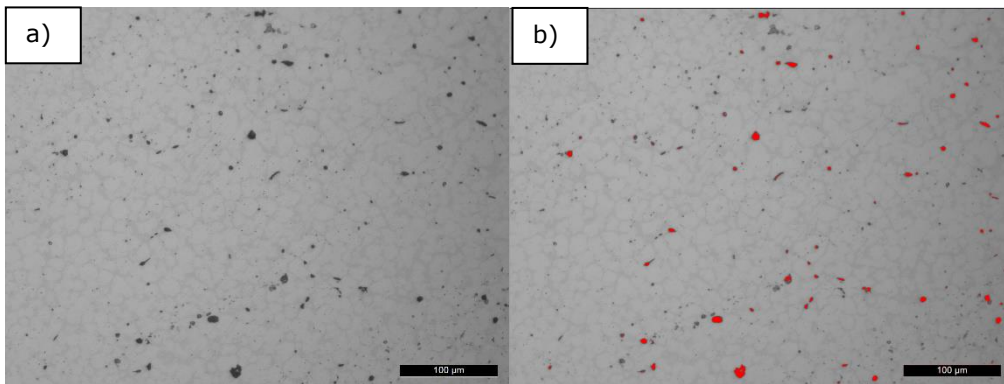


Figure 4.42 KS-IC-45 porosity: a) before, b)after measurement

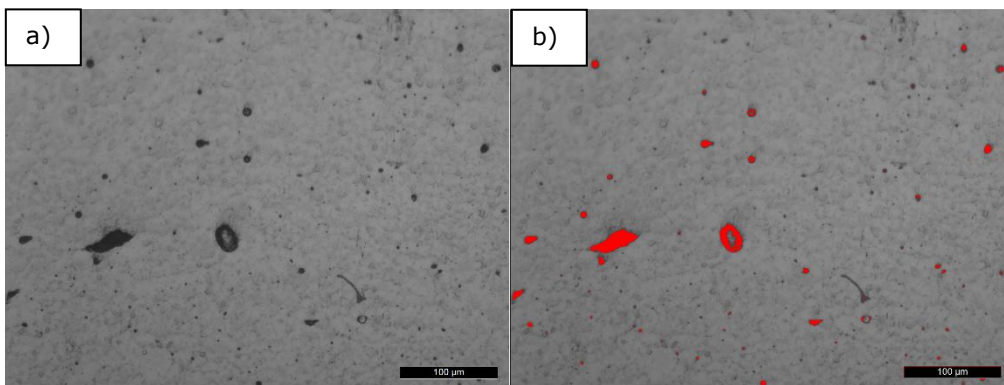


Figure 4.43 KS-IC-55S porosity: a) before, b)after measurement

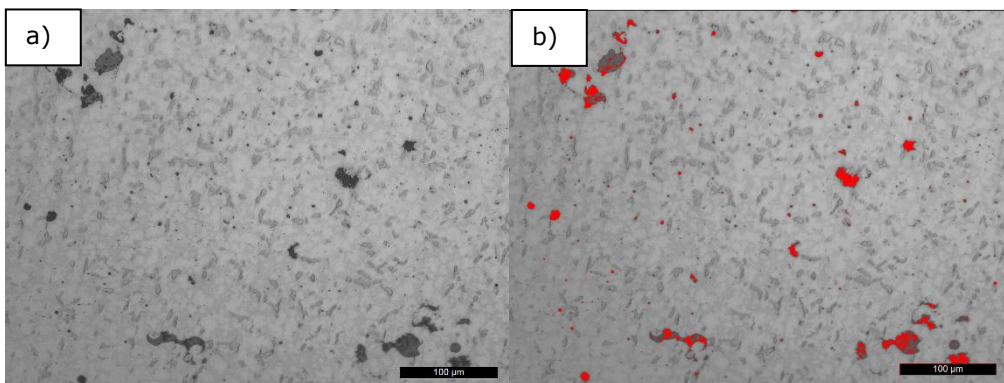


Figure 4.44 KS-IC-55 porosity: a) before, b)after measurement

The difference in porosity percent between the KS-IC-55S and KS-IC-55 can be explained by the fact that the last one has a higher content in the elements that favours the self-fluxing process, namely Si (See Table 4.1). Also because KS-IC-45 has a lower chromium content it makes it a more ductile material, having at the same

time the equivalent Si content as the KS-IC-55 powder and the rest of the alloying elements in low content, manages to make this type of powder easier to process. Also the dark gray phases that can be confused with porosity by the image processing software are phases rich in chromium and silicon see chapter 4.7.2.

Compared to other studies on the same type of powders but through other deposition processes a significant reduction of porosity was observed. For example Xiao J. K. et al deposited NiCrBSi through the atmospheric plasma spray process 2.3%, adding zirconium to the composition lowered the porosity to 0.6% [125]. Zoran Bergant in his work remelted the as-sprayed coatings in the furnace with the protective atmosphere of argon, managing to obtain a percentage of 0.83% porosity [126]. And Kamiri et al succeeded by remelting with oxyacetylene flame using a torch to obtain a minimum porosity of 1.9% [127].

4.7.4. Hardness

The term hardness, as used in industry, can be defined as the ability of a material to withstand to a permanent pressure or deformation when is in contact with an indenter under load [128]. Vickers indenter is a diamond tip with a with the angle at the top of 136 °. The test consists in pressing the known indenter in the test material with a predetermined load.

Microhardness measurements were performed along the cross section of the NiCrBSi Coatings, using a micro Zwick hardness tester. The applied load used to determine the Vickers microhardness was 3 N (± 0.3 kgf) for 15 seconds for each indentation; distance between measurements was 0.15 mm. The results were extracted using the TestXpertZHV μ software, the interface of the working device.

In order to test the hardness of the coatings, from the parts that were inductive remelted with the optimized parameters on a diameter of 160mm, for each type of powder were extracted 3 samples obtained from different parts of the material and prepared metallographically. On each sample, 7 measurements were made from the outside to the substrate. Table 4.18 shows the average values for each indentation

Table 4.18 Indentation values of remelted samples

| Distance [mm] | 0.05 | 0.2 | 0.35 | 0.5 | 0.65 | 0.8 | 0.95 | HRC Hardness |
|--------------------|------|-----|------|-----|------|-----|------|--------------|
| KS-IC-45 [HV 0.3] | 380 | 381 | 380 | 380 | 381 | 371 | 365 | 38 |
| KS-IC-55S [HV 0.3] | 573 | 591 | 636 | 639 | 585 | 584 | 590 | 53 |
| KS-IC-55 [HV 0.3] | 733 | 753 | 695 | 702 | 695 | 748 | 720 | 60 |

Was observed as higher amount of chromium, it results in a higher hardness. Depending on the customer's requirements, all three types of powder can be used, only considering that a high hardness brings problems in further processing it was tried another procedure on the KS-IC-45 type samples.

4.7.5. Adhesion

The chromium content in the coating besides the fact that it improves the corrosion resistance, also raises the hardness of the coating but a hard coating is not

enough in the technological exploitation. Adhesion to the substrate is one of the most important properties of the coatings deposited by thermal spraying. In the case of coats deposited by any thermal spraying process, there is just a mechanical bonding between the coating and the substrate, the particles being mechanically anchored to the substrate as can be seen in Figure 4.10, it also can be seen that before the remelting process there are present delamination, cracks and a deficient anchoring on the interface. Applying the secondary process of remelting by high frequency currents, at the boundary a metallurgical connection is formed between coatings and substrate which leads to a higher resistance.

To investigate whether the coating has good adhesion, all three samples were cut into sections and prepared metallographically. Indentation measurements were made at various points on the interface using Brinell and Vickers indenters.

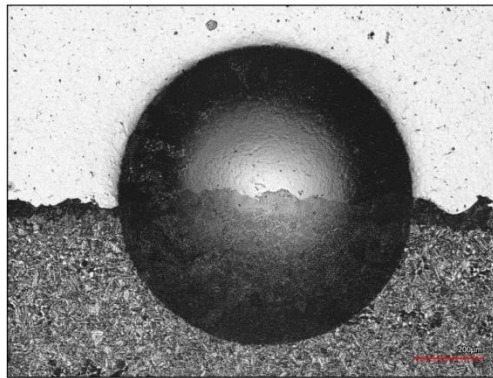


Figure 4.45 Micrographs of Brinell indentation 187.5 kgf

In the case of Brinell type indentation, indentations were made with the application of forces increasing in load up to a weight of 187.5 kgf. Figure 4.45 shows the trace left after the indentation of the coatings used the KS-IC-45 type powder, an imprint that is representative for all 3 types of coatings.

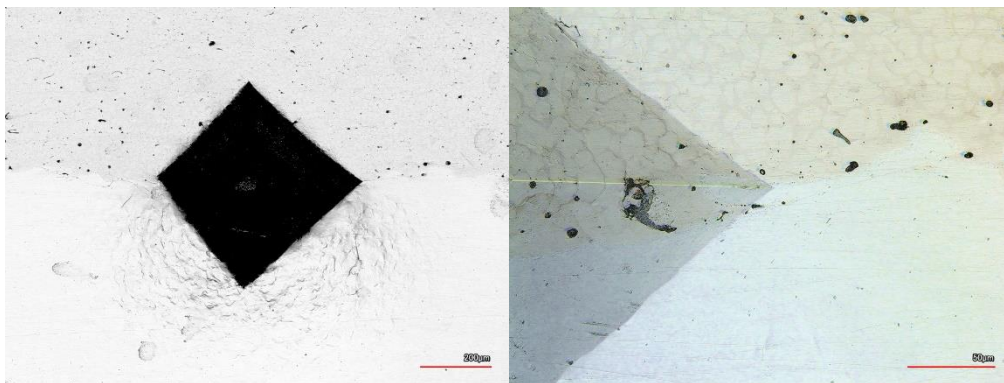


Figure 4.46 Micrographs of Vickers indentation, applied forces: 1200N

Due to the fact that in the case of using the Brinell type indenter with a ball diameter of 2.5 mm no cracks were observed at the interfaced coat-substrate, indentations of type Vickers were tried. This type of indenter having a pyramid type head with an angle of 136 degrees, it introduces much more stresses into the substrate coating interface which can lead, if the adhesion is not good to the microcracks. As in the case of Brinell, metallographic samples were prepared, and indentations were made at the interface with a maximum pressing force of 1200N and a holding time of 15 seconds. Figure 4.46 shows that no micro cracks appeared at the interface.

These results show a very good optimization of the remelting process, for all 3 types of powder, at the same time they show a low presence of internal stresses and a high resistance to exfoliation due to external applied forces.

4.7.6. Tribological behaviour

When using bore cylinder type parts, it is desirable that the coefficient of friction be as small as possible. A high coefficient of friction leads to the introduction of additional energy into the tribological system. This energy can translate over time into damage to the whole assembly due to micro deformations on the surface of the coating, the introduction of vibrations in the assembly or damage by wear of the surfaces. A pin on disk assembly was used to determine the coefficient of friction. The pieces were polished to obtain a flat surface, then they were cleaned with acetone, against the tested sample was chosen a static ball made of WC-Co with a diameter of 6mm, and a pressing force of 10N. The test took place with a sliding speed of 15cm/s on a circle with a diameter of 12 mm and the test stopped after 25000 rotations equal to 942 linear meters, almost double from the parameters used for the as-sprayed coatings. The obtained results of the friction coefficient and wear track are presented in Figure 4.47 to Figure 4.49

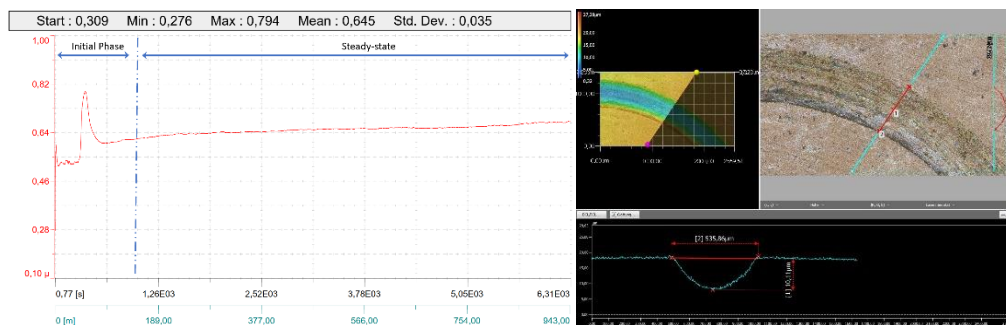


Figure 4.47 Friction coefficient and wear track of KS-IC-45

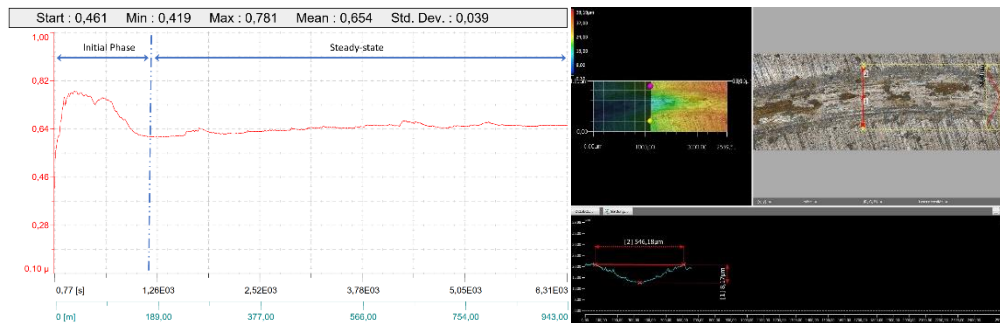


Figure 4.48 Friction coefficient and wear track of KS-IC-55S



Figure 4.49 Friction coefficient of KS-IC-55

Following the tests and microscopic investigations it can be seen that the coating obtained from the KS-IC-45 powder has a slightly higher coefficient of friction than the other two, this can be attributed to the fact that this powder has a modest hardness compare to the other two (see subchapter Hardness). Also from the segment of the track you can see a semi-round worn section according to the shape of the ball, for the other 2 types of powder, coating being harder it can be seen that the counterpart ball was worn, followed by an irregular section on the coating, one with a width much larger than depth. But in conclusion it can be seen that after the process the results are comparable to laser deposition processes founded in technical literature, possibly even a lower coefficient of friction [129]. It is also observed that compared to the as-sprayed coatings, following the remelting process, the coefficient of friction passes from the incipient phase directly to the steady state phase without a transition period, which can be explained by the fact that the coating is much more compact. Also was observed that the trace generated in the coatings is more round, that this is due to the degree of penetration of the counterpart in the material, resulting that the ball did not suffer a pronounced wear

The wear rate is quantified by measuring the wear groove and determining the amount of removed material of both sample and ball. The wear rate K is calculated with the equation:

$$K = \frac{V}{L * d} \quad 4.6$$

4.7 - Characteristics and properties of remelted coatings 93

$$V = 2\pi rA \quad 4.7$$

$$A = \frac{h}{6s}(3h^2 + 4s^2) \quad 4.8$$

$$K = \frac{2\pi r h(3h^2 + 4s^2)}{6Lds} \quad 4.9$$

Where: K=Wear rate [$\mu\text{m}^3/\text{Nm}$]

V= volume [μm^3]

L= normal load [N]

d= testing distance [m]

r= pin end radius [mm]

A= cross-section area [μm^2]

h= height [μm]

s= length [μm]

Table 4.19 Wear measurements

| Powder | h[μm] | s[μm] | Wear rate [mm^3/Nm]* 10^{-5} | Friction coefficient |
|-----------|--------------------|--------------------|---|-------------------------|
| IC-KS-45 | 10.1 | 535 | 1.35 | 0.681 |
| IC-KS-55S | 8.1 | 546 | 1.11 | 0.645 |
| IC-KS-55 | 8.7 | 543 | 1.18 | 0.654 |

The Pin-On-Disk tribological investigation revealed a wear rate of $1,11 \cdot 10^{-5} \text{ mm}^3/\text{Nm}$ for the KS-IC-55S remelted NiCrBSi coatings, compared to a higher value, of $1.35 \cdot 10^{-5} \text{ mm}^3/\text{Nm}$ in the case of IC-KS-45.

As it is observed that the IC-KS-55S type coatings have a better resistance to sliding wear, it can be concluded that they have a more compact structure as a result of the melting process, compared to the IC-KS-55 type coatings and a higher hardness than those of type IC-KS-45

4.7.7. Corrosion behaviour

In the marine industry that works in offshore regions, most parts inevitably present the risk of corrosion. In order to reduce this effect, they are covered with a protective coating which must have a very good corrosion behaviour. Corrosion is an irreversible destruction phenomenon that occurs as a result of chemical or electrochemical reactions.

NiCrBSi-type coatings are sustainable for providing functioning safety and good corrosion resistance, which leads to an extended service lifetime of the components. In order to have a good corrosion resistance the coatings must have a low porosity. At the same time this porosity must be not interconnected, otherwise the electrolyte reaches the substrate that does not have a good corrosion resistance

and begins to exfoliate the superficial layer. Also, the coatings must have a very good adhesion to the substrate; this makes the exfoliation process of the superficial layer very difficult, in the case of the existence of interconnected porosity.

Figure 4.50 shows a cylinder which was coated with KS-IC-45 powder. This part had an interconnected porosity and was tested under real operating conditions. It is observed that after two years of work under offshore conditions the electrolyte penetrated beneath the coating and began to corrode the substrate; after some time the coating was exfoliated. The picture shows the cylinder turned in the lathe and blasted in order to deposit a new coating for a new test.



Figure 4.50 Corroded cylinder sample

Another set of samples were prepared for electrochemical testing. Before the electrochemical corrosion tests, the coated surfaces were polished to obtain a flat surface, due to the fact that the samples were extracted from the deposit on the cylindrical surface with a diameter of 160 mm. Following the preparation of the flat surface, they were grounded until they reached a specified roughness ($R_a \approx 0.1$) and then they were covered in resin to achieve a work tested surface of 1 cm^2 . The corrosion behaviour of NiCrBSi coatings was investigated by electrochemical testing in aqueous solution with a concentration of 3.5% NaCl + 5% H_2SO_4 . A saturated calomel electrode (SCE) was used as a reference electrode, a platinum electrode as an auxiliary electrode and the samples represented the working electrode. The samples were polarized in a potential range from - 1000 mV to +1000 mV, applied between the platinum electrode and the working electrode.

A classification of the corrosion resistance of NiCrBSi powder alloys is achieved: following the process of sintering by electromagnetic induction the as-sprayed coating formed from the KS-IC-55 powder remelted by induction is nobler compared to KS-IC-45. The polarization curves presented in Figure 4.51 show that it has a more positive potential and a lower total current density. As expected due to higher chromium content, the area of positive potential is considered in more detail in Figure 4.52 from which it can be analysed that powders with higher content in Cr have the ability to passivate after passing through the critical point. The coating with low chromium content has a reduced ability to form a passivation layer which leads to more intense corrosion.

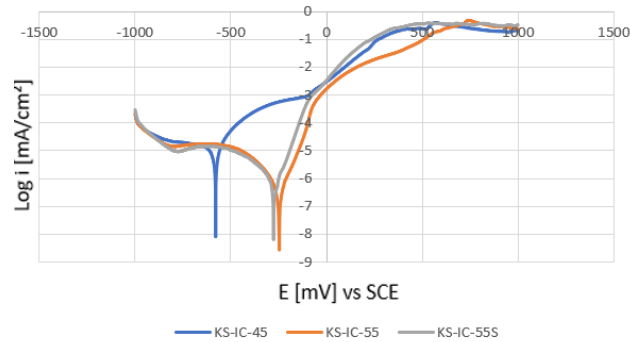


Figure 4.51 Polarization curves of NiCrBSi coatings

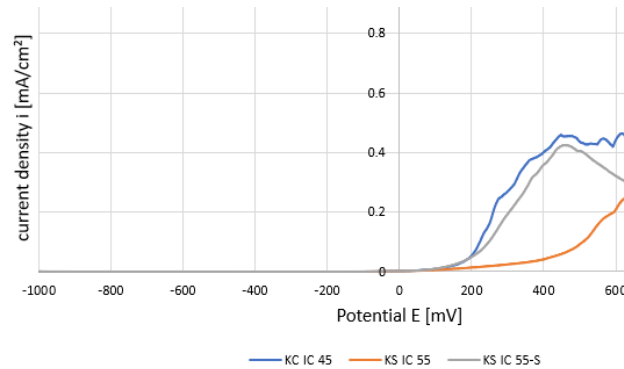


Figure 4.52 Polarization curves of NiCrBSi coatings in 3.5% NaCl + 5% H₂SO₄, passivating part

In the literature Jin-Kun Xiao et al., deposited NiCrBSi-type coatings with the addition of Zr (procedure of depositing was Atmospheric plasma spraying) and tested them in a solution of 3.5% NaCl, a less acidic solution than the solution used in the present work. After testing it was observed that an E_{cor} of -550 was obtained, comparing the coatings obtained by us with these results, it is observed that the KS-IC-45 type powder is in that range, and the other two behave much better, having an E_{cor} at half compared to the one obtained by Jin and the team [130].

Theoretically in the compact materials the corrosion is uniformly distributed, which in the present case, in the coating materials which are composed of several component phases there is a localized corrosion. First time the nickel phase is more likely to be corroded which is like a matrix in all three types of powder, at the intersection of the phases rich in nickel with those rich in chromium or boron. Due to the electrolyte at these joints galvanic microcells are formed which leads to the weakening of the coating. After the corrosion of the soft nickel type phase around the hard phases, the hard phases consisting of boron and chromium are extracted from the coating leaving a emptiness, and the process started again.

The results presented in Table 4.20 and the polarization curves illustrated in Figure 4.51 show that the KS-IC-55S and KS-IC-55 powder types have almost the same corrosion resistance, although the KS IC-55S powder has a chromium content of 3% lower and KS IC 55 has the iron content greater. It can be concluded that, the increase of the chromium content has the effect of increasing the corrosion resistance of the layer, and Fe reduces the anticorrosive properties of the coating. Because the KS-IC-55 powder has a higher Cr content and also has a higher amount of Fe in the structure, the corrosion properties are diminished, reaching approximately those presented by KS-IC-55S.

Table 4.20 Corrosion values of NiCrBSi coatings

| Sample | E_{cor} [mV] vs SCE | I_{cor} [mA*cm ⁻²] |
|-----------|-----------------------|----------------------------------|
| KS-IC-45 | -570 | $7.94 \cdot 10^{-7}$ |
| KS-IC-55S | -270 | $4.60 \cdot 10^{-7}$ |
| KS-IC-55 | -230 | $4.30 \cdot 10^{-7}$ |

Following the results obtained by electrocorrosion tests, the KS-IC-45 type sample resulted as the weakest in terms of corrosion resistance, but not much below the others. Since this type of coating requires much lower processing costs and times, it has been decided that an extra test will be carried out for this type of coatings. The tests were made in collaboration with the specialized and DAkkS accredited laboratory of Caterpillar Global Mining Europe GmbH. This coating was tested for corrosion in salt mist.

A new set of samples was deposited on the cylinders with the ring section and 220mm outer diameter, were remelted with the extrapolated optimum parameters specified in Table 4.16. After the process the samples were turned and polished in order to obtain an $R_a = 0.8 \mu\text{m} \pm 0.3 \mu\text{m}$. The cylinder was cut in half, the first part being prepared for the neutral salt spray test as seen in Figure 4.53.



Figure 4.53 Sample before salt spray test

From the second part a sample was taken and metallographically prepared in order to observe the structure of the coating in the section before the salt spray test. In Figure 4.54 it can be observed that the coatings has a thickness of about one mm.

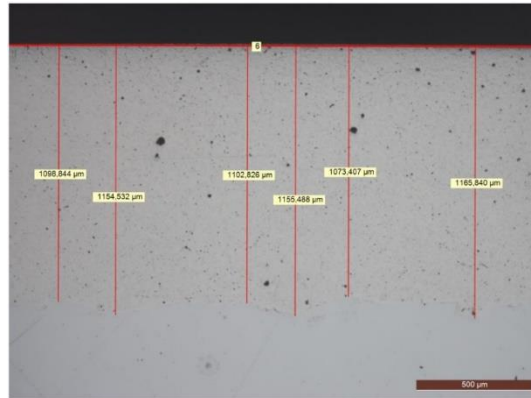


Figure 4.54 KS-IC-45 before Salt spray test

The samples were investigated according to DIN EN 9227 AASS: 2017-07, in the saline environment, the solution was prepared to obtain the neutral saline test. The measured pH of the solution was between 6.5 and 7.2, the sodium chloride concentration was 50g/l \pm 5g/l, after was added sufficient amount of glacial acetic acid in order to reduce the Ph to 3, and obtain an acid solution. The test was carried out in a saline test chamber, the test temperature was 35 °C and the duration of the examination stopped at 480 hours, with the visual investigation of the samples every 48 hours.



Figure 4.55 KS-IC-45 after 480 hours Salt spray test

Figure 4.55 shows the situation after the salt spray test. A clear reaction of the coating with the environment can be observed, but there is no recognized corrosion of the base metals. Towards to better evaluate the existing attack, a cross-section was made

Figure 4.56 shows the corroded piece after exposure to acid saline fog for 480 hours. In the most attacked part by the aggressive environment. It also presents the area from which the metallographic sample was extracted in order to observe the coating behaviour in cross section.

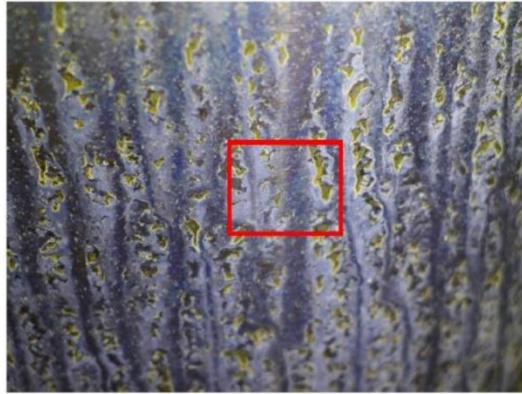


Figure 4.56 Attacked area of KS-IC-45

After 480 hours, in the cross section it is observed that the coating was attacked on a maximum depth of 70 μ m (see Figure 4.57). As this is observed it leads to a selective corrosion, the matrix, which appears darker dark in the cross section, it is finds formed from the nickel-rich phase and is preferably attacked

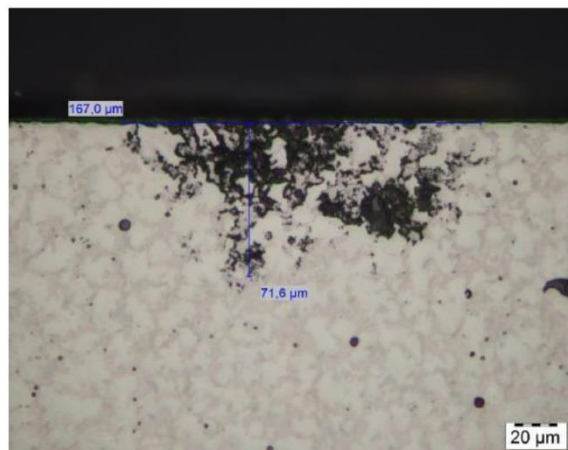


Figure 4.57 Corrosion depth on KS-IC-45

As can be seen from the electrocorrosion tests and the results presented in Table 4.20. The powder KS-IC-45 has a much lower electrocorrosive potential compared to the other two types of powder, at the same time the corrosion current is twice higher than in powder situation KS-IC-55S and KS-IC-55 which makes it most susceptible to corrosion in highly aggressive environments. As a result of the extra test obtained in collaboration with the test laboratory of Caterpillar Global Mining Europe GmbH, it resists in very good conditions to corrosion in saline fog, reaching up to 200 hours without visible optical pitting. At 480 hours under the test conditions, the coating has a corroded pit only on a depth of 70 μ m, and also not on the entire exposed surface, this depth represents only 6.3% of coating total thickness. It can be concluded that this type of coating behaves very well in the vitreous conditions in

4.7 - Characteristics and properties of remelted coatings 99

which hydraulic cylinders will be subjected. It can be seen from Figure 4.57 that the acid solution attacks the matrix which is rich in nickel. At the same time, the other two types because present a much higher chromium content and the electro corrosion result are better it can be concluded that they are less affected by the vitreous conditions to which the offshore aggregates are exposed. KS-IC-45 was chosen to apply extra tests, because from an engineering point of view (processing, costs and processing times, the price of Chromium, the price of powder) it has a very high efficiency and a good profitability.

To observe how the obtained coatings behave in marine environments that have a mostly neutral to basic pH [131], a new test was made for all 3 types of powder studied in this work. The NiCrBSi powder was deposited on cylindrical samples with a diameter of 70 mm and a length of 120 mm, melted and then turned, grinded and polished to a Ra of 0.12 and Rz of 1.2. after which they were covered on half of them and introduced in the testing chamber. The testing solution was prepared in the same way in accordance with the DIN EN 9227 NSS: 2017-07 norm only that acetic acid was not added at the end. The temperature of the solution during the test was 35°, the testing room temperature was 48.5° and spraying pressure was one bar.



Figure 4.58 KS-IC-45 before(left) and after (right) salt spray test

After testing, corrosion points were observed on the surface of KS-IC-45 type parts. In Figure 4.58 it is observed with the exposed eye that irregularities in the coating structure appeared on the surface of the piece. These pieces were cut and investigated in section (Figure 4.59). A corrosion penetration depth of only 34.4 micrometers was observed in the most destroyed part of the coating. Because the coating is at least 900 micrometers thick, this surface destruction does not affect the quality of the thermal coating.

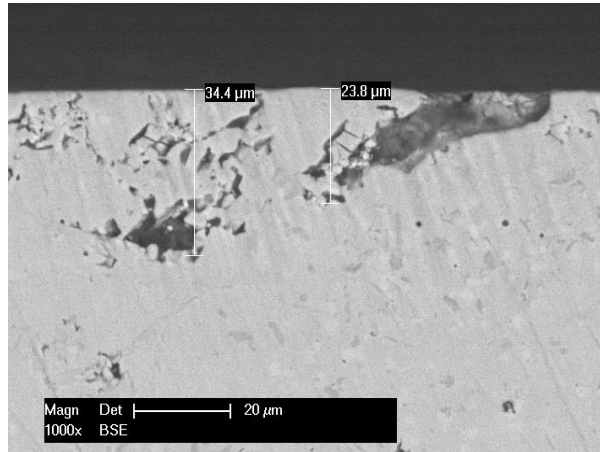


Figure 4.59 Cross section of KS-IC-45 coating after salt spray test

These punctual corrosion can be explained by the fact that during the remelting process due to the fact that this type of powder has a lower chromium content in the structure, some small islands with a low chromium content were formed, which favoured a local corrosion, this led to the formation of galvanic micro cells.



Figure 4.60 KS-IC-55S before(left) and after (right) salt spray test



Figure 4.61 KS-IC-55 before(left) and after (right) salt spray test

No visible damage was observed for the samples investigated and covered with the other two types of powder on the outer surface(Figure 4.60 and Figure 4.61). However, these were also cut and investigated in cross section. In Figure 4.62 the structure of the material is observed; on the surface, no traces of corrosion are noticed, the micron non-regularities being as a result of the mechanical processing.

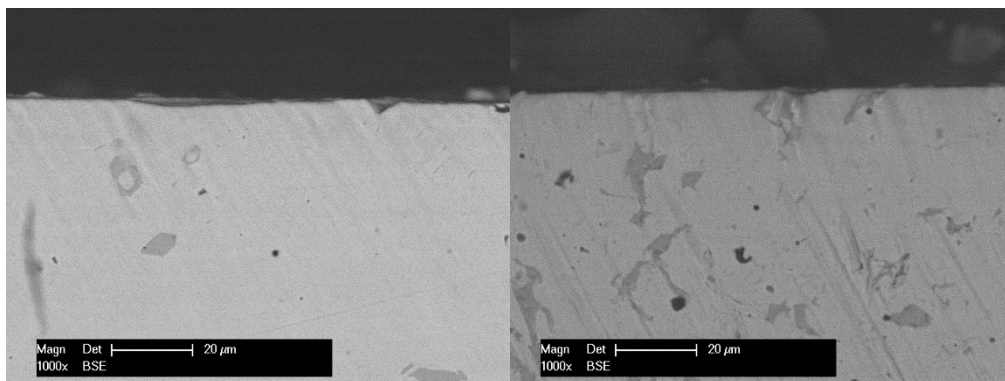


Figure 4.62 Cross section of KS-IC-55S(left) and KS-IC-55 (right) coating after salt spray test

In conclusion, an addition of chromium in the chemical composition of the powder brings a surplus of quality in the corrosion resistance of the final coating. But due to the fact that this element also brings an excess of hardness in the layer, forming some phases likely to introduce internal stresses in the coating and during the cooling process, if care is not taken on the heating parameters, cracks can form. That is why it is suitable in the industry to use KS-IC45 type powders for parts that do not work in a strongly aggressive environment, and KS-IC-55S type powders for parts that work in the open sea.

5. General conclusion, unique contributions and upcoming work

5.1. General Conclusion

The experiments were based on the introduction of a new process for remelting NiCrBSi-type coats sprayed with oxyacetylene flame in the case of new parts or in the case of replacement for worn coatings deposited by other types of processes. The experiments took place on three different types of powder with the aim of optimizing the remelting process for different hardness requirements from the hydraulic cylinder industry.

Attempts to improve NiCrBSi-type layers by heating them with high frequency currents have led to the following conclusions:

- As a feedstock material, the powder used was in the dimensions + 106-45 having a spheroidal shape due to the method of obtaining (by the gas atomization with water collection process), in the cross-section having very high encapsulated holes or porosity. The substrate used was a quenched and tempered 42CrMo4V type steel, with a mechanical strength of 911 MPa (N/mm²)

- The spraying of the three types of powder was done with the help of a specialized company in repairing used hydraulic cylinders. Calculating the necessary deposition parameters, resulted for the samples of diameter 160mm a deposition speed of 833mm/s, the rotation of the shaft being 95 rotations and an advance of 4mm per rotation, the deposition being made in 6 passes with a final coating thickness of 1.3mm

- After deposition, the coatings showed a porosity of up to 15% and a low adhesion to the substrate.

- The inductor type used for remelting these coats were chosen as a rectangular section of 20x10 mm with a wall thickness of 1 mm, continuously cooled with distilled water at a cooling temperature of 15 degrees Celsius.

- The optimization of the three types of layers was done considering the DTA curves obtained in the laboratory and compared to those given by the powder manufacturer. Using the Thaguchi method, was reduced the number of tests from 81 tests (as is normal for an arrangement of 3 factors influencing the process distributed on 4 levels) at only 16 experiments plus the verification experiment, for each of the three types of powder.

- The optimal working distance between the inductor and the heating piece was obtained as 7mm, with an influence on the substrate on a maximum depth of 7 mm and a lamellar sorbitic structure on the first 20 microns at the coating-substrate interface.

- After remelting, the coats were investigated in respect of the developed microstructure with a coat thickness higher than 1 mm and a reduced porosity from 15% down to 0.5% in the case of the coating obtained from the KS-IC-45 powder.

- The presence of chromium boride and nickel boride phases brought a high contribution to achieved hardness. Hardness increasing from 38 HRC in the case of KS-IC-45 powder which has the lowest chromium content of only 6 wt .% to a hardness of 60HRC in the case of KS-IC-55 powder with a content of 13% Cr

- Very good adhesion following the inductive melting process

- Similar friction coefficient of 0.64 was observed in the case of KS-IC-55S powders compared to 0.68 in the case of less hard KS-IC-45 powders.

- At the same time, a good corrosion resistance of the alloy formed after the remelting process was observed, in the case of KS-IC-45 type powder after the neutral salt spray test of 1000 hours, a corrosion penetration depth of only 3.5 micrometres was observed and in the case of testing in an acid environment a penetration of only 75 microns, which at a coating of 1000mm does not present a problem in terms of corrosion. In the case of the other 2 types of powder, no local corrosion attack was observed on the surface of the coating when tested in neutral salt spray.

In conclusion, the KS-IC-45 powder is suitable for use in industry with a hardening process applied before the polishing process, because the surface of the first 10 micrometres will be hard and meet the quality requirements of hydraulic cylinder industry. Inside, the coating is ductile and presents an exemplary machinability in comparison with the coatings obtained from the other two types of powder. The remelting parameters can be extrapolated up to 1000mm diameters, which in the case of coatings obtained from hard powders, due to the internal stresses that form during cooling, it is not possible to realize it without a preheating in the furnace of the entire part.

5.2. Personal contributions

The purpose of this work was to obtain a process for remelting NiCrBSi-based coatings that can be subsequently implemented in industry and also to reduce the operator's influence on the process (which is currently the case of flame torch remelting).

Personal contributions to this study can be said to have been the following:

- Study of the specialized literature that covers the heating of materials by different processes and the behaviour of different materials at temperature

- Choosing different concentrations of chromium in powders and calculating the deposition parameters for the given diameter of 160 mm

- Understanding the need for a subsequent remelting process on NiCrBSi coats

- Optimizing the work element considering its section and the behaviour of the coating when a magnetic field is applied

- Following the optimization of the working element, the selection of the optimal method for improvement of the remelting process, considering a minimum number of tests and also a low production cost. Choosing the Taghuci method to the detriment of other methods.

- Optimizing the working distance considering the quality requirements, the influence on the substrate and the residual stresses that may exist in the parts passed once through the process of use in industry

- Comprehensive characterization of remelted coatings using different methods

- Choosing a type of powder and implementing the process in the industry in the collaborating company

From an economic point of view, KS-IC-45 Powder was chosen to be implemented in industry. Industrial up to diameters of 125mm and any length all three types of powder are suitable. During coating of components with higher values for the diameter and length (>200 mm) using hard powders the remelting step cannot

be realised only with the preheating given by the inductor, because the temperature is dissipated and the cooling in the melting moment is high. This problem induces an high degree of internal stresses in the hard coatings. KS-IC-45 being a ductile material does not form cracks on cooling. That's why the industry agree this type of powder. The coating has a good corrosion resistance and a good machinability.

5.3. Future work

The present work through its theoretical and experimental study led to obtaining a new type of process for obtaining coatings for new hydraulic cylinders and for reconditioning used ones, it can be said that this study contains only a small part of the hydraulic industry.

Taking into account these considerations, one can go further on the following research directions:

- Obtaining coatings with a much higher chromium content, with a preheating in the oven before inductive melting
- Deposition of coatings by the HVOF process in a coating thickness of less than 200 microns with subsequent inductive melting
- Laser Cladding for NiCrBSi powder with inductive preheating of the substrate at the same time as deposition

LISTA PUBLICAȚIILOR REZULTATE ÎN URMA TEZEI DE DOCTORAT, PUBLICATE SUB AFILIERE UPT

Ing. Petru Cristian VĂLEAN doctorand

1. Lucrări științifice publicate în reviste indexate ISI

1.1. N. Kazamer, D.T. Pascal, G. Mărginean, V.A. Șerban, W. Brandl and **P.C. Vălean** "Aspects concerning the wear and corrosion behavior of WC-CoCr coatings and respectively DLC/WC-CoCr systems", 8th International Conference on Nanomaterials – Research & Application (Nanocon 2016), Brno, Czech Republic, pp. 383-388, 2017.

1.2. **Vălean P-C**, Kazamer N, Pascal D-T, Muntean R, Baranyi I, Mărginean G, Șerban V-A. "Characteristics of Thermal Sprayed NiCrBSi Coatings before and after Electromagnetic Induction Process". Acta Polytechnica Hungarica, Obuda, Hungary, Vol 16, Nr 3, pp 7-18, 2019.

1.3. Kazamer N, **Vălean P**, Pascal D T, Muntean R, Mărginean G, Șerban V A. "Development, optimization, and characterization of NiCrBSi-TiB₂ flame-sprayed vacuum fused coatings". Surface and Coatings Technology, Volume 406, 25 January 2021, 126747.

1.4. Kazamer N, Muntean R, **Vălean P**, Pascal D T, Mărginean G, Șerban V A. "Comparison of Ni-Based Self-Fluxing Remelted Coatings for Wear and Corrosion Applications". Materials 2021, 14(12), 3293

2. Lucrări științifice publicate în volumele unor manifestări științifice (Proceedings) indexate BDI (cu specificarea BDI)

2.1. N. Kazamer, **P.C. Vălean**, D.T. Pascal, R. Muntean, G.M. Mărginean and V.A. Șerban "Microstructure and phase composition of NiCrBSi-TiB₂ vacuum furnace flame-sprayed coatings", The 7th International Conference on Advanced Materials and Structures – AMS '18, IOP Conference Series: Materials Science and Engineering, 2018

2.2. D.T. Pascal, N. Kazamer, R. Muntean, **P.C. Vălean**, G. Mărginean and V.A. Șerban "Electrochemical corrosion behaviour of high temperature vacuum brazed WC-Co-NiP functional composite coatings" The 7th International Conference on Advanced Materials and Structures – AMS '18, IOP Conference Series: Materials Science and Engineering, 2018

2.3. **P.C. Vălean**, N. Kazamer, R. Muntean, D.T. Pascal, Y. Kilic, G. Mărginean and V.A. Șerban "Investigations on the characteristics of thermally sprayed NiCrBSi coatings fused by flame and inductive processing", The 7th International Conference on Advanced Materials and Structures – AMS '18, IOP Conference Series: Materials Science and Engineering, 2018

2.4. L. Păduraru, L. Nedeloni, R. Muntean, D.T. Pascal, N. Kazamer, **P.C. Vălean** and M.-D. Nedeloni "Investigations on dry sliding wear and corrosion resistance of thermal sprayed molybdenum coatings", The 7th International Conference on Advanced Materials and Structures – AMS '18, IOP Conference Series: Materials Science and Engineering, 2018



106 Lista publicatiilor

- Article • [Open access](#)
Comparison of ni-based self-fluxing remelted coatings for wear and corrosion applications 2 Citations
Kazamer, N., Muntean, R., Vălean, P.C., ...Mărginean, G., Șerban, V.-A.
Materials, 2021, 14(12), 3293
[Show abstract](#) ▾ [Related documents](#)
- Article
Development, optimization, and characterization of NiCrBSi-TiB₂ flame-sprayed vacuum fused coatings 5 Citations
Kazamer, N., Vălean, P., Pascal, D.-T., ...Mărginean, G., Șerban, V.-A.
Surface and Coatings Technology, 2021, 406, 126747
[Show abstract](#) ▾ [Related documents](#)
- Article • [Open access](#)
Characteristics of thermally sprayed NiCrBSi coatings before and after electromagnetic induction remelting process 2 Citations
Vălean, P.C., Kazamer, N., Pascal, D.T., ...Mărginean, G., Șerban, V.-A.
Acta Polytechnica Hungarica, 2019, 16(3), pp. 7–18
[Show abstract](#) ▾ [Related documents](#)
- Conference Paper • [Open access](#)
Microstructure and Phase Composition of NiCrBSi-TiB₂ Vacuum Furnace Fused Flame-Sprayed Coatings 4 Citations
Kazamer, N., Vălean, P.C., Pascal, D.T., ...Mărginean, G.M., Șerban, V.A.
IOP Conference Series: Materials Science and Engineering, 2018, 416(1), 012001
[Show abstract](#) ▾ [Related documents](#)
- Conference Paper • [Open access](#)
Electrochemical Corrosion Behavior of High Temperature Vacuum Brazed WC-Co-NiP Functional Composite Coatings 1 Citations
Pascal, D.T., Kazamer, N., Muntean, R., ...Mărginean, G.M., Șerban, V.A.
IOP Conference Series: Materials Science and Engineering, 2018, 416(1), 012003
[Show abstract](#) ▾ [Related documents](#)
- Conference Paper • [Open access](#)
Investigations on Dry Sliding Wear and Corrosion Resistance of Thermal Sprayed Molybdenum Coatings 2 Citations
Păduraru, L., Nedeloni, L., Kazamer, N., ...Vălean, P.C., Nedeloni, M.D.
IOP Conference Series: Materials Science and Engineering, 2018, 416(1), 012027
[Show abstract](#) ▾ [Related documents](#)
- Conference Paper • [Open access](#)
Investigations on the Characteristics of Thermally Sprayed NiCrBSi Coatings Fused by Flame and Inductive Processing 1 Citations
Vălean, P.C., Kazamer, N., Muntean, R., ...Mărginean, G., Șerban, V.A.
IOP Conference Series: Materials Science and Engineering, 2018, 416(1), 012002
[Show abstract](#) ▾ [Related documents](#)
- Conference Paper
Aspects concerning the wear and corrosion behavior of WC-CoCr coatings and respectively DLC/WC-CoCr systems 5 Citations
Kazamer, N., Pascal, D.-T., Mărginean, G., ...Brandl, W., Vălean, P.C.
NANOCON 2016 - Conference Proceedings, 8th International Conference on Nanomaterials - Research and Application, 2016, pp. 383–388
[Show abstract](#) ▾ [Related documents](#)

Bibliography

- [1] A. Demirbas, "Global renewable energy projections," *Energy Sources, Part B: Economics, Planning, and Policy*, pp. 212-224, 2009.
- [2] Cost of corrosion trends in oil and gas corrosion, Duxford: Woodhead Publishing, 2017.
- [3] C. M. Cotell, J. A. Sprague and F. A. Smidt, *Surface engineering*, ASM International, 1994.
- [4] C. M. Pogan, *Wear resistance improvement of titanium by surface alloying using electron beam irradiation*, Timisoara: Editura Politehnica, 2011.
- [5] S. Tanthadiloke, P. Kittisupakorn, P. Boriboonsri and I. M. Mujtaba, "Devise of a W serpentine shape tube heat exchanger in a hard chromium electroplating process," *Chinese Journal of Chemical Engineering*, vol. 27, no. 1, pp. 218-225, 2019.
- [6] J. Mendelsohn, P. Howley, M. Israel, J. Grey and C. Thompson, *The molecular basis of cancer*, Philadelphia: Saunders, 2014.
- [7] S. Siegmann and C. Abert, "100 years of thermal spray: about the inventor Max Ulrich Schoop," *Surface & Coatings Technology*, vol. 220, pp. 3-13, 2013.
- [8] ASM International, *Handbook of thermal spraying*, Ohio: ASM International, 2004.
- [9] M. Kroemmer, *Praxis des thermischen spritzen*, Dusseldorf: Thiebes Druck GmbH, 2014.
- [10] L. Pawlowski, *The science and engineering of thermal spray coatings*, 2008: John Wiley and Sons.
- [11] S. Kumar, "Overview of wire arc spray process: a review," *Journal of composition theory*, vol. Volume XII, no. Issue VII, 2019.
- [12] L. Pawlowski, *The science and engineering of thermal spray coatings*, John Wiley & Sons, 2008.
- [13] F. Asinger, *Mono-olefins: chemistry and technology*, 2013.
- [14] J. B. Durkee, *Cleaning with solvents: science and technology*, 2013.
- [15] TEKNOS, *Handbook for corrosion protection of steel surfaces*, Teknos Oy, 2013.
- [16] V. Vanmore and U. Dabade, "Development of laval nozzle for micro abrasive jet machining [MAJM] processes," *Procedia Manufacturing*, vol. 20, pp. 181-186, 2018.
- [17] S. Ebnesajjad, "Surface Preparation of Metals," in *Handbook of adhesives and surface preparation*, 2011, pp. 83-106.
- [18] SinaEbnesajjad and A. H.Landrock, "Material surface preparation techniques," in *Adhesives technology handbook (Third Edition)*, 2015, pp. 35-66.

- [19] "DVS Regelwerk," DVS Verband, [Online]. Available: <https://www.dvs-regelwerk.de/en/topics/Procedures%20and%20devices/Arc%20welding>. [Accessed 25 06 2018].
- [20] P. Vuoristo, "Development trends in thermal spray technologies," Thermal spray coatings in paper processing and printing industries, TUT Finland, 2012.
- [21] C. Brendt, "The origins of thermal spray literature: new surfaces for a new millennium," in *Proceedings of the international thermal spray conference*, 2001.
- [22] M. A. R. & D. G. M. G. D. Lunn, "A study of wire breakup and In-flight particle behavior during wire flame spraying of aluminum," *Journal of thermal spray technology*, p. 1947–1958, 2017.
- [23] D. V. R. a. M. V. R. Dominick V. Rosato, *Plastic product material and process selection handbook*, Elsevier Science, 2004.
- [24] N. V. I. D. A. G. a. A. M. Yu.S. BORISOV, "Study of effect of electric arc spraying modes on structure and properties of pseudoalloy coatings," *Schientific and technical*, 2013.
- [25] C. Abert and S. Siegmann, "100 years of thermal spray: About the inventor Max Ulrich Schoop," *Surface and coatings technology*, vol. 220, pp. 3-13, 2013.
- [26] "ETSS course," GSI SLV, Munchen , 2017.
- [27] A. L. Horner, A. C. Hall and J. F. McCloskey, "The effect of process parameters on twin wire arc spray," *Coatings*, 2015.
- [28] V. B. M. D. S. S. A. Z. Klaus Erich Schneider, *Thermal spraying for power generation components*, 2006.
- [29] A. Guraydin, "Analysis of bimetallic adhesion and interfacial toughness of kinetic metallization coatings," Faculty of california polytechnic state university, San Luis Obispo, 2013.
- [30] M. P. Fuste, J. Picas and M. T. Baile, "Effect of oxygen/fuel ratio on the in-flight particle parameters and properties of HVOF WC-CoCr coatings," *Surface and coatings technology*, 2011.
- [31] R. J. K. Wood and M. Roy, "Tribology of thermal-sprayed coatings," in *Surface engineering for enhanced performance against wear*, 2013, pp. 1-43.
- [32] R. J.K.Wood, "Tribology of thermal sprayed WC-Co coatings," *International journal of refractory metals and hard materials*, pp. 82-94, 2010.
- [33] H. Singh, M. Kaur and N. Bala, "High velocity oxy-fuel spraying and surface finish," in *Reference module in materials science and materials engineering*, 2016.
- [34] E. Jonda and L. Łatka, "Comparative analysis of mechanical properties of WC-based cermet coatings sprayed by HVOF onto AZ31 magnesium alloy substrates," *Adv. Sci. Technol. Res*, pp. 57-64, 2021.
- [35] C. Dong, A. Wu, S. Hao and Z. L. T. Xu, "Surface treatment by high current pulsed electron beam," *Surface and coatings technology*, pp. 620-624, 2003.
- [36] J. Davis, *Handbook of thermal spray technology*, ASM International, 2004.

- [37] E. Toyserkani, A. Khajepour and S. Corbin, *Laser cladding*, London: CRC Press, 2000.
- [38] D. Bartkowski, W. Matysiak and K. Wojtko, "Stellite-6 surface layers reinforced with hard and refractory WC particles produced on steel for metal forming," *IOP conference series: Materials science and engineering*, 2018.
- [39] "SLM Solutions," [Online]. Available: <https://www.slm-solutions.com/products-and-solutions/powders/>.
- [40] E. Musk, "Tweeter," [Online]. Available: <https://twitter.com/elonmusk/status/375737311641628672>.
- [41] F. Vollertsen, K. Partes and J. Meijer, "State of the art of laser hardening and cladding," in *Proceedings of the third International WLT-conference on lasers in manufacturing, 14-17*, Munich, 2005.
- [42] "Ebpglobal," Electron beam processes Ltd, [Online]. Available: <https://www.ebpglobal.com/why-does-electron-beam-welding-need-a-vacuum/>.
- [43] J. Pollefliet, "Applications of power electronics," *Power Electronics*, 2018.
- [44] D. Murzin, K. Levada and V. Belyaev, "Ultrasensitive magnetic field sensors for biomedical applications," *Sensors*, 2020.
- [45] M. Mehdizadeh, *Microwave/RF applicators and probes for material heating, sensing, and plasma generation*, Elsevier Inc, 2015.
- [46] "Fluxtrol," [Online]. Available: <https://fluxtrol.com/magnetic-flux-control-in-induction-heating>.
- [47] L. W. McKeen, *Fluorinated coatings and finishes handbook: the definitive user's guide, second edition*, Elsevier, 2016.
- [48] V. Vologdin, *Poverhnostnaia zagalca inductionnim sposobom.*, Moscova: Metalurgizdat, 1939.
- [49] a. Rudnev, D. Loveless and R. L. Cook, *Handbook of induction heating*, New York, 2017.
- [50] D. Schieber, *Electromagnetic induction phenomena*, Springer Science & Business Media, 2012.
- [51] C. Oldřich, "Faraday's law of electromagnetic induction in two parallel conductors," *International journal of applied electromagnetics and mechanics*, vol. 54, pp. 263-280, 2017.
- [52] D. W. Jordan, "D. E. Hughes self-induction and the skin-effect," *Centaurus*, vol. 26, no. 2, 1982.
- [53] G. S. Smith, "A simple derivation for the skin effect in a round wire," *European journal of physics*, vol. 35, no. 2, 2014.
- [54] B. S. Guru and H. R. Hiziroglu, *Electromagnetic field theory fundamentals*, Cambridge University Press, 2009.
- [55] R. Martin, *Electromagnetic field theory for physicists and engineers: Fundamentals and applications*, 2009.

- [56] D. Gerada, A. Mebarki, N. L. Brown, C. Gerada, A. Cavagnino and A. Boglietti, "High-speed electrical machines: technologies, trends, and developments," *IEEE Transactions on industrial electronics*, vol. 61, no. 6, pp. 2946-2959, 2014.
- [57] J. Davies, *Conduction and induction heating*, IET, 1989.
- [58] Shia-ChungChen, P. SonMinh, Jen-AnChang and Sung-WeiHuang, "Mold temperature control using high-frequency proximity effect induced heating," *International communications in heat and mass transfer*, vol. 39, no. 2, pp. 216-223, 2012.
- [59] F. S. Bergeret, A. L. Yeyati and A. Martín-Rodero, "Inverse proximity effect in superconductor-ferromagnet structures: from the ballistic to the diffusive limit," *Physical review*, 2005.
- [60] S. L. Buck, A. Shelton, B. Stoehr, V. Hadyanto, M. Tang, T. Morimoto and T. DeLawyer, "Influence of surround proximity on induction of brown and darkness," *Journal of the optical society of america*, vol. 33, no. 3, pp. A12-A21, 2016.
- [61] S. Tahkur, "<https://electricalengineering.quora.com/>," [Online]. Available: <https://electricalengineering.quora.com/What-is-proximity-effect?ch=1&share=ff6af271>. [Accessed 2020].
- [62] D. Hömberg and J. SokoLowski, "Optimal shape design of inductor coils for surface hardening," *SIAM Journal on control and optimization*, vol. 42, no. 3, pp. 1087-1117, 2006.
- [63] A. Canelas, J. R. Roche and J. Herskovits, "Inductor shape optimization for electromagnetic casting," *Structural and Multidisciplinary optimization*, vol. 39, 2009.
- [64] S. Chaki, S. Aono, N. Andoh, Y. Sasaki, N. Tanino and O. Ishihara, "Experimental study on spiral inductors," in *Proceedings of 1995 IEEE MTT-S International Microwave Symposium*, Orlando, FL, USA, 1995.
- [65] A. T. Burkov, A. Heinrich, P. P. Konstantinov, T. Nakama and K. Yagasaki, "Experimental set-up for thermopower and resistivity measurements at 100-1300 K," *Measurement science and technology*, vol. 12, no. 3, 2001.
- [66] G. Wouch, "Eddy currents: levitation, metal detectors, and induction heating," *American journal of physics*, vol. 46, no. 5, 1978.
- [67] J. Pendry, A. Holden, D. Robbins and W. Stewart, "Magnetism from conductors and enhanced nonlinear phenomena," *IEEE Transactions on microwave theory and techniques*, vol. 47, no. 11, pp. 2075-2084, 1999.
- [68] V. Rudnev, "Heat treat today," [Online]. Available: <https://www.heattreattoday.com/processes/induction-heating/induction-heating-technical-content/dr-valery-rudnev-on-equipment-selection-for-induction-hardening-single-shot-hardening-part-2/>.
- [69] Huy-TienBu and H.-J. Hwang, "Modeling a working coil coupled with magnetic flux concentrators for barrel induction heating in an injection molding machine," *International journal of heat and mass transfer*, vol. 86, pp. 16-30, 2015.

- [70] V. I. Rudnev. [Online]. Available: <https://inductotherm.sfo2.cdn.digitaloceanspaces.com/wp-content/uploads/sites/11/2019/08/01160900/117.pdf>.
- [71] D. K. Kim, Y. Y. Woo, K. S. Park, W. J. Sim and Y. H. Moon, "Advanced induction heating system for hot stamping," *The international journal of advanced manufacturing technology*, vol. 99, pp. 583-593, 2018.
- [72] V. Rudnev, D. Loveless and R. L. Cook, "Heat treatment by induction," in *Handbook of induction heating*, New York, 2017.
- [73] N. Bayındır, O. Kükreer and M. Yakup, "DSP-based PLL-controlled 50–100 kHz 20 kW high-frequency induction heating system for surface hardening and welding applications," *IEE Proceedings - Electric power applications*, vol. 150, no. 3, 2003.
- [74] V. Geetha and V. Sivachidambaranathan, "An overview of designing an induction heating system for domestic applications," *International journal of power electronics and drive system (IJPEDS)*, vol. 10, 2019.
- [75] S. A. AghaMirjalily, "Effects of joule heating on shock train structure, mathematical modeling with modification of k- ω shear stress transport," *Acta astronautica*, vol. 188, pp. 326-333, 2021.
- [76] D. U. Shin, S. RyongRyu and K. WooKim, "Simultaneous heating and cooling system with thermal storage tanks considering energy efficiency and operation method of the system," *Energy and buildings*, vol. 205, 2019.
- [77] M. R. Tarla, "Successive cooling/heating methods to decrease Gglobal warming.," *Design Engineering*, no. 05, p. 2021.
- [78] M. Zhan and H. Yang, "Casting, semi-solid forming and hot metal forming," *Comprehensive materials processing*, 2014.
- [79] B.-A.Behrens, A.Bouguecha, I. Lüken, J.Mielke and M.Bistron, "Tribology in hot forging," in *Comprehensive materials processing*, 2014.
- [80] k. Holmberg and A. Matthews, *Coatings tribology: properties, mechanisms, techniques and applications in surface engineering*, Elsevier, 2009.
- [81] S. Ghimisi, *Elemente de tribologie*, Bucuresti : Matrix Rom, 2005.
- [82] M.M.Khruschov, "Principles of abrasive wear," *Wear*, vol. 28, no. 1, pp. 69-88, 1974.
- [83] A.A.Torrance, "Modelling abrasive wear," *Wear*, vol. 258, no. 1, pp. 281-293, 2005.
- [84] A. Misra and I. Finnie, "A review of the abrasive wear of metals," *Jurnal of engineering materials and technologies*, vol. 104, pp. 94-101, 1982.
- [85] M. Salot, "Study on Wear resistance of Al-Si alloy using a 3-body dry abrasive wear testing machine," in *NCIMEAT: Indus Univeristy*, Ahmedabad, 2016.
- [86] E. Raask, *Erosion wear in coal utilization*, United States: US department of energy, 1987.
- [87] S. R.More, D. V.Bhatt and J. V.Menghani, "Recent research status on erosion wear – an overview," *Materials today proceedings*, vol. 4, no. 2, pp. 257-266, 2017.

- [88] H. Zhang and Z. Zhang, "Transparent wear-resistant multifunctional polymeric nanocoatings," in *Multifunctionality of polymer composites*, 2015.
- [89] D. H. Buckley, *Surface effects in adhesion, friction, wear, and lubrication*, Elsevier, 1981.
- [90] SantiagoMaya-Johnson, J. Santa and AlejandroToro, "Dry and lubricated wear of rail steel under rolling contact fatigue - wear mechanisms and crack growth," *Wear*, vol. 380, pp. 240-250, 2017.
- [91] A. Leteleanu, "Cercetari privind comportarea la coroziune a materialelorcompozite cu matrice metalica cu baza aluminiu armata cu grafit si carbura de siliciu," *Metalurgia >nternational*, vol. 4, 2012.
- [92] W. D. C. Jr and D. G. Rethwisch, *Fundamentals of materials science and engineering: An integrated approach*, 2018.
- [93] D. I. Fuente, J.G.Castaño and M.Morcillo, "Long-term atmospheric corrosion of zinc," *Corrosion Science*, vol. 49, no. 3, pp. 1420-1436, 2007.
- [94] D. Pascal, *Development of high temperature vacuum brazed WC-Co-NiP functional composite coatings*, Timisoara: Editura Politehnica, 2017.
- [95] N. Kazamer, *Development, optimization and characterization of NiCrBSi-TiB2 vacuum fused flame-sprayed coatings*, Timisoara: UPT, 2019.
- [96] "www.csun.edu," California state university northridge, [Online]. Available: http://www.csun.edu/~bavarian/Courses/MSE%20528/microindentation_hardness_testing.pdf. [Accessed 25 07 2018].
- [97] J. Goldstein, D. Newbury, D. Joy and C. Lyman, "Scanning electron microscopy and X-ray microanalysis," *Springer*, 2013.
- [98] FEI, *An introduction to electron microscopy*, 2010.
- [99] R. Muntean, *Development of catalyst materials based on carbon nanofibers for electrochemical cell applications*, Timisoara: UPT, 2016.
- [100] T. Sokoltsova, *Development of a standardless miniature XRF setup for the analysis of actinides : coupling MC methods with fundamental parameters*, Paris: L'université Paris-Saclay, 2021.
- [101] "Toray inovation by chemistry," [Online]. Available: <https://www.toray-research.co.jp/en/technicaldata/techniques/SEM.html>. [Accessed 05 08 2020].
- [102] L. Fedrizzi, L. Valentinelly, S. Rossy and S. Segna, "Tribicorrosion behaviour of HVOF cermet coatings," *Corrosion science*, vol. 49, no. 7, pp. 2781-2799, 2007.
- [103] L. W. Xu, N. Lin, L. B. Zaho, C. Ma, Z. Y. Wang and Y. H. He, "Improvement in wear and corrosion resistance of Ti(C,N)-based cermets via aluminium nitride additions," *Vacuum*, vol. 168, 2019.
- [104] B. S. Mann, V. Arya, A. K. Maiti, M. U. B. Rao and P. Joshi, "Corrosion and erosion performanceof HVOF/TiAlN PVD coatings and candidate materials for high pressure gate valve aplication," *Wear*, vol. 260, pp. 75-82, 2006.
- [105] B. S. Mann, V. Arya and P. Joshi, "Advanced high-velocity oxygen fuelcoating and candidate materials for protecting LP steam turbine blades against droplet

- erosion," *Journal of materials engineering and performance*, vol. 14, no. 4, pp. 478-494, 2005.
- [106] X. C. Zhang, B. S. Xu, F. Z. Xuan, S. T. Tu, H. D. Wang and Y. X. Wu, "Rolling contact fatigue behaviour of plasma-sprayed CrC-NiCr cermet coatings," *Wear*, vol. 265, pp. 1875-1883, 2008.
- [107] ASM International, Alloy phase diagram, ASM Handbook, 2005.
- [108] Z. Bergant and J. Grum, "Quality improvement of flame sprayed, heat treated and remelted NiCrBSi coatings," *Journal of Thermal Spray Technology*, vol. 18, pp. 380-391, 2009.
- [109] t. Liyange, G. Fisher and A. P. Gerlich, "Influence of alloy chemistry on microstructure and properties in NiCrBSi overlay coatings deposited by plasma transferred arc welding (PTAW)," *Surface & Coatings Technology*, vol. 205, pp. 759-765, 2010.
- [110] M. Larsson, "Introduction to a new standardized test method for mixes, the gustavsson flowmeter funnel," in *EURO PM 2013*, Gothenburg, 2013.
- [111] j. Su, X. Qiu, F. Xiang and Y. Ruan, "Effect of preheating temperature on microstructure and properties of 42CrMo4/38MnVS6 heterogeneous laser welded joint," *Metals*, 2019.
- [112] P. J. Cunat, "Alloying elements in stainless steel and other chromium-containing alloys," in *Euro inox*, Paris, International Chromium Development Association, 2004.
- [113] R. S. Ruffini, "Fluxtrol.com," Fluxtrol manufacturing, 1981. [Online]. Available: <https://fluxtrol.com/magnetic-flux-control-in-induction-installations>.
- [114] M. Rycroft, "Induction heating applications in the metals industry," *EE Publisher*.
- [115] D. J, Introduction to electrodynamics, Cambridge University Press, 2017.
- [116] "RDO INduction," Induction heating solution, [Online]. Available: <https://rdoinduction.com/components-of-induction-heating.html>. [Accessed 23 05 2020].
- [117] J. M. Miguel, J. M. Guilemany and S. Vizcaino, "Tribological study of NiCrBSi coating obtained by different processes," *Tribology International*, vol. 36, no. 3, pp. 181-187, 2003.
- [118] V. Rudnev, D. Loveless, R. Cook and M. Black, Handbook of induction heating, Michigan: Marcel Dekker Inc., 2003.
- [119] G. Taguchi and S. Konishi, Taguchi methods, orthogonal arrays and linear graphs, tools for quality american supplier institute, American Supplier Institute, 1987, pp. 8-35.
- [120] R. R. Sreenivas, C. G. Kumar, R. S. Prakasam and P. J. Hobbs, "The taguchi methodology as a statistical tool for biotechnological applications: A critical appraisal," *Biotechnology Journal*, vol. 3, pp. 510-523.

- [121] G. Box and W. G. H. J. Stuart Hunter, *Statistics for experiments: Design innovation and discovery*, 2nd edition, Hoboken, New Jersey: John Wiley and Sons Inc, 2005.
- [122] J. L. Rosa, A. Robin, M. B. Silva, C. A. Baladan and M. P. Peres, "Electrodeposition of copper on titanium wires: Taguchi experimental design approach," *Journal of materials processing technology*, vol. 209, no. 3, pp. 1181-1188, 2009.
- [123] V. A. Vaidya, "Application of taguchi for optimization of process parameters improving thickness variation in single stand cold rolling mill," *International refereed journal of engineering and science*, vol. 5, no. 5, pp. 15-23, 2016.
- [124] "Stahl Online," [Online]. Available: https://www.stahl-online.de/wp-content/uploads/2019/06/MB450_Waermebehandlung_von_Stahl_Haerten_Anlassen_Vergueten_Bainitisieren.pdf?fbclid=IwAR1owXbz-LaxOQ7jK4OuPn0mU7uE6h8Be8HAVTznSSUbRywFJUVT89thhfU.
- [125] J. K. Xiao, Y. Q. Wu, W. Zhang, J. Chen, X. L. Wei and C. Zhang, "Microstructure, wear and corrosion behaviours of plasma sprayed NiCrBSi-Zr coating," *Surface & Coatings Technology*, vol. 360, pp. 172-180, 2019.
- [126] Z. Bergant and J. Grum, "Porosity evaluation of flame sprayed and heat treated nickel based coatings using image analysis," *Image Anal Stereol*, vol. 30, pp. 53-62, 2011.
- [127] M. R. Karimi, H. R. Salimijazi and M. A. Golozar, "Effects of remelting process on porosity of NiCrBSi flame sprayed coatings," *Surface Engineering*, vol. 32, no. 3, pp. 238-243, 2016.
- [128] P. Fauchais, J. J. Heberlein and M. Boulos, *Thermal spray fundament: from powder to part*, Springer, 2014.
- [129] A. Garcia, M. Fernandez, J. Cuetos, R. Gonzalez, A. Ortiz and M. Cadenas, "Study of the sliding wear and friction behaviour of WC+NiCrBSi Laser cladding coatings as a function of actual concentration of WC reinforcement particles in Ball-on-Disk test," *Tribol Lett*, p. 41, 2016.
- [130] J.-K. Xiaoa, Y.-Q. Wua, W. Zhanga, J. Chenb, X.-L. Weia and C. Zhanga, "Microstructure, wear and corrosion behaviors of plasma sprayed NiCrBSi-Zr coating," *Surface & Coatings Technology*, vol. 360, pp. 172-180, 2019.
- [131] Otilia Antonaru; Laura Alexandrov; Eugen Anton, "Evaluarea initiala a mediului marin," Institutul Național de Cercetare Dezvoltare Marină "Grigore Antipa", Constanta, 2012.
- [132] V. A. Bukanin, A. N. Ivanov, A. E. Zenkov and V. V. Vologdin, "Induction Hardening of External Gear," *IOP Conference Series: Materials Science and Engineering*, vol. 327, no. 3, 2018.
- [133] A. Vasiliev, I. Pozniak and V. Greshnov, "Modeling and investigation of hardening processes," International scientific colloquium, Hannover, 2003.
- [134] C. Laird and L. Buchinger, "Hardening behavior in fatigue," *Metallurgical Transactions A*, vol. 16, pp. 2201-2214, 1985.

- [135] G. E. Totten, Handbook of residual stress and deformation of steel, ASM International, 2002.

Personal information

Petru Cristian Valean

Nationality: Romanian

Birth date: 16.06.1991

E-mail: petru.valean@student.upt.ro

Education:

Doctoral studies:

Polytechnical University of Timisoara, Romania – Faculty of Mechanical Engineering,
Department of Materials Engineering and Manufacturing

2016 - Present

Westphalian University of Applied Science, Germany – Faculty of Mechanical
engineering, department of material science and testing

2016-2021

Master degree

Polytechnical University of Timisoara, Romania – Faculty of Mechanical Engineering

2014-2016

Bachelor degree

Polytechnical University of Timisoara, Romania – Faculty of Mechanical Engineering,

2010-2014

Languages

English – professional proficiency ; German – working proficiency